Mass transfer from giant donors

by

Konstantin Pavlovskii

A thesis submitted in partial fulfillment of the requirements for the degree of

Doctor of Philosophy

Department of Physics
University of Alberta

Abstract

In this thesis we study MT from giant and subgiant donors in binary stars. We develop a MT simulation framework based on the MESA set of stellar libraries, which is suitable to study extremely high MT rates and predict the stability of MT. We find that the MT from giant donors is much more stable than previously thought: the currently used critical initial mass ratios are approximately two times lower than the ones predicted by our improved MT framework. We foresee that this improvement of stability will substantially affect the rate of double compact mergers in the Galaxy, which are the sources of gravitational radiation detectable by the gravitational observatories, such as the Advanced LIGO. We find that a non-degenerate He remnant obtained from an evolved main sequence star by rapid mass loss, as a donor to the three known ultra-compact X-ray binaries – 4U 1626-67, 4U 0614+09, and 4U 1916-053 can explain the anomalously high MT rates in them. We develop an improved magnetic braking prescription that can be used to study the evolution of low-mass X-ray binaries with a giant or subgiant donor. We find that this prescription can explain the extremely high MT rate observed in such binaries, for example in Sco X-1.

Preface

The research for this thesis was conducted in collaboration with Prof. Natalia Ivanova and Prof. Craig Heinke at the University of Alberta. The thesis is substantially based on the following published, submitted and prepared papers: Pavlovskii & Ivanova (2015b); Heinke et al. (2013); Pavlovskii & Ivanova (2013, 2015a); Pavlovskii et al. (2015)

The Section 1.4.3 of this thesis contains text published as Pavlovskii, Konstantin & Ivanova, Natalia, "Ultra-compact X-ray binaries with high luminosity: a key for a new scenario," *Proceedings of the International Astronomical Union*, Volume 291, pp. 468-470, which was written by myself with the assistance of Prof. Natalia Ivanova. In this work I was responsible for the simulations and analysis of results, Prof. Natalia Ivanova was the author of the theoretical concept.

Chapters 2, 3, 4, 5, 6.1, 6.2 of this thesis contain text published as Pavlovskii, K. & Ivanova, N. "Mass transfer from giant donors," *Monthly Notices of the Royal Astronomical Society*, Volume 449, Issue 4, p.4415-4427, 2015. I was responsible for the theoretical content of the above paper except for the theoretical part of the Section 2.3 and condition (23), which were written by Prof. Natalia Ivanova. I was also responsible for the simulations and analysis of the results. Prof. Natalia Ivanova was also the supervisory author, she assisted me with the composition of the manuscript and was involved with the main concept formation.

Chapter 6.2 of this thesis contains the material from the paper in preparation by Pavlovskii, K., Belczynski, C. and Ivanova, N. "Stability of the MT and black hole-black hole binaries formation", in which I am the author of the theoretical concept relating to the stability of MT, Prof. Belczynski investigates the relationship between the rate of mergers and the stability of MT, I am responsible for the simulation and analysis of results and Prof. Natalia Ivanova assists us with the composition of the manuscript and analysis of results.

Chapter 6.3 of the thesis contains text submitted to the *Monthly Notices of the Royal Astronomical Society* as a manuscript by Pavlovskii, K. & Ivanova, N., "Mass transfer and magnetic braking in Sco-X1". I was responsible for the simulation and analysis of results. Prof. Natalia Ivanova was the author of the general concept of the new magnetic braking prescription.

Chapter 6.4 of the thesis contains text published as Pavlovskii, Konstantin & Ivanova,

Natalia, "Ultra-compact X-ray binaries with high luminosity: a key for a new scenario," *Proceedings of the International Astronomical Union*, Volume 291, pp. 468-470 (see above) and as the Section 2.2 of the published paper by Heinke, C. O.; Ivanova, N.; Engel, M. C.; Pavlovskii, K.; Sivakoff, G. R.; Cartwright, T. F.; Gladstone, J. C., "Galactic Ultracompact X-Ray Binaries: Disk Stability and Evolution," The Astrophysical Journal, Volume 768, Issue 2, article id. 184, 2013, in which I was responsible for the numerical simulations and Prof. Natalia Ivanova was the author of the theoretical concept.

Dedications

I would like to dedicate this thesis to those people who provided me with non-academic support during my doctoral program: my wife Elena (emotional and technical support); my daughter Alisa (emotional support), my supervisor Prof. Natalia Ivanova (emotional and technical support); my mother (emotional support); Yarik Fiveyskiy (inspirational and creative support).

Acknowledgements

I would like to thank my supervisor, Prof. Natalia Ivanova for her intensive academic support. I also acknowledge the financial support provided by the Golden Bell Jar Scholarship and the University of Alberta Doctoral Recruitment Scholarship.

Table of Contents

List of Tables

List of Figures

Chapter 1

Introduction

1.1 Importance of close binary stars

Many stars do not solely interact with their neighboring stars as point masses but are sufficiently close to affect each others evolution in a noticeable way. Such binary stars that appreciably affect each others evolution are called close binaries. They are unique physical laboratories that allow one to test and constrain unknown parameters in such theories as condensed matter, physics of plasma, and general relativity through the comparison between observations and the output of the respective numerical models.

Binary stars that are sufficiently close to each other can exchange matter and produce a very important natural phenomenon of X-ray binaries. In these binary stars matter from one star is accreted onto another (its compact companion, e.g. a black hole or a neutron star), which results in X-ray radiation. The star that accretes mass is called accretor, and the star that gives its mass away is called donor. Studies of mass transfer (MT) in X-ray binaries are important tools for constraining the equation of state of neutron stars and accretion theories. High energy X-ray radiation is poorly absorbed by the interstellar matter and thus can be detected at a long distance, which gives us an exciting possibility to study the sources located in distant galaxies. MT in binaries can be steady or runaway (unstable) MT. Runaway MT, unlike steady MT, changes the orbital parameters of a binary system substantially over one period (crossing timescale) of the binary, for a detailed discussion refer to Chapter 5. Having a stable or unstable MT also affects substantially the ensuing evolution of the binary stars. A clear separation of the possible evolutionary channels is important for our understanding of the formation of compact binaries. E.g., double white-dwarf binaries were thought in the past to be formed via two common envelope events, while more recent detailed simulations of MT with low-mass red giant donors show that the first episode of MT was stable (Woods et al.,

2012). It is important to study the formation of compact binaries because they are a well-known source of gravitational radiation, detectable by the planned eLISA mission.

Understanding the stability of MT in binaries with massive stars is important to determine the rate of double compact object mergers. Double compact object merger occurs when two black holes or a black hole and a neutron star merge in the course of binary evolution. For example, when massive giant donor causes a runaway MT when it overflows its Roche lobe (see Chapter 5), the common envelope is in some cases ejected from the system, forming a close binary consisting of two compact objects. These mergers are the key source of gravitational radiation that would be detectable in the near future by detectors like Advanced LIGO (Laser Interferometer Gravitational-Wave Observatory). Through this mechanism the rate of detectable gravitational events depends on the theory of MT from giant donors to compact accretors and can vary by at least an order of magnitude depending on the stability criteria for such MT. It is possible in some cases to develop these stability criteria for a range of systems without detailed simulations (see Chapter 5), but in other cases the only currently feasible way to predict, whether or not the MT will be stable in a given binary system, is to conduct long-term detailed simulations with one-dimensional stellar codes.

Low-mass X-ray binaries (LMXBs) are a subtype of X-ray binaries, in which the mass of the donor is less than 1.5 $M_{\odot}$. The formation of this type of binaries requires angular momentum to be lost from the binary system in order to shrink their orbital separations to the observed values and to provide ongoing mass transfer. For binaries with non-degenerate donors, the most effective mechanism of angular momentum loss is magnetic braking. Magnetic braking is a mechanism by which the angular momentum of a rotating star is carried away by the outflowing matter. Due to the magnetic field of the star, the outflowing matter partially co-rotates with the star as it is ejected away from it. This mechanism leads to the reduction in the angular momentum of single rotating stars. In a binary magnetic braking acts on the non-degenerate donor, slowing down its rotation and simultaneously the donor is being synchronized with the accretor by the means of tidal interaction. As a result, the angular momentum of the whole binary decreases.

Unfortunately, it appears that either this mechanism or the long-term evolution of these binaries are not understood correctly because the simulated MT rates in LMXBs strongly (by approximately an order of magnitude) disagree with the observations of persistent LMXBs, where the theoretical value of MT rate is systematically below the observed one (Podsiadlowski et al., 2002). In this paper, the authors conduct 100 detailed evolutionary binary calculations for the systems consisting of a neutron star and non-degenerate donor star with various initial periods and masses of the donor. Then they calculate the probability distribution for the value of MT rate depending on the orbital

period of the system. Most observed LMXBs have higher MT rates than those rates that are the most probable for a given period.

Calculating long-term evolution of X-ray binaries is especially complicated because it requires truly detailed stellar models to keep track of the changes in the structure and mass loss response of the donor. In addition, various physical effects were found to be significant: irradiation of the donor star by the X-ray radiation from the accreting star (Podsiadlowski, 1991), tidal deformation of the donor and eccentricity of the system (Petrova & Orlov, 1999; Sepinsky et al., 2007, 2009) and the evolution of the accretor. In this thesis we do not consider these effects. We limit our consideration to the structural changes of the donor as given by a one-dimensional stellar code and employ a semi-hydrodynamical model of MT and magnetic braking. Even these simulations require both an extremely robust stellar code and a realistic model of gas flows from the donor to the accretor.

There are a number of observed LMXBs for which current theory can not explain the observations. For example, Sco X-1, an X-ray binary that according to observations consists of an evolved but anomalously light subgiant, an evolved star, which is much less dense than a MS (MS) star of its mass and a heavy compact accretor, most likely a neutron star. The mass of the subgiant is so small that there is no conceivable way a star of this mass could evolve to reach the advanced evolutionary phase of a giant or subgiant. The commonly adopted picture is that the MT from this star to its compact companion makes this configuration possible, but what drives the MT at the observed rate is not understood. In this system the MT rate mainly depends on the rate at which the angular momentum is removed from the system. However, neither gravitational radiation nor current magnetic braking schemes provide the amount of braking torque sufficient to drive the observed MT rate. It remains approximately an order of magnitude higher than it should be according to the commonly used magnetic braking scheme.

There is a subclass of LMXBs called ultra compact X-ray binaries (UCXBs) because their periods are less than 1 hour. Among them, there are also several UCXBs which have anomalously high MT (MT) rates. These high MT rates could neither be explained with a hypothesis of MT from helium white dwarfs (WDs) nor from normal carbon-oxygen (CO) WDs. However, if the He-rich core of the donor star is exposed as a result of fast mass loss (as presumably happens in a CE event), the MT rate from a non-degenerate donor (He-rich remnant) is much higher. This hypothesis requires fast mass loss to strip the outer hydrogen-rich envelope of a red giant first and then the He-rich remnant to be placed into a binary system. Numerical calculations performed in the frame of this thesis validate this hypothesis and explain the observations (Heinke et al., 2013).

1.2 Approaches to binary simulations

A commonly used approach (which is also adopted in the framework we use) is to consider the non-inertial reference frame, that co-rotates with the components. It is also assumed that the rotation of both components is synchronized and the whole system rotates as a rigid body around its own center of mass. In this case one has to take into account additional fictitious forces within this frame, namely centrifugal force, Euler force and Coriolis force. The latter two forces are usually neglected in comparison to the centrifugal force, which dramatically simplifies the calculations because both remaining forces – centrifugal and gravitational are potential by nature and therefore one can introduce a potential corresponding to them, which is commonly called the "Roche potential":

$$\Phi_{\rm Roche} = \Phi_{\rm cent} + \Phi_{\rm grav}, \tag{1.1}$$

where $\Phi_{\rm Roche}$ is the Roche potential, $\Phi_{\rm cent}$ is the potential of centrifugal force, $\Phi_{\rm grav}$ is the gravitational potential. For the description of the Roche potential it is a common approach to use a dimensionless system of units, in which the angular velocity, binary separation and the gravitational constant are taken to be unity. If the origin of a Cartesian coordinate system is located at the center of mass of the binary system, the angular velocity is parallel to the z axis, and the donor and accretor are located at the x axis, then the Roche potential can be written in the following way (in the aforementioned dimensionless system):

$$\Phi_{\rm Roche} = -\frac{q}{(q+1)\sqrt{\left(-\frac{1}{q+1}-x\right)^2+y^2+z^2}} - \frac{1}{(q+1)\sqrt{\left(\frac{q}{q+1}-x\right)^2+y^2+z^2}} + \frac{1}{2}\left(-x^2-y^2\right), \tag{1.2}$$

where q is the mass ratio of the left (negative x) binary component to the right one. The MT problem then can be approximately solved by considering fluid (gas) that flows within this potential (Lubow & Shu, 1975a).

The two lobes of the equipotential surface, to which the first Lagrangian point, L_1, belongs are then called the Roche lobes. The Roche model is widely employed in the studies of binary stars. MT between the components in binary stars is often dramatically boosted when dense layers of one of the components go beyond its Roche lobe (that can be very roughly described as a three dimensional potential well that surrounds the component). This is referred to as the Roche lobe overflow (RLOF) by this component. It can happen either when due to natural evolutionary expansion the volume of a component grows to exceed the volume of its Roche lobe or when due to overall angular momentum loss from a binary, the Roche lobe of a component gradually shrinks and descends onto its dense layers. The donor is assumed to take the shape of its Roche lobe at

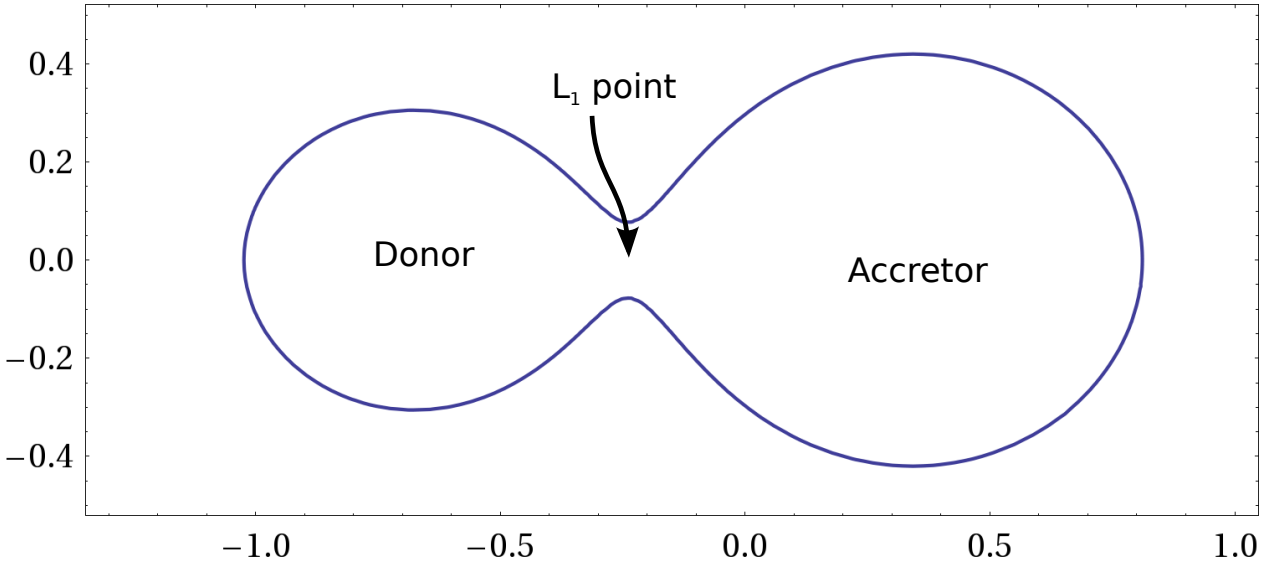

Figure 1.1: Schematic depiction of the Roche lobe (L_1) overflow in a binary with the mass ratio (donor to accretor) of 0.5. Donor's photosphere matches the equipotential, drawn with the blue solid line. The MT occurs through the L_1 nozzle. The unit of length is binary separation.

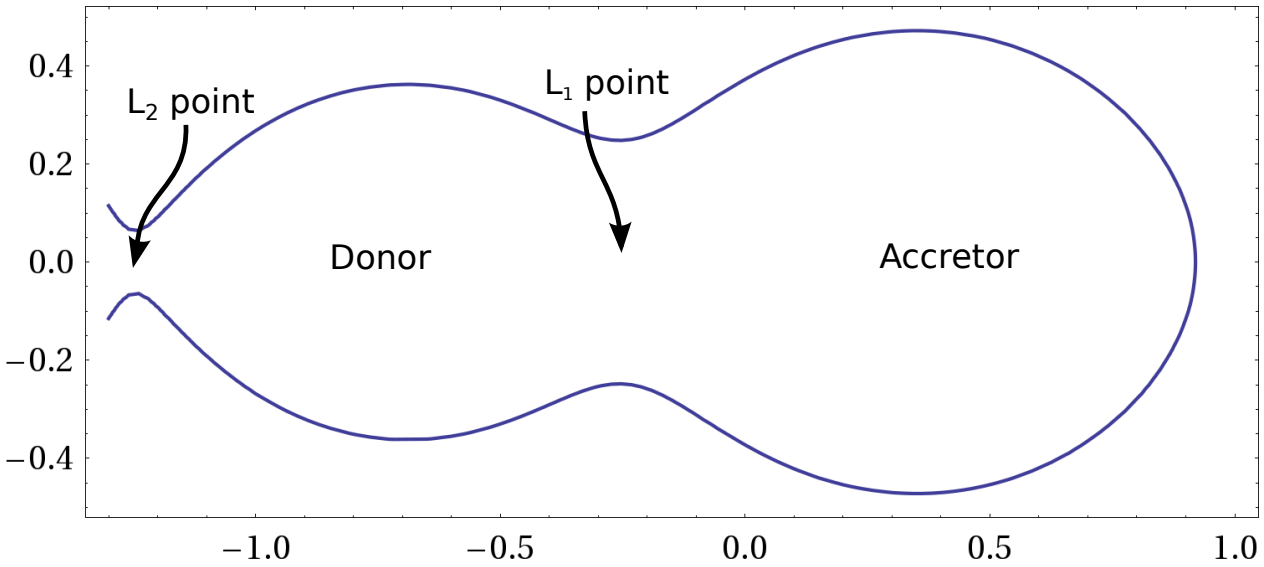

Figure 1.2: Schematic depiction of the L_2 overflow in a binary with the mass ratio (donor to accretor) of 0.5. Donor's photosphere matches the equipotential, drawn with the blue solid line. The MT occurs through both the L_1 nozzle and L_2 nozzle. The unit of length is binary separation.

the moment of RLOF, however all thermodynamical parameters of this donor are usually taken from a one-dimensional stellar code following the rule or simplified assumption called *volume correspondence*. According to this assumption, the thermodynamical parameters, such as pressure, temperature, density and others at a radius R of the one-dimensional model are the same at a Roche equipotential surface with enclosed volume $(4/3)\pi R^3$. Usually the donor star is assumed to end at its photosphere, characterized by the optical depth of 2/3.

In the case of steady (stable) MT, the material of the donor flows approximately through the inner Lagrangian point, L1, to the accretion disk that is formed around the accretor if the latter is compact, e.g. a neutron star or a black hole. The evolutionary way of the single stars is defined by their mass and composition. During the MT mass is removed from the donor, therefore the donor is deflected from its normal evolutionary way. The donor in some cases may undergo substantial transformations as a result of MT. The material from this accretion disk is accreted onto the donor if the MT rate doesn't exceed the Eddington limit for the accretor, i.e. if the luminosity generated by accretion does not exceed the Eddington luminosity for the accretor. When the rate of MT is high enough to cause the orbital parameters of the system to evolve on the system crossing timescale (binary period), the material of the donor might form a cloud engulfing the binary system, and the system no longer behaves like a set of two relatively compact objects. In this case the MT is called unstable.

One of the factors that determines whether or not an episode of MT is stable is the relationship between the response of the donor's radius to mass loss and that of the Roche lobe volume. This response in many cases proceeds on the dynamical timescale of the donor and in general its study requires three-dimensional (magneto-)hydrodynamical simulations that would also take into account heat exchange, ionization, element mixing and so on.

A star, even if it is a member of a binary system, evolves much like a single star would unless its interaction with the component is sufficiently strong. For this reason up to a certain point the evolution of binary stars can be treated with one-dimensional evolutionary codes designed for the single stars. When the interaction between a simulated star and its component becomes sufficiently strong to affect its evolution, the single-star evolutionary codes become insufficient. Unfortunately, the subsequent evolution becomes much more complex at this point. To date, there are a few approaches that allow one to simulate in a very approximate manner the binary system as a whole or on the component-by-component basis. The approaches include:

- direct hydrodynamical simulations which are based on three-dimensional hydrodynamical codes (see e.g. Rasio & Livio, 1996),

- implicit models of MT, based on the one-dimensional model of the donor, in which the

donor's radius is considered to be always equal to the volume-radius of the Roche lobe and the MT rate is chosen to satisfy this condition (see e.g. Ivanova & Taam, 2004),

- explicit models of MT, in which the one-dimensional donor is allowed to grow larger than the Roche lobe, but MT rate is calculated on the basis of simplified semi-hydrodynamical models of gas flows (see e.g. Paczyński & Sienkiewicz, 1972).

All of these approaches employ serious simplifications in physics and multiple ad-hoc assumptions. Typically, no approach can be trusted on the whole range of timescales encountered in binary evolution. For this reason before attempting to simulate a binary system, one should pick a concrete physical process that one needs to simulate and from there pick a method of simulations that is assumed to work satisfactorily on the timescales of the chosen process. For example, 3D hydrodynamical models are expected to work on the dynamical timescale of the whole binary system, also called crossing time. On this timescale the physical processes in the donor which these codes do not track (convection, radiation, nuclear energy generation, etc.) are not expected to affect the results. Implicit and explicit models of MT are most often used in conjunction with one-dimensional stellar codes and are expected to work well on longer timescales, such as evolutionary and thermal (Kelvin-Helmholtz) timescales of the donor. These models, however, can't be expected to give realistic results in those cases when the orbital parameters of the binary system vary substantially over the crossing timescale because the use the Roche lobe potential approximation, which is only expected to work when the Euler term is negligible compared to the centrifugal term (see Chapter 5).

In our research we concentrate mainly on the behavior of the giant stars. Here giant refers to a certain evolutionary stage of single stars, at which they are relatively expanded and possess convective envelopes of a sufficient depth (over 30% of their mass). Note that giant stars could be either on red giant branch or asymptotic giant branch. We study how these giant stars transfer their material to their binary companions once they overfill their respective Roche lobes. We conduct numerical simulations that are to show the processes that take place in a binary system once the mass loss starts. We then consider to naturally expand our results to the underdeveloped giant stars with shallow convective envelopes and also to massive stars. Unfortunately, the evolution of single stars of high mass (more than 10 $M_{\odot}$) becomes much more complex. For example, they may possess multiple convective layers at the giant stage. Among other complications, the quantity and width of these layers might strongly depend on the adopted assumptions about the opacity of the stellar material (opacity tables). For this reason alone any results concerning massive stars should be taken with great caution.

Binary MT can proceed on various timescales – from the dynamical timescale of the donor

star (its sound crossing time) to the evolutionary timescale, on which the structure of a single star would evolve. The intrinsic complexity of the problem with studying binary MT is in part due to the extreme width of the involved range of timescales. To make the study feasible we primarily concentrate on the range of timescales larger than the dynamical timescale, on which the internal structure of the stars cannot be considered constant. Shorter timescales are currently the domain of hydrodynamical codes, e.g., SPH codes which among other things ignore the stellar evolution.

This choice of the physical process and timescales restricts us to the use of detailed stellar evolutionary codes, which are still, unfortunately, predominantly one-dimensional. Namely, we have chosen to use the `MESA` set of stellar libraries[1]. `MESA` is described in Paxton et al. (2011a, 2013). This set includes the stellar evolutionary code, `MESA/star`. In our opinion, this code can be considered the state-of-the-art stellar code in the area of stellar evolution. This code describes very well the evolution of single stars but is not, unfortunately, designed to treat the fast-paced processes that occur when a giant star exchanges mass with its companion. For this reason we had to introduce certain modifications to it and adjust certain free parameters to ensure that the results are compatible with physical reality.

The `MESA` code includes a binary module, `MESA/binary` which is designed to simulate binary systems (Paxton et al., 2015). Among other things this module can simulate MT from one binary component to another. We introduce improvements to this module in order to enable it to treat the extremely fast MT that happens in some cases when the mass-losing component is a giant star.

We call the set of improvements to both `MESA/star` and `MESA/binary` our MT simulation framework. This framework, unlike its predecessors, allows one to consider much shorter timescales, which are practically on the edge of the dynamical timescale, and much higher MT rates.

Below we cover in brief the content of this thesis, separated in two parts. The first part, the larger one, is the list of methodological improvements offered in this work, the second is dedicated to the astrophysical applications of the improved methods.

1.3 Methodological improvements

This section describes the approaches to simulating MT in a binary star where material is transferred from a giant donor to a compact accretor. First the scope of the problem is described. Then, I make an overview of the historically used and commonly accepted methods. Finally, I focus on

[1] Modules for Experiments in Stellar Astrophysics, http://mesa.sourceforge.net

the methods suggested in this work and on the improvements they offer.

1.3.1 Outer layers of giant stars

Giant stars, including red giants and asymptotic giant branch stars, have vast outer convective envelopes. On the top of these envelopes, according to the current stellar models, there are superadiabatic layers, in which the logarithmic gradient of temperature with respect of pressure, $P\partial T/T\partial P$ is much higher than it would be in an isentropic environment (difference between these gradients is comparable to the gradients themselves). Superadiabatic layers are formally convective, but convective heat transfer in them is ineffective compared to radiative due to a combination of reasons. It is believed that the major contributing factor to the inefficiency of convection is low density in the superadiabatic layers. It is important to study the structure of these layers because of the role they might play in the reaction of a giant to mass loss (both radial response and the temperature of the giant). We develop a prescription for the approximate mass of superadiabatic layers in stars of various masses and radii with convective envelopes. As we show, it is important to know the mass of superadiabatic layer to properly take into account the effect of recombination that occurs in the outer layers of the giant stars during mass loss. It turns out that this effect mainly affects the temperature of the donor star and to a lesser extent its radial response to mass loss.

Previously the response of giant stars to mass loss was studied on simplified models that did not include superadiabatic convection. The first step to understanding the response employed polytropic gaseous spheres – normal, condensed, and composite polytropes (Hjellming & Webbink, 1987). The condensed polytrope model considers a polytropic spherical star consisting of ideal gas with a massive material point at its center. The index of the polytrope is taken to produce a star with a constant profile of specific entropy versus mass. Although this model doesn't include the superadiabatic layer, by employing this model it becomes possible to predict the radial response of the star to mass loss analytically, without detailed simulations, by solving the Lane-Emden style equations with proper boundary conditions. By conducting detailed simulations we show in Chapter 5 that these predictions hold for large giants, whereas compact giants exhibit less expansion, and therefore tend to have more stable MT. Using the results of Hjellming & Webbink (1987), stability thresholds for various modes of MT were derived by Soberman et al. (1997).

Later, Ge et al. (2010) studied mass loss response of detailed stellar models to fast mass loss. It was assumed in their study that the profile of specific entropy versus mass doesn't change appreciably during the mass loss. The starting model for mass loss was obtained from a detailed one-dimensional stellar code and did contain superadiabatic layer. However, after the original superadiabatic layer was removed during the mass loss, it did not reconstitute itself and the ensuing

remnants did not have strong superadiabatic convection in their outer layers, unlike the starting model. Additional details about this model can be found in Chapter 3. It has been shown (Ge et al., 2010; Woods & Ivanova, 2011) that those models that don't include superadiabatic convection and those that do give quite different results with respect to the response of giant stars to mass loss, namely models without superadiabatic convection predict more expansion, which leads to underestimated stability of MT from giant donors. This decreased stability leads to, e.g., increased predicted number of double compact objects, whose mergers are detectable sources of gravitational radiation (see Chapter 6.2).

In Chapter 2 of this thesis I show that the shape of these layers is defined by the partial ionization of hydrogen and helium and that partial ionization can impede the growth of superadiabaticity in these layers through the increased heat capacity of gas at constant pressure. I explain the features of the temperature gradient seen in the outer layer.

1.3.2 Single stars subjected to fast mass loss

Modern 1D stellar codes are very well suited to calculate the evolution of single stars. However, a star in a close binary could be subjected to fast mass loss rate as a result of binary MT. This mass loss could change the structure of the donor star on timescales which can't be adequately tracked by the modern evolutionary stellar codes. In this regime the conventional equations governing photospheric boundary conditions, convection and recombination may fail. As a result of fast mass loss, stellar material may experience local Lagrangian accelerations, comparable to the local effective gravitational accelerations. These acceleration terms are partially taken into account in advanced stellar codes in the frames of the Heyney-type hydrodynamical treatment, in which they are added to the stellar pressure equations. There are, however, other stellar equations which depend on these acceleration terms. Convection can not be considered to occur in an inertial reference frame, as it is done in all currently used stellar codes. In a non-inertial frame additional fictitious forces need to be considered along with the external gravitational force field, because these terms together drive convective instability. The same is true for the photospheric boundary condition, which should also be rewritten for a non-inertial frame.

Chapter 3 of this thesis explores the limitations of stellar codes relating to fast MT and explains the numerical effects that arise in this case, including those found earlier by other authors but unexplained.

1.3.3 MT in binaries

This section is dedicated to simulating long-term (thermal or even nuclear-timescale) MT in binaries with one-dimensional detailed stellar codes, including the initial response to mass loss. The primary problem in this field is interdependence between the mass loss rate from the donor and the extent to which the donor overfills its Roche lobe. Three dimensional hydrodynamical simulations of this process on thermal or evolutionary timescales are not currently feasible, hence one has to use one-dimensional detailed stellar models and infer the MT rate from additional considerations.

In implicit MT models, which are suitable for donors with dense outer layers and/or low mass loss rates, the donor is assumed to always remain within its Roche lobe and the mass loss rate is chosen to satisfy this assumption. However, the explicit MT models show that those donors that experience high MT rates and/or have substantially rarefied envelopes can overfill their Roche lobes by more than 30% during the MT (see e.g. Pavlovskii & Ivanova, 2015b). In this case implicit MT models are obviously not applicable and there is currently no alternative to using the explicit MT models. In the explicit models a stream of gas is considered that flows from the outer layers of the donor through the L_1 point to the accretor. The parameters of this stream depend on the extent of the RLOF of the donor. The density and velocity of the gas flow at its L1 neighborhood cross-section can be calculated if simplifying assumptions on the thermodynamical processes that occur in the stream as it flows to the cross-section and shape of potential are made.

In Chapter 4 of this thesis I consider improvements to the existing explicit MT models that would decrease the number of simplifying assumptions and allow one to track whether or not the equipotential of the outer Lagrangian point of the donor, called either L_2 or L_3 depending on the mass ratio, is overfilled in the process of MT.

1.3.4 Common envelope events

In an extreme case of very fast mass exchange the material drawn from the donor can form a common envelope that engulfs both components and strongly affects the further evolution of the system. The common envelope could later be expelled, carrying mass and angular momentum away from the system. As a result, a very close binary forms, which can later merge. Through this mechanism the expected rate of detectable gravitational wave events depends on whether or not certain binary systems eject their envelope or whether or not they experience common envelope events.

It is obvious that a common envelope event dramatically modifies the binary system even if the envelope is not ejected. It is therefore important to understand when or if the common envelope

event takes place in a given binary system. To understand this, among other things, needs detailed structural models to simulate the binary system before the common envelope event. The common envelope event proceeds on a range of timescales and always starts with low rate (e.g. evolutionary and then thermal timescale) MT. In some cases, when it is known in advance that the common envelope event does take place and when it happens relatively fast, the three-dimensional hydrodynamical models might be of use. One could, for example, simulate the ejection of the envelope using hydrodynamical codes. Unfortunately, these codes are quite limited in terms of physics that's taken into account, especially heat transfer.

In some cases though, the simulation of slow (for example, thermal-timescale) MT preceding the common envelope event is required. Also some systems are known to have delayed dynamical instability (Webbink, 1985), and the stability of some systems is questionable. Delayed dynamical instability does not appear immediately after the RLOF (RLOF). Instead, for example, the first RLOF leads to stable MT, after which a part of the hydrogen-rich envelope is lost and the donor detaches. That lost envelope was radiative initially. Later, the donor overfills the Roche lobe again and the remaining envelope is consumed to expose its middle convective layer (which is still hydrogen-rich). At this point the donor expands dramatically and experiences a very fast dynamically unstable MT and a common envelope event.

In these cases one needs detailed structural models, which are usually one-dimensional due to computational limitations. In the case of fast MT, in addition to the detailed stellar models, one needs a MT model that treats the way material is transferred between the components in a simplified semi-hydrodynamical way. Here, "semi-hydrodynamical" means that although Navier-Stokes equations are used to track the flow of gas, the models of flows are simplified to the degree that allows one to conduct simulations without the use of three-dimensional hydrodynamical codes. Such models have existed since at least 1970s (Paczyński & Sienkiewicz, 1972; Savonije, 1978) and haven't changed much since then (Kolb & Ritter, 1990; Ge et al., 2010). They are simplified due to the inherent incompatibility between a three-dimensional flow of gas between the components and one-dimensional models of the donor and accretor. The basic idea of these models is to consider a steady stream of gas flowing from the donor to the accretor and then use Navier-Stokes equations and additional assumptions to find the density and velocity of the gas at some cross-section of this stream. In Section 4.1 of this thesis I propose how to improve the stream models.

One of the cases where a common envelope event can take place is when a more massive star leaves the main sequence (MS) earlier than its less massive counterpart, expands and overfills its Roche lobe, thereby starting the MT. A classical understanding is that if the donor has a deep convective envelope at the moment of RLOF, then the ensuing MT will be unstable and will ultimately

lead to a common envelope event. This is based on semi-analytical models of MT suggested and explored by Hjellming & Webbink (1987) and Soberman et al. (1997). In Chapter 5 of this thesis I show that this assumption is incorrect and that it is possible to determine the fate of the binary system in a more precise way even without detailed stellar simulations.

Further, I derive the applicability limits of the currently used Roche and L_1 MT approximations (see Chapter 5). I show that the Roche approximation becomes invalid when the orbital parameters of the system change substantially on its crossing timescale, and that the L_1 MT approximation fails when the equipotential corresponding to the outer Lagrangian point of the donor is overfilled. I subsequently show that these applicability limits are comparable to each other.

1.4 Applications

This section is focused on how to apply the new knowledge from the previous section in practice.

1.4.1 New stability thresholds

The application of the new MT simulation framework immediately leads to a new stability picture for the giant stars that are subject to MT.

Population synthesis codes, e.g. `StarTrack` (Belczynski et al., 2012), `Brussels` (De Donder & Vanbeveren, 2004), `SeBa` (Portegies Zwart & Verbunt, 1996) with the latest updates by Toonen & Nelemans (2013) are used, among other things, to estimate the merger rates of the double compact objects (i.e., black holes and neutron stars) in the Galaxy. These mergers are an important source of the gravitational radiation, detectable by observatories such as Advanced LIGO. To achieve this goal, population synthesis codes make statistical evolutionary predictions. These codes use a set of criteria to determine whether or not in a given binary system there will be runaway MT from a giant donor when it overfills its Roche lobe (for a review see Toonen et al., 2014). These criteria are based on the structure of the donor, mode of MT and the donor-accretor mass ratio at the onset of the RLOF. Here, the mode of MT is defined by the fraction of mass, lost from the donor, which is accreted and by the specific angular momentum of the material lost from the system. For example, the Brussels code assumes that when the donor of a certain mass grows larger than a certain radius it acquires a convective envelope. If by the time of the RLOF this radius is achieved, then it is considered that MT will be unstable. SeBa and StarTrack decide whether or not the MT is stable by comparing the logarithmic derivatives of the donor radius and Roche lobe radius with respect to the donor mass – $\zeta_{\rm RL} = d\ln R_{\rm RL}/dM_{\rm d}$ and $\zeta_{\rm d} = d\ln R_{\rm d}/dM_{\rm d}$ at the moment of RLOF.

In essence, the Brussels code thresholds are based on the assumption that as the donor develops

a sufficiently deep convective envelope, its radial mass loss response becomes substantially negative (it expands in response to mass loss) and results in a runaway MT. StarTrack and SeBa rely on the assumption that if a donor expands faster than the Roche lobe during the MT (at the moment of RLOF), then the mass-transfer is self-amplifying and therefore unstable.

In Section 6.2 of this thesis we suggest improvements to these techniques based on the detailed simulations. Our simulations also show that the MT from the massive giants could become unstable not only when they develop a deep convective envelope, as initially thought, but also when they are very underdeveloped, of very low radii. We think that this additional instability region is caused by sufficiently flat regions of the entropy-mass profile, which are a feature of the underdeveloped massive giants.

New stability criteria are shown as a table that covers giants of various masses and radii at the onset of the RLOF. This result can be immediately used to supplant the existing criteria in the population synthesis codes, which will hopefully lead to substantially different merger rates of the double compact objects in the Galaxy.

1.4.2 Simulations of the Sco X-1 binary

Section 6.3 of this thesis revisits the problem of the evolution and formation of a well-known X-ray binary, Sco X-1. This binary contains a subgiant donor, which, if it was a single star, would never be able to reach this stage of evolution due to its extremely low mass. It is commonly assumed that this donor lost a significant fraction of its mass after it evolved to the subgiant stage. A multitude of binary simulations are conducted to pinpoint the possible evolutionary scenarios. As a result it is shown that the commonly used magnetic braking prescription based on the Skumanich law (angular velocity decreases with time as $t^{-0.5}$ or braking torque is proportional to the cube of angular velocity) and calibrated for MS stars is not sufficient to explain the detailed evolution of the Sco X-1 system, where the donor is a subgiant.

The new magnetic braking model, which takes into account increased mass loss rate from the subgiant, is suggested to explain the observations. The key feature of this model is that it takes into account the increased isotropic stellar wind from the subgiant, which is ignored in the commonly used models. Detailed simulations show that the new model works much better for Sco X-1 and possibly for a range of other systems, predicting approximately an order of magnitude higher mass accretion rate than the old model, which is consistent with the observations. However, it turns out that it is not possible to constrain the initial parameters of the binary system using just the known period, mass ratio and mass accretion rate. By considering the anticipated effective temperature of the donor, we could infer from our detailed simulations that the systems with donor ZAMS mass

$\gtrsim 1.6\ M_\odot$ are unlikely to be the progenitors of Sco X-1 because these progenitors produce hotter donors than observed.

1.4.3 Simulations of UCXBs

UCXBs are accreting systems with periods less than 1 hour, which qualifies them to contain a degenerate donor-companion. A group of three UCXBs – 4U 1626-67, 4U 0614+09, 4U 1916-053 – exhibit unusually high MT rates for a WD donor. We find that the existing theoretical models, gravitational radiation or tidal torque from a circumbinary disk, produce too low MT rates compared to the observations. Even replacing the WD with a slightly evolved MS donor with a He-rich core does not resolve the puzzle.

A naked He core that is formed in a CE event can be larger than a WD of the same mass. It is crucial that if prior to the CE the giant's core was non-degenerate, then during and immediately after the envelope ejection it experiences thermal readjustment. This leads to a fast MT onto a companion, with MT rates reaching $10^{-2} M_\odot \mathrm{yr}^{-1}$ at the peak. After the peak, the MT rates are smaller but still sufficient to keep the remnant out of thermal equilibrium for a while (Ivanova, 2011).

Hence, to understand high-MT UCXBs, we consider self-consistent He remnants. While previous studies considered evolution of initially homogeneous He stars, we formed them via simplified CE event by evolving a 5 $M_\odot$ star and stripping its hydrogen rich envelope. We considered cases before the start of the He core burning prior to CE, and after. The formed He remnants were evolved with different fast mass loss rates. The MT rates of UCXBs were then obtained assuming that these out-of-thermal-equilibrium remnants are placed in a binary with a neutron star companion to start the MT, and the binary evolution is driven by gravitational wave radiation only. The remnants formed with an initially higher mass loss rate drive a higher MT rate under gravitational wave radiation because they are further out of their thermal equilibrium – for the same remnant mass, they are more inflated and colder.

We find that this range of MT rates can be maintained if the donor is a remnant of an out-of-thermal-equilibrium naked core of a giant that was revealed in a very recent episode of a common envelope (CE) event.

We also find that the observed variations in He abundances in accretion disks of these mysterious fast-MT UCXBS do not necessarily require a WD donor. They can be explained by different duration of He core burning that took place in donor before or after the start of the MT. Depending on the post-CE orbital separation and on the mass and entropy of a He remnant, MT can start when the donor either:

- has not yet started He burning – this can be applicable to 4U 1916-053, where the observed accretion disk is nitrogen-rich;
- is going through He burning – in this case the disk will be C/O rich, as observed for 4U 1626-67 and 4U 0614+09;
- has already completed He burning. In this case we find that the donor is less likely to be inflated enough to provide the observed MT rates.

Chapter 2

Outer layers of giant stars

This Chapter describes the course of the entropy profile in unperturbed giant stars, energetics of the outer layers of their convective envelopes, and its connection to the phenomenon of recombination induced by mass loss. It is important to study these issues because the way they treated in the existing one-dimensional stellar codes affects the response of giant to mass loss and, eventually, the outcome of the Roche lobe overflow by a giant donor. We consider in detail the profile of specific entropy and heat transfer in the outer layers of the giant stars (applicable to both red giants (RG) and asymptotic giant branch (AGB) stars).

2.1 Convective envelope

As it is well-known, stars of giant type have outer convective envelopes of varying depth. Subgiants typically have shallow convective envelopes, as they become more developed their convective envelope deepens. Heat transfer in convective envelope is believed to take place through both convection and radiation transfer. Nowadays convection in detailed one dimensional stellar models is treated with the Mixing Length Theory of Convection (MLT), a simplified approach with free parameters that is based on the description of sinking and rising blobs of material (for details, refer to e.g. Cox & Giuli (1968)). Radiation transfer is usually described on the basis of photon diffusion approximation.

In MLT, the relative efficiency of heat transfer via two mechanisms (radiative and convective) can be characterized by the ratio of radiative and convective conductivities (see equation 7.12 in Kippenhahn & Weigert, 1994):

$$\frac{\sigma_{\rm rad}}{\sigma_{\rm conv}} = \frac{3acT^3}{c_P\rho^2\kappa l_{\rm m}^2}\sqrt{\frac{8H_P}{g\delta}}, \tag{2.1}$$

where $l_{\rm m}$ is the mixing length and H_P is pressure scale height. $\delta = -\left(\partial \ln\rho/\partial \ln T\right)_P$ is a quantity

that characterizes the thermal expansion properties of a medium. T is temperature, c_P is the heat capacity of the gas at constant pressure, ρ – density, κ – Rosseland mean opacity, g – magnitude of the effective external force field.

In the framework of MLT, convective efficiency directly depends on two free parameters – on how far a blob rises or sinks before it mixes with the environment (which can be seen in Equation 2.1 directly as $l_{\rm m}$), and on the linear size of convective blobs (used in Equation 2.1). These free parameters are best calibrated from observations and are not obtained from physical considerations.

Strictly speaking, in a convective zone the real logarithmic gradient of temperature with respect to pressure is denoted as ∇ and is defined as $\nabla = d\ln T/d\ln P$, is always higher than the local adiabatic logarithmic gradient of temperature with respect to pressure ($\nabla_{\rm ad} = \left[\partial \ln T/\partial \ln P\right]_s$), calculated at constant specific entropy s. In this sense one could call the convective regions "over-adiabatic", and this would mean that the logarithm of temperature falls off with the logarithm of pressure faster than it would in an adiabatically stratified star ($\nabla > \nabla_{\rm ad}$).

However, the degree of over-adiabaticity varies quite a bit along the convective zone. Deep inside the convective envelope the difference between the above-mentioned nablas is small compared to the nablas themselves. There, convective heat transfer is very efficient compared to the radiative heat transfer and therefore the actual temperature gradient almost matches the adiabatic gradient. The situation is, however, different close to the outer surface of the convective envelope. There the difference between the gradients is so large that it's comparable to the gradients themselves.

As mentioned in the Introduction, the treatment of the phenomenon of strongly over-adiabatic (also called superadiabatic) convection is considered to be the advantage of the detailed stellar models over the simple models, e.g. isentropic polytropic spheres of ideal gas (Hjellming & Webbink, 1987) or models with frozen specific entropy profile with respect to mass (Ge et al., 2010). In some cases the mass loss responses of the giants simulated with these two different strategies are drastically different. This hints that the structure of the superadiabatic layer at the top of convective envelopes defines the response of giant stars to certain modes of mass loss. For this reason we explore the structure of the superadiabatic layer in great detail in this section.

In this thesis, for the efficiency of convection, we adopt the relation between conductivities of convective and radiative heat transfer denoted by $\sigma_{\rm conv}/\sigma_{\rm rad} = 1/U$. Larger values of U correspond to less efficient convection and accordingly to a larger over-adiabaticity.

As mentioned above, in red giants, due to a combination of factors U increases in the vicinity of the stellar surface to the extent that the real gradient of temperature becomes substantially detached from the adiabatic gradient ($\nabla > \nabla_{\rm ad}$) (see Figure 2.1). This figure was obtained by evolving a 5 $M_\odot$ red giant of solar metallicity in `MESA` until its radius reaches 70 $R_\odot$ for the first time.

The radiative gradient $\nabla_{\rm rad}$ is also shown in this Figure. Radiative gradient is the logarithmic derivative of temperature with respect to pressure, which is required to transfer the total heat solely by radiative diffusion.

Let us consider in detail what affects the behavior of the efficiency of the convection $1/U$ and of the overadiabaticity $\nabla - \nabla_{\rm ad}$. In the region where both quantities have simultaneous slow-down in their almost monotonic decrease towards the center (see Figure 2.2), hydrogen and helium change their degree of ionization (see Figure 2.3). The degrees of ionization affect U and $\nabla - \nabla_{\rm ad}$ by strongly changing the heat capacity of the medium c_P and the Rosseland mean opacity (see Figure 2.4).

For the range of densities and temperatures in the envelope, the heat capacity of a partially ionized gas is higher than that of both neutral and fully ionized gases (ionization consumes a part of the heat transferred to the gas without increasing the kinetic energy of its molecules). The three major jumps in c_P, from highest to lowest temperature, are associated with the following recombinations:

- double ionized helium $\rightarrow$ single ionized helium;
- single ionized helium $\rightarrow$ neutral helium;
- ionized hydrogen $\rightarrow$ neutral hydrogen.

Let us discuss the reason for two overadiabaticity plateaus in the area of interest marked with the solid opacity curve in Figure 2.4. In this area, partial recombination of elements affects the convective efficiency mainly through c_P, because opacity does not vary much there. Due to the change in monotonicity of c_P at half-ionization, recombination of either hydrogen or helium impedes the growth of overadiabaticity towards the surface while the ionization fraction is between 100% and 50%, but when the ionization fraction is lower than 50% the recombination, on the other hand, accelerates the growth of overadiabaticity (see Equation 2.1 and Figure 2.4). Because of this, the areas where the growth of overadiabaticity is impeded (plateaus) are shifted with respect to the maxima of c_P. The initial stage of partial recombination of hydrogen is able to completely suppress the growth of overadiabaticity towards stellar surface in the envelope; the initial recombination of helium also impedes it to a large extent. The shape of the superadiabatic layer, hence, is substantially affected by the recombination of hydrogen and helium.

At the final stages of hydrogen recombination, the opacity falls sharply by a few orders of magnitude. As a result, the radiative gradient, which is proportional to opacity, falls below the adiabatic gradient (Figure 2.1). We call this region the "surface radiative zone". It takes place outside the temperature range shown in Figures 2.2-2.4, at $\lg T < 3.73$. The spatial size of the

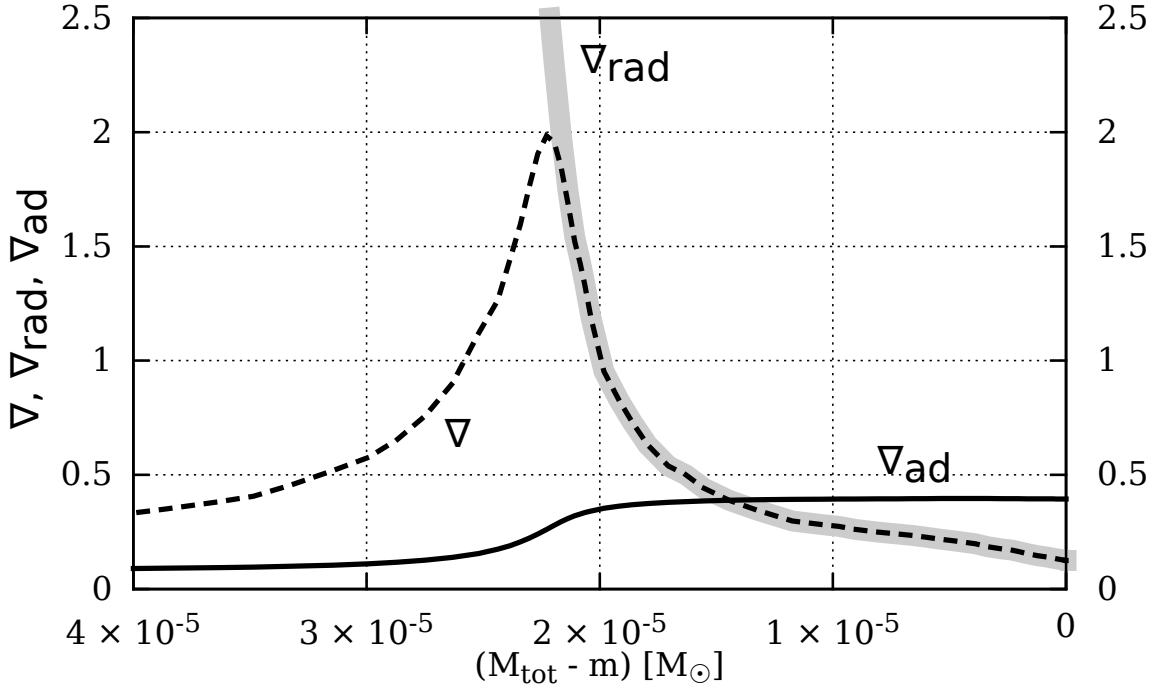

Figure 2.1: Interplay of temperature gradients ∇, $\nabla_{\rm rad}$ and $\nabla_{\rm ad}$ in the vicinity of the hydrogen ionization boundary of a 70 $R_\odot$, 5 $M_\odot$ red giant. The radiative gradient is shown with a solid gray line, adiabatic gradient – solid black line, actual gradient – dashed line; m is the mass coordinate and $M_{\rm tot}$ is the total giant's mass. Near the surface, where $\nabla_{\rm rad} < \nabla_{\rm ad}$, this giant has a surface radiative zone. A superadiabatic zone is where $\nabla_{\rm rad} > \nabla_{\rm ad}$ but convection is not efficient enough, and the actual gradient ∇ exceeds $\nabla_{\rm ad}$ by a value comparable to the gradient itself.

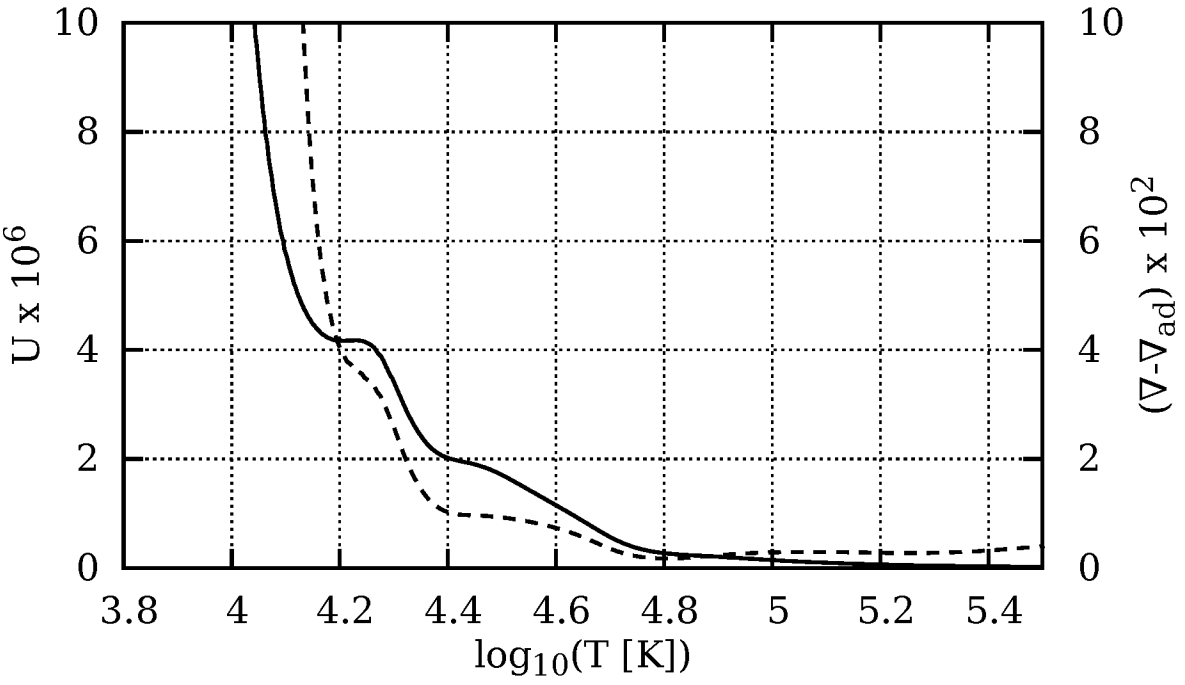

Figure 2.2: Overadiabaticity $\nabla - \nabla_{\rm ad}$ (solid) and U (dashed) in the outer layers of a 5 $M_\odot$ and 50 $R_\odot$ red giant.

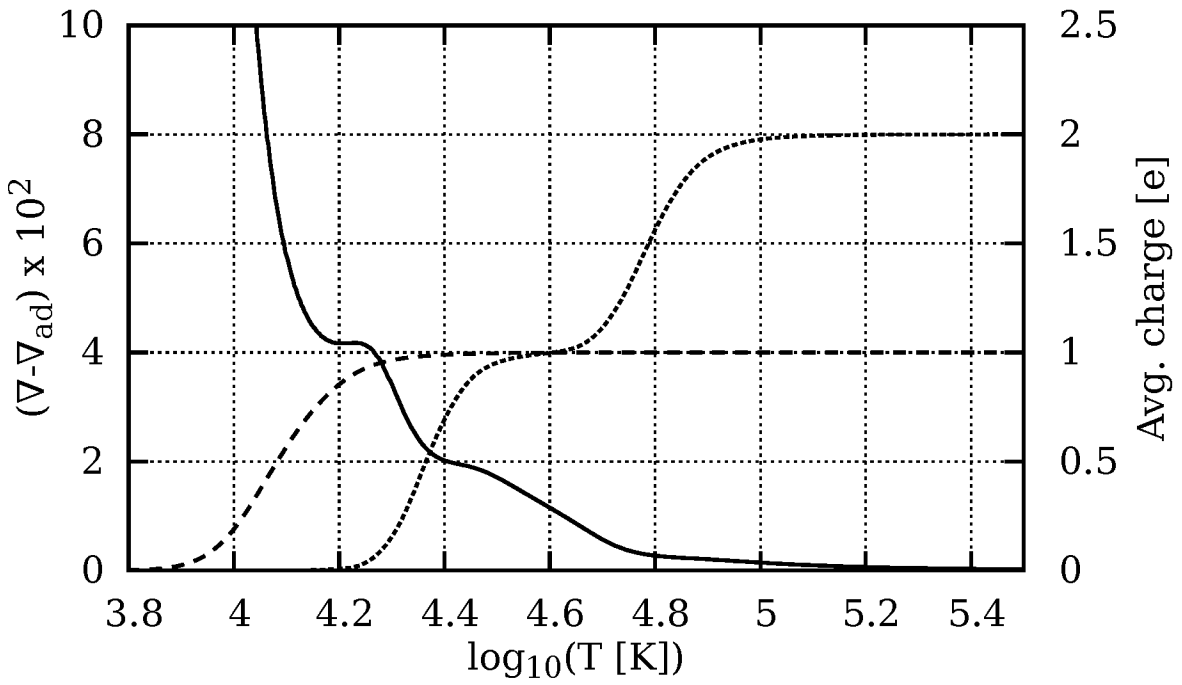

Figure 2.3: Overadiabaticity $\nabla - \nabla_{\rm ad}$ (solid) and average charges of helium (dotted) and hydrogen (dashed) in the outer layers of a 5 $M_\odot$ and 50 $R_\odot$ red giant. Note that behavior of overadiabaticity and partial ionization zones is strongly coupled.

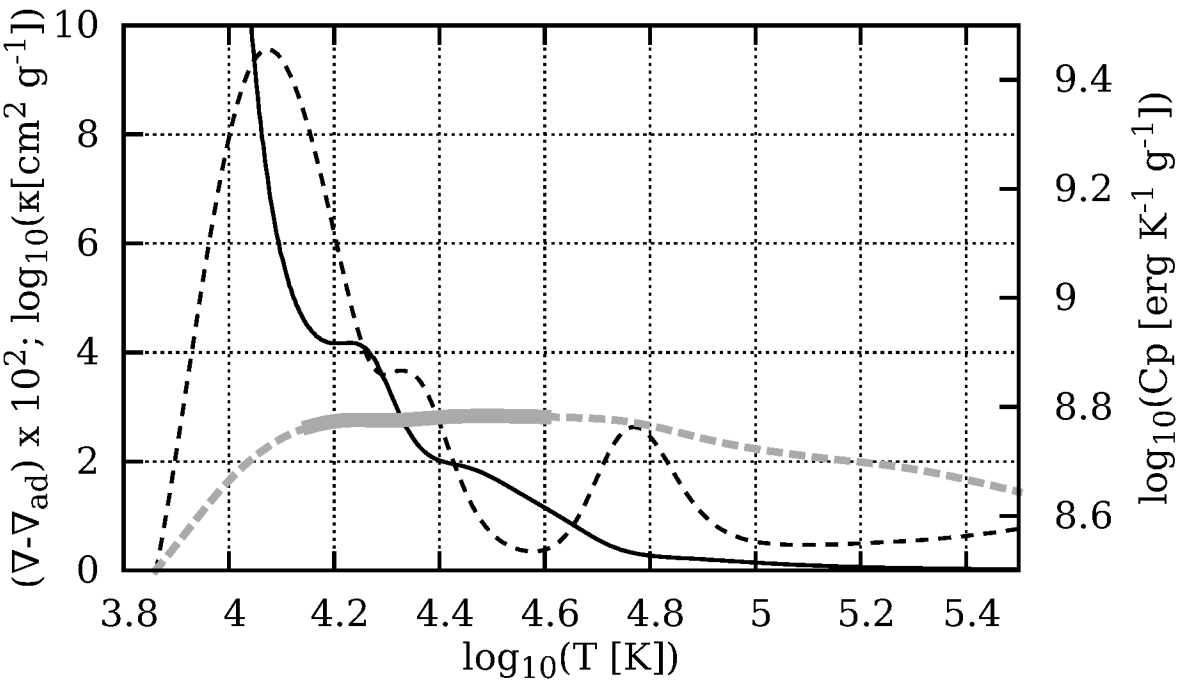

Figure 2.4: Overadiabaticity $\nabla - \nabla_{\rm ad}$ (solid black), Rosseland mean opacity κ (gray solid in the area of interest and gray dashed elsewhere) and specific heat capacity at constant pressure c_P (dashed black) in the outer layers of a 5 $M_\odot$ and 50 $R_\odot$ red giant.

surface radiative zone is of the order of the mixing length. Hence it is plausible that convective blobs overshoot the boundary between the superadiabatic layer and the surface radiative zone (see also Kuhfuss, 1986).

2.2 Mass of superadiabatic layers in convective donors

For analysis of superadiabatic layers and radiative zones, we introduce the quantity $m_{\rm sad}$, the mass of these layers. We measure $m_{\rm sad}$ from the stellar surface to the point near the start of the entropy drop, m_0. Since the convection is never fully adiabatic, the entropy profile in the envelope is not flat, and there is no sharp transition between the entropy plateau and the entropy drop (see Figure 2.5). For consistency between stars of different masses, we therefore choose to define m_0 as the point where entropy is

$$S(m_0) = S_{\rm min} + 0.9(S_{\rm conv} - S_{\rm min}). \tag{2.2}$$

Here $S_{\rm min}$ is the local *minimum* of entropy in the outer layer of the star and $S_{\rm conv}$ is the (maximum) value of entropy in the convective envelope.

Clearly, it can be seen in Figure 2.6 that the mass of this shell varies between giants of different masses and radii. From the behavior of the envelope's simplified analytical solution (see e.g. Figure 10.2 in Kippenhahn & Weigert, 1994), we expect that overadiabaticity of convective envelopes becomes substantial at about the same pressure, to an order of magnitude. Indeed, in realistic stellar models for stars of different masses, the pressure at the bottom of the superadiabatic layer does not vary much from $P(m_0) \approx 10^5 {\rm dyn/cm^2}$. In this case, we can estimate $m_{\rm sad}$ by simply considering a pressure drop. The equation of hydrostatic equilibrium over the superadiabatic layer and radiative zone is

$$\frac{dP}{dm_{\rm sad}} = \frac{G(m_0 + m_{\rm sad}(r))}{4\pi r^4}. \tag{2.3}$$

As the pressure at the top of the superadiabatic layer (photospheric pressure) is much less than at its bottom, we find

$$m_{\rm sad}(R) \approx \frac{4\pi R^4 P_0}{G M_{\rm tot}} \approx 1.1 \times 10^{-10} M_\odot \frac{(R/R_\odot)^4}{(M_{\rm tot}/M_\odot)}. \tag{2.4}$$

Indeed, as illustrated in Figure 2.6, stars with convective envelopes at *any* evolutionary stage have $m_{\rm sad}$ which can be found using this relation. This approximation has only limited, though still very good, applicability to more massive stars, where $m_{\rm sad}$ is comparable to the total mass of the star's envelope (we note also that it is well known that in massive stars almost the entire convective envelope could be superadiabatic).

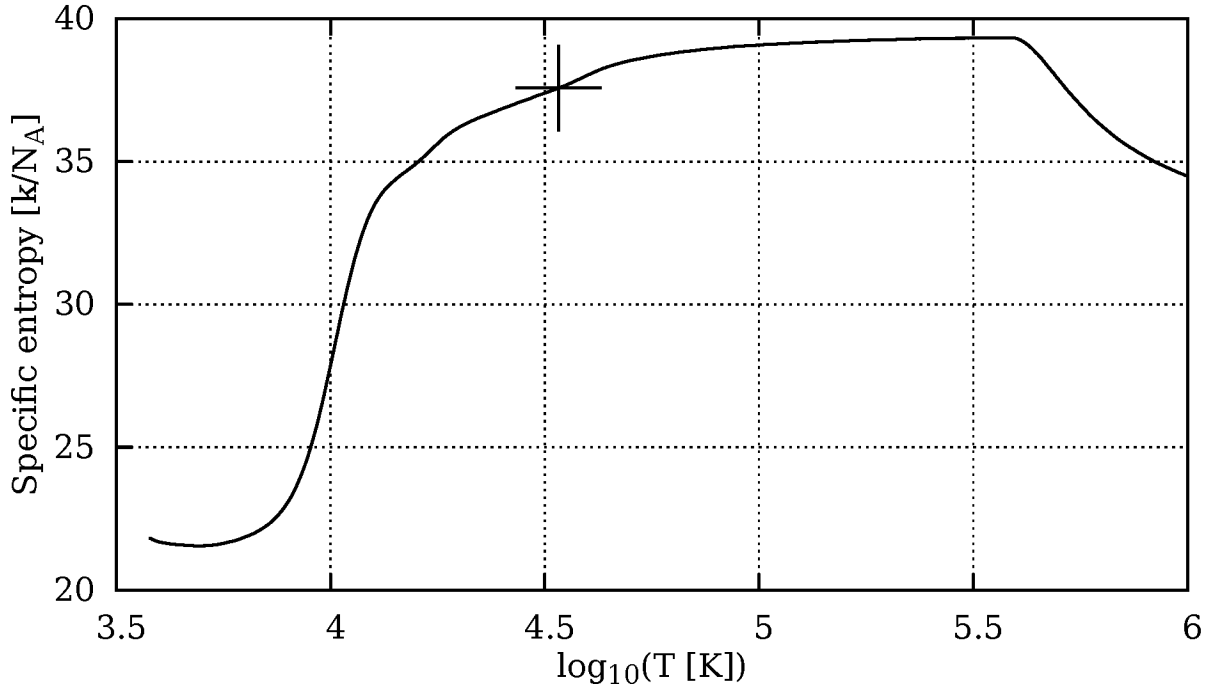

Figure 2.5: Specific entropy in the outer layers of a 14.6 $M_\odot$ and 500 $R_\odot$ red giant, the cross denotes the bottom of the superadiabatic layer calculated as per Equation 2.2.

It is important to note that this is the mass of the superadiabatic layer and surface radiative zone in a star *unperturbed* by ML. Mass loss affects both our assumptions about the pressure drop (as the star is not in hydrostatic equilibrium anymore), and the entropy profile.

We see from the preceding analysis that while the mass of the superadiabatic layer is relatively small in low-mass giants, it grows for more massive stars, increasing substantially as the star is evolving and expanding. Stellar models that have a constant entropy profile are therefore not justified, as the error in the case of massive stars could be enormous. We will also show in §2.3 that the mass of the superadiabatic layer helps estimate its rate of energy generation for each ML rate, and how to find the timesteps that provide valid results for the radial response on the ML.

2.3 Energetics of the superadiabatic layer

We saw a hint in § 2.1 that the formation of a superadiabatic layer is to a certain extent governed by recombination, hence this layer might be energetically important for obtaining the correct ML response. Energetically, recombination enters the structure equations through the gravitational energy term, which is the last term in the energy generation equation and is defined as:

$$\epsilon_{\rm g} = -T \left(\frac{\partial s}{\partial t} \right)_m \tag{2.5}$$

The $\epsilon_{\rm g}$ term can be found directly from the Equation 2.5, using only one temporal derivative of the entropy which is derived from the EOS. Alternatively, $\epsilon_{\rm g}$ can be calculated by subtracting two terms that depend on temporal derivatives of thermodynamic quantities, for example:

$$\epsilon_{\rm g} = -T c_P \left[(1 - \nabla_{\rm ad} \chi_T) \frac{1}{T} \left(\frac{\partial T}{\partial t} \right)_m - \nabla_{\rm ad} \chi_\rho \frac{1}{\rho} \left(\frac{\partial \rho}{\partial t} \right)_m \right]. \tag{2.6}$$

Here, $\chi_\rho = \left(\partial \ln P / \partial \ln \rho \right)_T$ and $\chi_T = \left(\partial \ln P / \partial \ln T \right)_\rho$. When mass is removed from the surface of a red giant, the partial ionization zones of hydrogen and helium discussed in § 2.1 move to areas that were previously fully ionized, deeper in the star. Recombination of these previously ionized areas leads to the release of recombination energy. One can estimate that the recombination energy of pure hydrogen is $W \sim 10^{13}$ erg g^{-1}. For the ML rate of $\dot{M} = 10^{-2}$ $M_\odot$ yr^{-1} the recombination energy release should be of the order of $W\dot{M} \sim 6 \times 10^{36}$ erg s^{-1}.

Let us consider now this mass loss on an example of a 5.0 $M_\odot$ and 50 $R_\odot$ red giant. Using our Equation 2.4 for the mass of the superadiabatic layer, we find that its total mass is about 10^{-4} $M_\odot$, though the part where hydrogen recombination energy is released is usually only a fraction of it, about 10^{-5} $M_\odot$ (see also Figure 2.7). The contribution of this recombination component alone in $\epsilon_{\rm g}$ in such a superadiabatic layer is expected to be of the order of 3×10^8 erg g^{-1} s^{-1}.

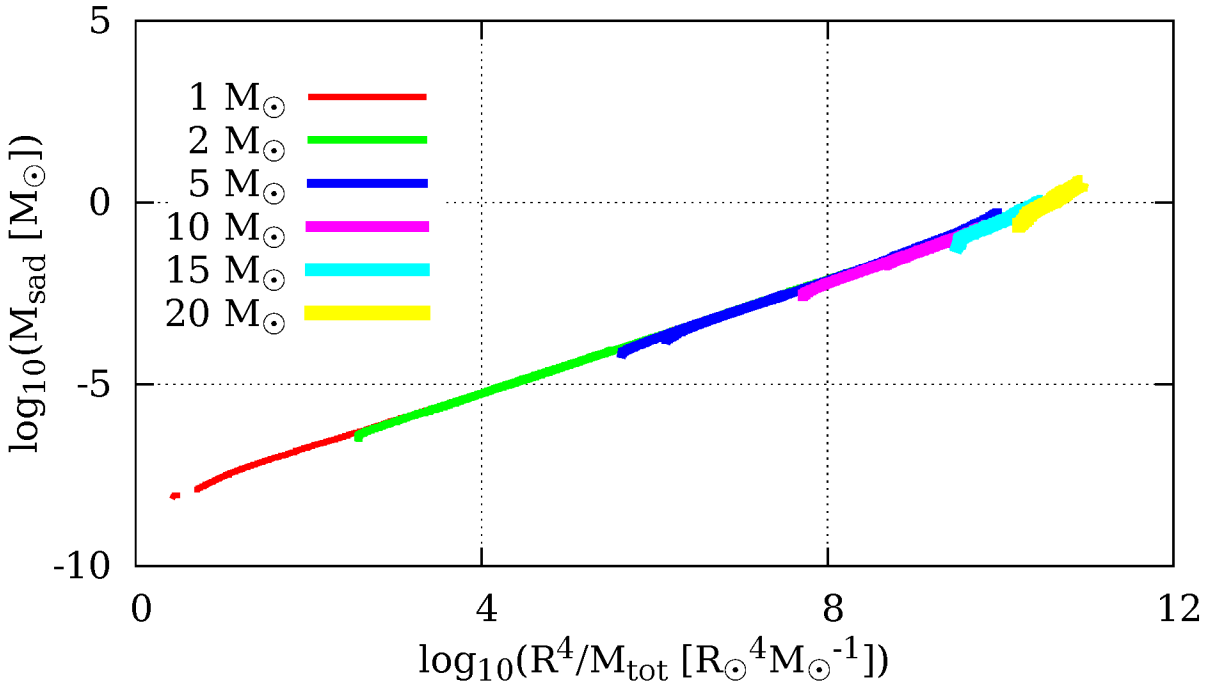

Figure 2.6: Total mass of superadiabatic layers and surface radiative zones in stars with convective envelopes of different masses and ages.

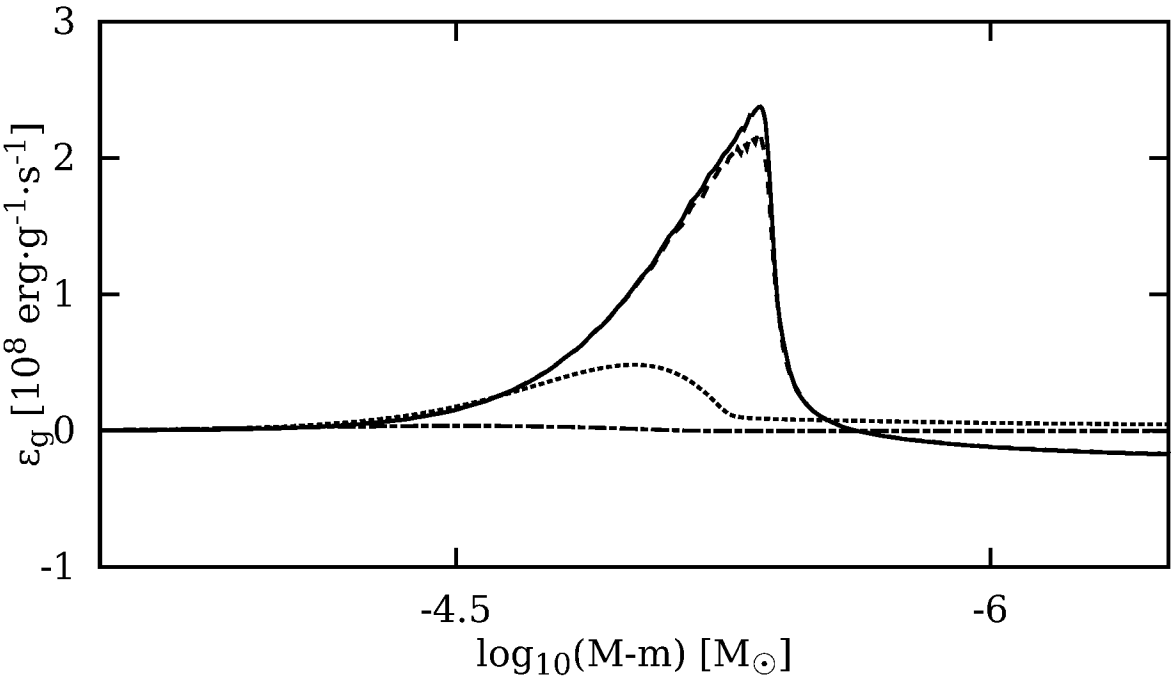

Figure 2.7: Values of ϵ_g in the same 5.0 $M_\odot$, 50 $R_\odot$ red giant subjected to the same constant ML rate of 10^{-2} $M_\odot$ yr^{-1} shown at the same moment of time: 0.1 *yr* since the start of ML. Dash-dotted, dotted, dashed and solid lines correspond to constant timesteps 10^{-1}, 10^{-3}, 10^{-5} *yr* and 10^{-6} *yr* respectively. The observed discrepancy in the values of ϵ_g is due to the inaccuracy of the first order formula used to calculate Lagrangian derivatives using the Equation 2.5 (see Section 2.3 for details).

We have checked what values of ϵ_g we obtain *in practice*, using the detailed stellar code of our choice, MESA. First, we tested the method where the entropy derivative is found using Equation 2.5, as it takes into account composition changes, unlike the second method that uses Equation 2.6. However, this method suffers from an inexact calculation of entropy from the EOS. After performing numerical tests, we found it to not be suitable for the small timesteps necessary for fast mass loss calculations: as the timesteps become smaller, the errors in the entropy values become comparable to their Lagrangian differences between subsequent timesteps. The two-component formula 2.6 always uses structural variables. Entropy, used in the formula 2.5, is never a structural variable: it is always derived from the structural variables through the tabulated EOS. In addition, composition artifacts can play a role in entropy fluctuations.

Second, we tested the method where the entropy derivative is found using Equation 2.6, see Figure 2.7. We found that the expected physically reasonable level of ϵ_g is only reached when the timestep is below $\approx 10^{-3}$ yr. We relate it to the inaccuracy of the first-order numerical differentiation formulae used in practice to calculate the right-hand side of (2.6) at larger timesteps. Note that the right-hand side of (2.6) is effectively proportional to the Lagrangian derivative of entropy[1], which is calculated indirectly through the corresponding derivatives of T and ρ. Therefore, the error in calculation of ϵ_g with formula (2.6) is, as expected, the most significant in the superadiabatic layer and surface radiative zone, because the second Lagrangian derivative of entropy is the highest there[2].

We do not suggest a complete formal procedure to calculate the errors in calculation of ϵ_g. Instead, we resort to a plain comparison of results obtained with various timestep selection approaches. For example, the comparison for one of our models (Figure 2.7) shows that if it loses not more than $\approx 1/1000$ of its initial m_{sad} in one timestep, then the calculation of ϵ_g in the superadiabatic layer is affected only marginally. Removing mass in such small timesteps is, however, quite resource intensive. We can foresee that the outlined numerical problem with a recombination zone that moves too fast in mass can be eventually resolved using a technique similar to the one used for calculating thin shell burning as in Eggleton (1967, 1973). However, for the purpose of the studies presented in this thesis, we can afford to use a numerically intensive way.

[1] If one neglects composition changes.

[2] We'd also like to mention that quite recently a new scheme for the calculation of ϵ_g was implemented in MESA, that follows a mixed Lagrangian-Eulerian approach. We performed a preliminary testing of this scheme on mass-losing red giants. Unfortunately, this new scheme is not suitable for our simulations yet because of severe numerical artifacts that it introduces under certain conditions. These artifacts have to be carefully studied and eliminated before we can consider incorporating this new scheme into our simulations. Because of this, we only discuss the standard purely Lagrangian scheme for the calculation of ϵ_g in this thesis.

In Section 6.1 we will show how inaccurate calculations of ϵ_g affect the radial response to the mass loss. While the numerical problems that we described in this section are native only to the code we use, when fast mass loss rate calculations are performed with another code, the numerically obtained ϵ_g has to be tested against its expected value that can be found using the method described in this section.

In this chapter we were focused on the thermal phenomena that take place during mass loss and affect mass loss response. In the next chapter we will describe the hydrodynamical effects that govern the response of the one-dimensional models of giant stars.

Chapter 3

Mass loss response of a single star

This chapter is dedicated to the problem of response on the mass loss of a single giant from the point of view of the Heyney-type one-dimensional hydrodynamical treatment. It describes the approaches used to model mass loss and challenges faced by modern one-dimensional stellar codes related to the hydrodynamical terms in the stellar equations. We also briefly review the applicability of the Mixing Length theory of convection, which is commonly used in one-dimensional codes, to the strongly non-hydrostatic giants.

3.1 Early approaches

The response of the giant donor itself to mass loss is a separate issue from the overall stability of MT, which, due to its complexity, requires realistic detailed stellar simulations. There are, however, a couple of alternative approaches to this question, which were historically used. The general idea of these approaches was to consider a one-dimensional model of the giant, neglect the hydrodynamical effects and set explicitly the distribution of specific entropy versus mass in the model. The historically first approach used the entropy-mass profile of a polytropic gaseous sphere, a so-called "composite polytrope" (Hjellming & Webbink, 1987), also see Soberman et al. (1997). Another approach, recently explored in the work of Ge et al. (2010), employed a realistic entropy-mass profile obtained from a detailed one-dimensional stellar model and assumed that this profile rests unchanged (frozen) during the mass loss. The response of the donor to mass loss was then calculated by changing the mass boundary condition to simulate the mass loss from its surface and tracking the dependence between the radius of the gaseous sphere and its total mass. This allowed one to obtain the commonly used logarithmic derivative of donor's radius with respect to its mass, $\zeta_{\rm donor} = \partial \log R_{\rm donor} / \log M_{\rm donor}$, first introduced by Hjellming & Webbink (1987).

3.2 Understanding hydrostatic adiabatic ML

In this Section we discuss how the adiabatic approach may affect the solution. We start with standard stellar equations, where the energy generation equation is

$$\left[\frac{\partial L}{\partial m}\right]_t = \epsilon_{\rm nuc}(\boldsymbol{X},P,T) - \epsilon_\nu(\boldsymbol{X},P,T) - \frac{1}{T}\left[\frac{\partial s}{\partial t}\right]_m , \tag{3.1}$$

where t is time, L is the luminosity, P is the pressure, T is the temperature, $\boldsymbol{X}$ is composition vector and s is the specific entropy that itself is a function of P, T and $\boldsymbol{X}$ through an adopted equation of state

$$s(m) = F(P,T,\boldsymbol{X}), \tag{3.2}$$

$\epsilon_{\rm nuc}(\boldsymbol{X},P,T)$ is nuclear energy generation and $\epsilon_\nu(\boldsymbol{X},P,T)$ is neutrino losses. The third term is often called gravity energy, $\epsilon_{\rm g}$.

The energy transport equation is

$$\left[\frac{\partial T}{\partial m}\right]_t = -\frac{Gm}{4\pi r^4}\frac{T}{P}\nabla(P,T,\rho,L,m,\boldsymbol{X},r) \ . \tag{3.3}$$

Here ρ is the density and $\nabla = d\ln T/d\ln P$ is the actual temperature gradient.

The hydrostatic adiabatic approach uses for its initial conditions a stellar model obtained with a regular stellar evolutionary code and governed by the stellar structure equations and the gray atmosphere boundary condition (there are more stellar structure equations, but we only provide the crucial ones). The adiabatic study then assumes that once ML begins, the entropy profile $s(m)$ is fixed (*"frozen"*).

It can be seen from the chain of Equations 3.1, 3.2 and 3.3 that $s(m)$ depends on $\left[\partial s/\partial t\right]_m$. The assumption of the entropy profile to be frozen throughout the mass-loss sequence sets the quantities $\left[\partial s/\partial t\right]_m = 0$ and $s(m) = s_0(m)$.

To set the quantities $s(m)$ and $\left[\partial s/\partial t\right]_m$ arbitrarily and independently one must, in general, abandon at least either Equation (3.3) or Equation (3.1).

For example, in the paper of Ge et al. (2010), where adiabatic approach is used, the authors abandon Equation (3.1). This abandoned equation asserts, essentially, the conservation of energy. The MLT relations (used in Equation 3.3) are assumed to still hold. Indeed, the conservation of energy in this approach doesn't hold, which can be easily seen by examining a stellar profile in the paper of Ge et al. (2010). In a model with a frozen entropy profile, according to the conservation of energy, the luminosity must be constant with respect to mass in any region where there is no nuclear

energy generation, or neutrino losses. However, in their Figure 2 the initial luminosity profile is not flat in such regions.

On the other hand, we may also imagine models with fixed entropy profiles that leave Equation (3.1) in force and break Equation (3.3) instead. In this way, we would obtain models with fixed entropy profiles that are generally non-compliant with MLT. These models should correspond to the case of very fast ML, for which the entropy profile is almost fixed, the MLT condition does not hold due to its limited domain of applicability (see App. 3.3.5), but Equation (3.1) is still in force.

We anticipate that consideration of the latter MLT-non-compliant models might shed light on the area of extremely fast ML, but for the purpose of this thesis we limit ourselves to "completely non-adiabatic" models, where the entropy profile is re-calculated at each step.

3.3 Modern approaches

There currently exists a number of one-dimensional detailed stellar codes which can be used to calculate the response of a star to mass loss. However, these codes are originally meant for stellar evolutionary calculations and hence don't always work well at short timescales (e.g., thermal or dynamical timescale). They either do not include any acceleration terms in their stellar structure equations, or include just one of them. In addition, these codes usually use the MLT, which in certain cases becomes inapplicable to the giants that experience mass loss. Let's consider these issues in detail.

All acceleration terms become important when the local Lagrangian (radial) acceleration in the stellar material becomes comparable to the local effective gravitational acceleration. We introduce the acceleration term Q, which is the ratio of the local Lagrangian acceleration to the local gravitational acceleration:

$$Q = \left[\frac{\partial^2 r}{\partial t^2}\right]_m \Big/ \frac{Gm}{r^2} \tag{3.4}$$

m is enclosed mass, r is distance to center at a certain spherical shell of the model.

3.3.1 Pressure acceleration term

A standard way to introduce hydrodynamical treatment into a stellar code is to use a truncated Navier-Stokes equation in spherical coordinates as the pressure equation. This equation will then contain a term, proportional to the local Lagrangian acceleration, which we will call for brevity *pressure acceleration term*:

$$\left[\frac{\partial P}{\partial m}\right]_t = -\frac{Gm}{4\pi r^4}(1+Q), \tag{3.5}$$

where P is pressure.

3.3.2 Transport acceleration term

Transport acceleration term appears in the transport (also called temperature) equation:

$$\left[\frac{\partial T}{\partial m}\right]_t = -\frac{Gm}{4\pi r^4}(1+Q)\frac{T}{P}\nabla, \tag{3.6}$$

In a purely radiative zone the transport acceleration term will vanish because there ∇ is proportional to $(1+Q)^{-1}$.

3.3.3 MLT acceleration term

Within the frames of the MLT, convective mixing stops when the local gravitational acceleration becomes equal with the opposite sign to the local Lagrangian acceleration. Indeed, convective conductivity is proportional to their sum (which is sometimes called *effective gravitational acceleration*). Despite this fact, in today's implementations of MLT *effective gravitational acceleration* in convective conductivity is supplanted with just local gravitational acceleration. This substitution might work well in cases when $Q \ll 1$ (most evolutionary calculations), but if a star experiences a high rate of ML, this is no longer the case.

3.3.4 Grey atmosphere boundary condition acceleration term

This term is analogous to the pressure acceleration term, but it appears in the gray atmosphere boundary condition:

$$P_{\rm bc} = \frac{2}{3}\frac{GM}{R^2\kappa}(1+Q) \tag{3.7}$$

where M, R, and P_{bc} are mass, radius and pressure at the outer shell of a stellar model, corresponding to the optical depth of 2/3, κ is Rosseland mean opacity there.

Modern evolutionary stellar codes use only the pressure acceleration term and neglect the transport acceleration term, the MLT acceleration term and the gray atmosphere boundary condition acceleration term discussed below. As a part of this thesis we modified the `MESA` stellar evolution code to take into account all the acceleration terms listed here (see App A).

3.3.5 MLT applicability

Modern one-dimensional stellar evolution codes are unable to treat convective heat transfer in a physically realistic way because of large computational complexity involved in the description of

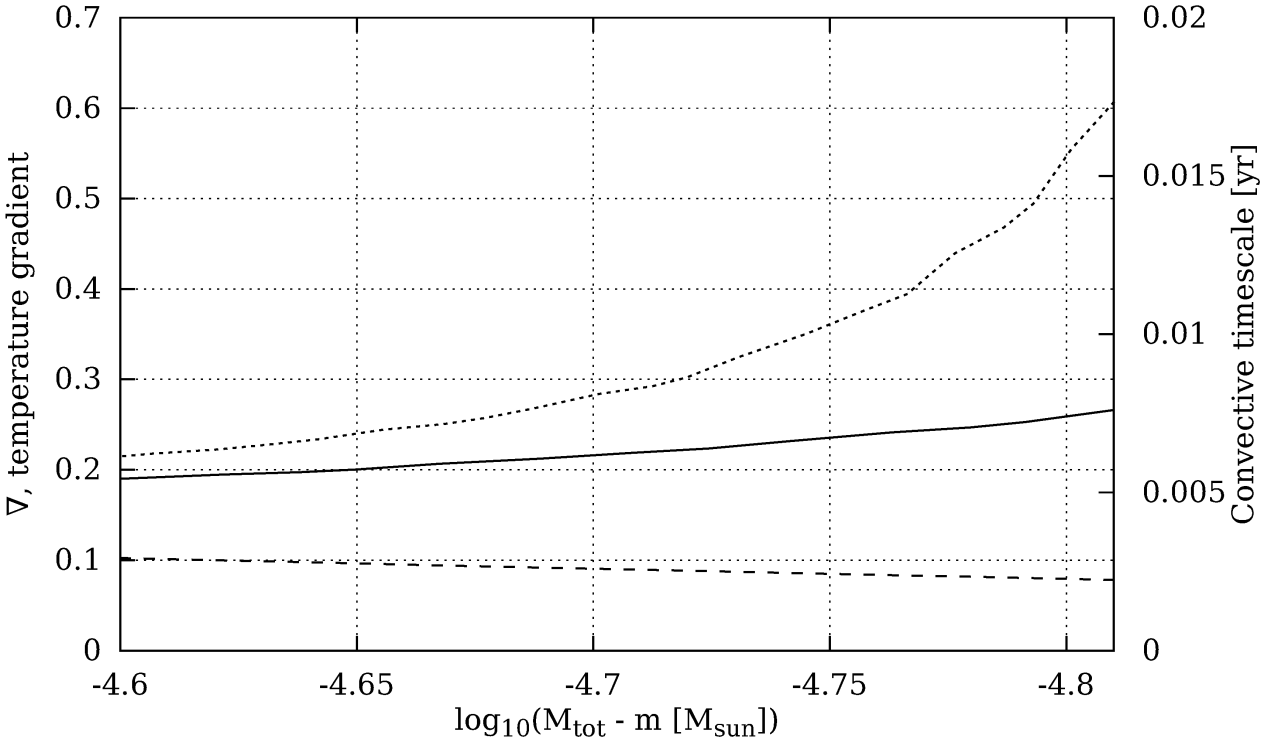

Figure 3.1: Temperature gradients in a 5.0 $M_\odot$ and 50 $R_\odot$ red giant subjected to the ML of 10^{-2} $M_\odot$ yr^{-1}. Solid curve is for the onset of the ML, short-dashed curve is 10^{-3} *yr* later. Long-dashed curve corresponds to the local convective timescale $2H_p/v_{\rm conv}$, where H_p is pressure scale height. Within a substantial part of superadiabatic layer temperature gradient rises by $\approx 50\%$ in comparison to its value at the onset of the ML. This change takes place on $1/2$ of the local convective timescale.

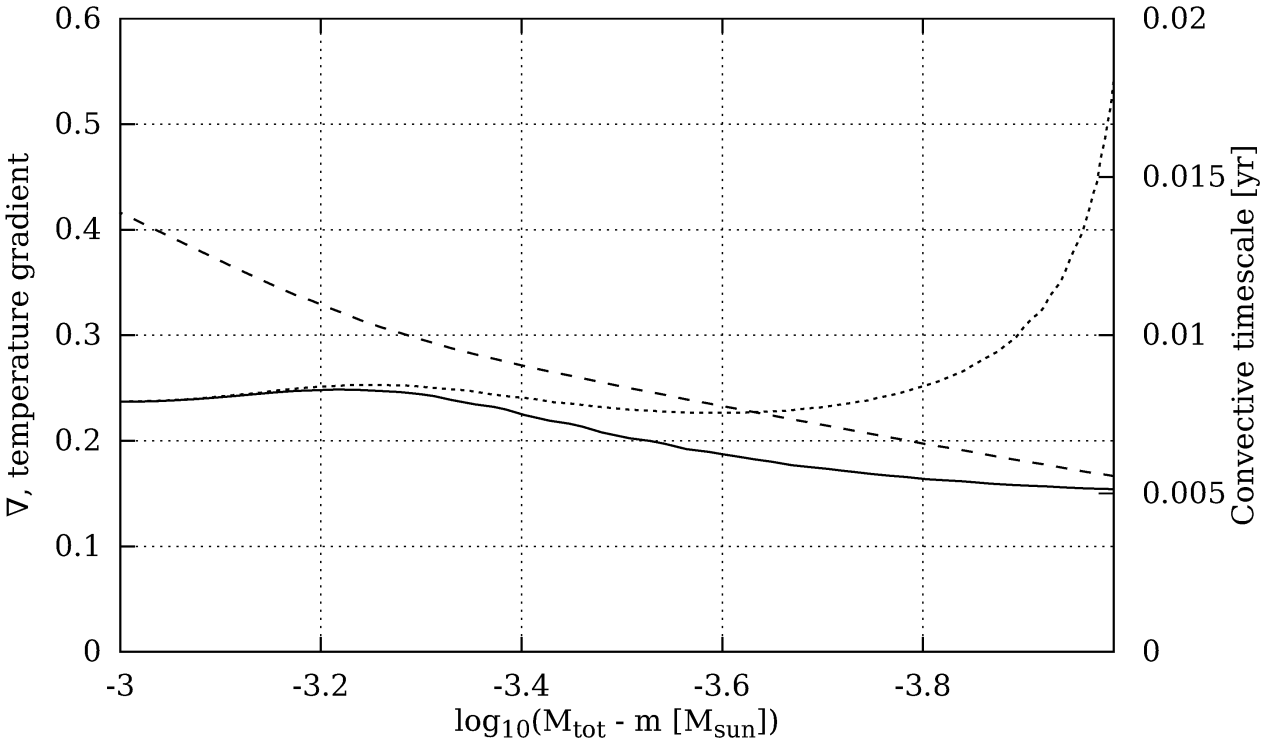

Figure 3.2: The same giant as in Figure 3.1 at the same moments of time, but subjected to the ML of 10^{-1} $M_\odot$ yr^{-1}. Layers just below the superadiabatic layer are shown. Temperature gradient decreases by $\approx 10-50\%$ during just $1/5$ of convective timescale. Mass of the layer where this change takes place is ≈ 10 times greater than the initial mass of the whole superadiabatic layer!

convective flows within a medium. To avoid this difficulty the majority of the codes use various types of the MLT. MLT is a set of analytical simplifications that allows one to obtain an approximate value of the full gradient of temperature ∇ in a one-dimensional medium subjected to external uniform gravitational field. The approximation at least requires that the temporal and spatial scales of changes in ∇ be less than $l_{\rm m}/v_{\rm conv}$ and $l_{\rm m}$ respectively where $l_{\rm m}$ is "mixing length" and $v_{\rm conv}$ is "convective velocity" – two related free parameters of the theory.

Both temporal and spatial conditions hold for the most part of the stellar evolution and for the most part of the stellar interior. However, for red giants spatial condition does not hold within the superadiabatic layer (see, e.g., Houdek et al. (1999)) and, as our calculations show (see Figure 3.1 and 3.2), temporal condition does not hold in the case of sufficiently fast ML. Indeed, the temperature gradient ∇ is drawn for two moments of time separated by time of the order of the local convective timescale and the values of the gradient differ by more than 50% within a substantial part of the superadiabatic layer.

3.4 Early response problem

There currently does not exist a comprehensive and self-consistent hydrodynamical simulation to treat the three-dimensional problem of MT in a binary. Even when three-dimensional simulations eventually become self-consistent, they would likely resolve only the question of the initial stability of the RLOF (RLOF), but not the long-term MT, which will remain a prerogative of one-dimensional stellar codes in the foreseeable future.

In a standard one-dimensional ML model, the stellar codes use the regular set of structure equations, but adopting the boundary condition that the total mass decreases with time. This boundary condition is an unavoidable reduction of the three-dimensional picture of the ML to one dimension. In other words, $\dot{M}$ represents our best understanding of the stream that is formed in the vicinity of L_1 and that carries the donor's material away from the donor. In this Section we examine the reaction of giants to the ML in one-dimensional stellar codes, explaining in particular the nature of the feature observed in the previous MT calculations.

3.4.1 Understanding the initial contraction of a red giant upon the instantaneous ML in 1D stellar codes

Passy et al. (2012) studied the response to mass loss with `MESA`. They compared the response of the red giants of several different masses to a set of fixed mass loss rates. Among other things, two opposite responses to ML were found: hydrostatic stellar models initially expanded in response to

ML, while models with hydrodynamical terms, on the opposite, initially shrunk. This behavior was observed for all considered fixed MT rates and giants.

In neither of these two approaches the ML experiment is close to what would happen in Nature, where MT never starts abruptly at some fixed high MT rate. However, it is important to understand what causes the dramatic difference between these two approaches.

Passy et al. (2012) provided the following explanation: *"...some energy that is stored in gravitational form in the hydrostatic models is actually in a kinetic form [in hydrodynamic models], leading to the star contracting instead of expanding"*, although how exactly the transformation of gravitational energy into kinetic leads to contraction was not explained.

Instead of the energy argument, we argue that the main reason for the radial response is due to the material being consumed from the surface of a red giant with linear velocity $\dot{m}/(4\pi r^2\rho)$, where r is the radius of a red giant, and ρ is the surface density. Note that this term intrinsically decreases the radius.

To validate that this term is dominant, we need to consider the involved stellar equations. For a star in hydrostatic equilibrium, $Q = 0$ (see Equation 3.5). In Figure 3.3 we illustrate how significant the acceleration term can be in the superadiabatic layer and surface radiative zone of a red giant at high ML rates.

Let's now consider the initial response after some (small compared to the dynamical timescale) time τ to ML $\dot{m} < 0$ of a red giant of initial mass M_0 without artificial viscosity or any other effects that would alter Equation (3.5).

If $P(m,t)$ is a smooth and bounded function and $m(t)$ and $r(t)$ are continuous and bounded, then

$$\lim_{t\to 0} a(m,t) = 4\pi R_0^2 \left[\frac{\partial P}{\partial m}\right]_{t=0} + \frac{GM_0}{R_0^2}, \tag{3.8}$$

where $a(m,t)$ is acceleration of the medium at mass coordinate m at the moment of time t. By integrating Equation (3.8), we get for the velocity v at the surface[1]:

$$v(t) = v_0 + \left(4\pi R_0^2 \left[\frac{\partial P}{\partial m}\right]_{t=0} + \frac{GM_0}{R_0^2}\right) t + o(t), \tag{3.9}$$

where $v_0 = v(0)$. To obtain the complete radial response, this velocity must be combined with the material consumption velocity, which is equal to

$$v_c(t) = \frac{\dot{m}}{4\pi\rho_0 R_0^2} + o(t), \tag{3.10}$$

[1]Here we use the "little-o" notation for the vicinity of zero. A brief definition of this notation is $f(t) = o(g(t)) \Leftrightarrow \lim_{t\to 0} f(t)/g(t) = 0$ (for details see, e.g., Kevorkian & Cole, 1985).

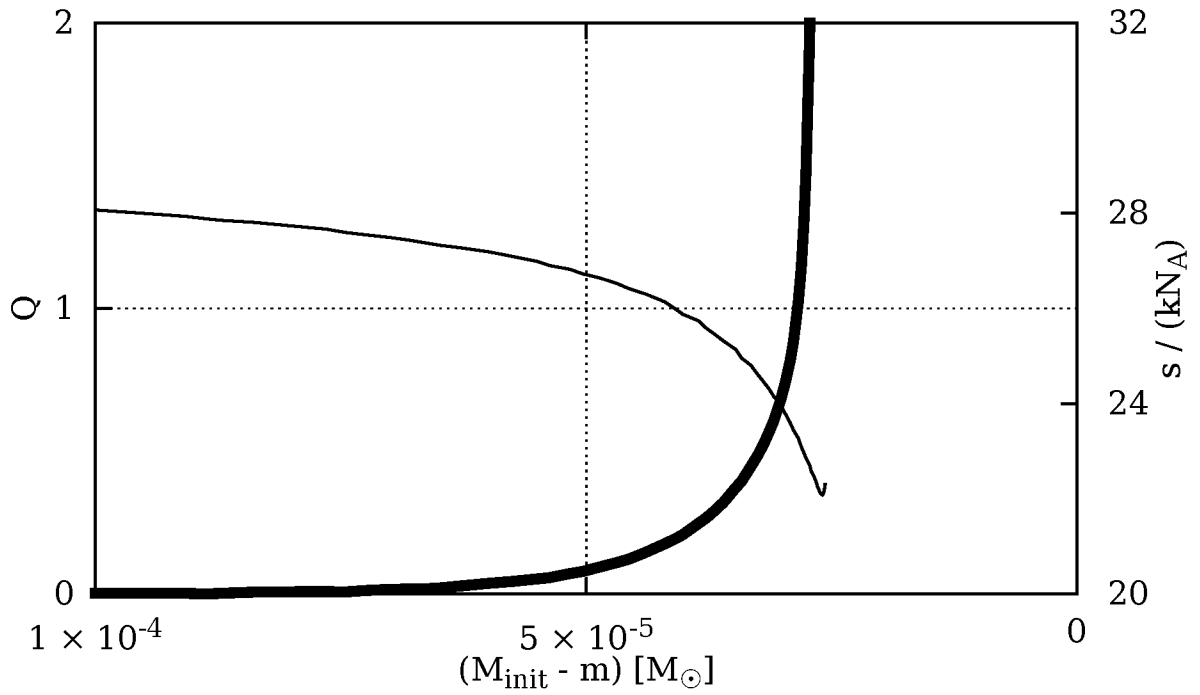

Figure 3.3: A red giant of initial mass 5.0 $M_\odot$ and radius 50 $R_\odot$ subjected to ML of 0.1 $M_\odot$ yr^{-1}. The entropy profile is shown with a thin line, the ratio Q of acceleration and gravitational terms is shown with a thick line. It is clear that Q is far from being negligible compared to unity within the superadiabatic layer and surface radiative zone.

where ρ_0 is the initial surface density of the star. Their sum must in turn be integrated in time. Thus, the complete radial response of a red giant to ML is given by:

$$\begin{aligned} R(t) &= R_0 + \left(\frac{\dot{m}}{4\pi R_0^2 \rho_0} + v_0 \right) t \\ &+ \left(2\pi R_0^2 \left[\frac{\partial P}{\partial m} \right]_{t=0} + \frac{GM_0}{2R_0^2} \right) t^2 + o(t^2) \end{aligned} \tag{3.11}$$

If the original star was in hydrostatic equilibrium, then $v_0 = 0$, and, according to Equation (3.8), the term, proportional to t^2 in Equation (3.11), would be equal to $o(1)t^2 = o(t^2)$, and hence is vanishing. The total radial response reduces to

$$R(t) = R_0 + \frac{\dot{m}}{4\pi R_0^2 \rho_0} t + o(t) \tag{3.12}$$

This result may be directly compared to the decrease in the radius of a stellar model that occurs during the first timestep after the start of the ML, divided by this timestep. This comparison helps to understand the role of the adopted outer boundary condition (see Section 6.1). We conclude that the contraction observed in the simulations of Passy et al. (2012) is neither a numerical error, nor a conversion of gravitational energy to kinetic, but a natural consequence of a finite pace of expansion of the one-dimensional envelope that was forced to experience a fast ML. At this point we finish our discussion of the behavior of single stars when subjected to mass loss. In the next chapter we will consider the treatment of self-consistent MT in a binary system from a giant donor to a compact accretor.

Chapter 4

Mass transfer in binaries

A self-consistent treatment of MT from donor to a compact accretor combines the response of the donor to mass loss, studied in the previous chapters, and the calculation of MT rate between the components. The calculation of MT rate is accomplished by using an improved explicit MT scheme which is described in this chapter.

4.1 Rate of the MT

We describe below an optically thick model for MT that we have adopted for our studies of hydrodynamic response to rapid MT in binaries.

We follow a conventional way to calculate the MT rate by integrating the mass flow over a "nozzle" cross-section that is taken on a plane perpendicular to the line connecting the centers of the two stars and passing through the L_1 point:

$$\dot{m} = \int_{\text{nozzle}} v_{\text{flow}} \rho_{\text{flow}} dS \tag{4.1}$$

Here v_{flow} is the velocity that the stream has within the nozzle, and ρ_{flow} is the density that the stream has at the same position. We note that the use of the nozzle cross-section only in the L_1 neighborhood implies that only the L_1 MT rate can be found, and the rate of ML via L_2/L_3 overflow cannot be calculated.

Furthermore, any scheme that finds an ML boundary condition for stellar one-dimensional codes adopts some set of simplifications to find the distribution of the stream's density and velocity throughout the nozzle, as well as the nozzle geometry. The flow is considered to be steady, which permits the use of the Bernoulli theorem along the streamlines. The standard assumptions are that the nozzle at L_1 coincides with the sonic surface of the flow (Lubow & Shu, 1976), and that

initial velocities are negligible at the origin of the streamlines. We adopt the same assumptions.

The MT rate then becomes dependent only on these assumptions:

- the adopted *geometry* of the donor and the nozzle;
- the *streamlines* – this assumption, coupled with the adopted evolution of the specific entropy along the streamlines, allows relating the donor's thermodynamical properties to those of the flow crossing the nozzle.

4.1.1 RLOF formalism and geometry of the problem

The fundamental simplifying assumption that governs the whole Roche lobe formalism is *volume correspondence*. More precisely, this is the assumption that thermodynamical parameters (pressure, density, composition, etc.) at a certain radius r in a one-dimensional stellar model are the same in three-dimensional space at a Roche equipotential whose enclosed volume is $(4/3)\pi r^3$. Whenever one-dimensional stellar evolution is considered in terms of RLOF formalism, the volume correspondence assumption is automatically used. Note that when a donor experiences a substantial RLOF this volume correspondence for thermodynamical parameters can be applied only far from the L_1 point, where the donor's material is almost at rest. The Roche lobe volume radius $R_{\rm L}$ is usually found using one of two well-known approximations (Paczyński, 1971; Eggleton, 1983). The area of the nozzle is then usually approximated by the area of an ellipsoid by taking the second-order term in the Roche potential expansion within the sonic surface near the L_1 point.

An additional simplifying assumption is applied when integrating the ML rate over the potential region between the Roche lobe potential Φ_L and the photospheric Roche potential $\Phi_{\rm phot}$ (note, that $\Phi_{\rm phot} > \Phi_L$). At this point, to avoid volume integrations, it is a common approach to implicitly break the volume correspondence assumption and replace it with the *pressure correspondence* assumption.

The pressure correspondence assumption asserts that the thermodynamical parameters (temperature, density and composition) at a point A in three-dimensional space are the same as at a point B in the one-dimensional model, provided that the pressure at the point A in three-dimensional space is the same as the pressure at point B in the one-dimensional model. If one applies this pressure correspondence far from the L_1 point and assumes, in addition, that

$$\mathbf{a} \cdot \nabla\Phi \ll |\nabla\Phi|^2 , \tag{4.2}$$

where $\mathbf{a}$ is the local Lagrangian acceleration, and Φ is the local Roche potential, then it becomes possible to replace the integral over radius with the integral over pressure. The benefit of the pres-

sure correspondence assumption is that one can avoid the painful calculation of the differential $d(\Phi(r))$, which requires volume integrations. We note that once a star is not in hydrostatic equilibrium, $Q \ll 1$ does not hold (see Section 3.4.1), and condition 4.2 cannot be satisfied. Hence, pressure correspondence should not be used for rapid mass loss.

RLOF during the evolution of a mass-losing red giant can however be very substantial. When an equipotential surface is far from the Roche lobe surface, the expansions obtained in the vicinity of the L_1 point break down since the expansions are truncated after the quadratic term. Higher-order terms are no longer negligible. Instead, we conduct the realistic Roche lobe integrations which employ the Runge-Kutta-Fehlberg integrator and the damped Newton-Raphson solver to obtain all geometrical parameters. These integrations have been conducted for 275001 mass ratios from 0.06 to 19.145 with an increment of $7 \cdot 10^{-5}$. For each mass ratio we calculate the nozzle areas and volume radii for 200 equipotentials lying between the L_1 potential and the L_2/L_3 potential. In addition to the use of a more precise relation between the star's volume and the Roche lobe volume, volume correspondence that is necessary for rapid mass loss and a non-simplified nozzle shape, this also allows us to track whether the donor overfills the L_2/L_3 equipotential during the MT.

4.1.2 Streamlines

For a rapid MT rate, an "optically thick" approximation is usually used (see Paczyński & Sienkiewicz, 1972; Savonije, 1978; Kolb & Ritter, 1990; Ge et al., 2010, and many others). The flow of matter towards L_1 in this approximation is adiabatic and streamlines go along the equipotential surfaces of the Roche potential. The photosphere corresponds to a Roche equipotential which lies outside the Roche lobe. Close to the L_1 point, the photosphere turns into the outer boundary of the optically thick flow which flows across the sonic surface along the Roche equipotential surfaces with the local adiabatic speed of sound (Kolb & Ritter, 1990).

To find the stream's density and sonic velocity at L_1, one is required to adopt the evolution of the specific entropy in the flow along the streamlines. Often the flow is taken to be polytropic – that is, the flow preserves a constant value of P/ρ^{γ} along a streamline, where γ is the adiabatic exponent. In certain cases, the polytropic stratification of the donor itself is adopted. Note that the stream's velocity, while locally sonic, is not constant across the nozzle. The flow also does not need to be isentropic if the donor is not isentropic – the streamlines can originate at different initial equipotentials.

We also assume that a flow is adiabatic. An adiabatic flow is not, of course, entirely polytropic due to, for example, recombination, that occurs as gas flows towards the sonic surface. It means that γ varies along an adiabat. For this reason, we employ a realistic equation of state taken from

MESA, that among other effects takes into account the ionization of elements in the mix and the radiative component of pressure. For test purposes, we also can consider the flow to be polytropic. We have verified that for those models that are provided as examples in this thesis, the effect of the adopted equations of state on mass flux does not exceed $\pm 4\%$.

An appealing modification to the standard optically thick model was discussed in Eggleton (2006). In that model, the streamlines can cross equipotentials. However, this comes at a cost of other simplifications: the flow has to have the same constant velocity over its cross-section. In addition, the model also adopts that the fluid is both isentropic and polytropic and the donor is in hydrostatic equilibrium, hence all the streamlines have the same value of their Bernoulli integral at their origin. Since we study the case of a donor's reaction where the donor is not in hydrostatic equilibrium, and we expect that the superadiabatic layer may affect the results, and the streamlines can originate in layers with different entropy, we cannot employ this method.

We also should mention that in our scheme we do not use any approximation for an optically thin MT stream that originates from above the photosphere. The primary reason for this is that we have not yet developed a model that would allow one to combine both optically thick and optically thin ML schemes when a donor overfills its Roche lobe. Kolb & Ritter (1990) have suggested that during RLOF, the total MT rate can be found by a summation of the MT of an optically thick stream, calculated as a function of the current RLOF, plus the maximum MT rate obtainable for an optically thin photospheric flow in the case of RL underflow, which is at the instant when a star exactly fills its Roche lobe. We are not confident whether this method would estimate correctly the contribution of an isothermal photospheric outflow in the case of a non-negligible RLOF, considering that both the geometrical cross-section and the potential of the nozzle for the isothermal flow (located now around the nozzle for the adiabatic flow) are changed substantially from those in the L_1 neighborhood. Hence, we do not use this approach.

The degree to which optically thin MT affects the behavior of stars before their photospheres overfill the Roche lobe depends on the rate of their intrinsic evolutionary expansion when their photospheres approach the Roche lobe. Relatively massive giants (5 $M_\odot$ and up), cross the interval of radii for which the optically thin MT is dominant in a short time thanks to their fast expansion. Hence, the fraction of the envelope they lose via optically thin transfer is small. On the other hand, less massive giants expand slowly and can lose a lot of mass through atmospheric ML before the optically thick mechanism kicks in. This decreases the mass ratio at the onset of RLOF and improves stability. We observed an extreme case, where with the Ritter (1988) prescription, a 0.89 $M_\odot$ giant could never actually overfill a $100R_\odot$ Roche lobe, and steadily lost the whole convective envelope via optically thin mechanism reaching an optically thin MT rate of $10^{-3.6}$ $M_\odot \mathrm{yr}^{-1}$! We therefore

Table 4.1: Simplifications eliminated in the optically thick MT schemes

Reference	GS	PC	PD	PS
Paczyński & Sienkiewicz (1972)				
Savonije (1978)				
Kolb & Ritter (1990)			•	
Ge et al. (2010)		○	•	
This work	•	•	•	•

GS – geometrical simplification for the nozzle, PC – pressure correspondence, PD – polytropic stratification of the donor, PS – along the streamlines P/ρ^{γ} is constant. Empty circle – simplified potential is adopted the effect of which is equivalent to the PC assumption.

warn the reader that the mode of MT from low-mass giants might be sensitive to the very uncertain model of optically thin MT.

We summarize the simplifications eliminated in the existing optically thick schemes and in our case in Table 4.1. For the technical details on the implementation of the method in `MESA` and use see Appendix A. Given that the model of self-consistent MT from a giant donor to a compact accretor is described, one must develop a criterion to judge whether or not a common envelope event takes place in the system, i.e. whether or not the MT in a given model is stable or runaway. In the next chapter I focus on these criteria.

Chapter 5

The onset of common envelope

This chapter describes the criteria of the onset of common envelope in a given binary system. I also introduce a simple method, which makes it possible to apply these criteria to binary systems without detailed binary simulations.

5.1 Currently used criteria for the stability of mass transfer

The MT rate and stability depend crucially on the response of the donor's radius to the ML compared to the response of its Roche lobe radius to the same ML (for foundations, see Webbink, 1985). The governing feature that shaped studies of MT in binary systems with giant donors was the wide acceptance of the theory that a convective donor would intrinsically expand as a reaction to ML. In the framework of this theory, the immediate response of a star to ML takes place on a dynamical timescale (to restore its hydrostatic equilibrium) – this assumes that no thermal effects can take place, and it was hence called an adiabatic response. It is characterized by the quantity known as the mass-radius exponent $\zeta_{\rm ad}$

$$\zeta_{\rm ad} \equiv \left(\frac{\partial \log R}{\partial \log M} \right)_{\rm ad} . \tag{5.1}$$

With polytropic models (including also composite and condensed polytropes), it was found that a convective donor would have $\zeta_{\rm ad} < 0$ (Paczynski, 1965; Hjellming & Webbink, 1987). The presence of a non-convective core increases the value of $\zeta_{\rm ad}$, which becomes positive once the relative mass of the core is more than 20% of the star's total mass (Hjellming & Webbink, 1987).

It is commonly assumed that MT is dynamically stable only if a donor remains within its Roche lobe, or when $\zeta_{\rm L} \leq \zeta_{\rm ad}$, where $\zeta_{\rm L}$ is the mass-radius exponent for the Roche lobe reaction to the MT.

Dependence of $\zeta_{\rm L}$ on the mass ratio, q, can be calculated analytically for a fixed fraction of accreted matter (accretion efficiency) if one uses an analytical approximation for the Roche lobe radius, e.g. the Eggleton approximation (Eggleton, 1983). This way for conservative MT it can be found that $\zeta_{\rm L}$ crosses zero when the mass ratio is $q_{\rm crit} \approx 0.788$, and is positive for a larger mass ratio. For completely non-conservative isotropic re-emission this critical mass ratio is ≈ 1.2 (Soberman et al., 1997).

The first episode of MT in a system in which both components were formed simultaneously happens when the initially more massive component reaches the end of the MS, expands and overfills its Roche lobe, hence the mass ratio (donor to accretor) at the onset of the first episode of MT is believed to be more than unity, for this reason the first episode of MT is commonly considered dynamically unstable.

Hjellming & Webbink (1987) showed that taking into account the core improves stability, however for all stars with relative mass of the core $\lesssim 0.45$ of the total stellar mass, the first episode of conservative MT will be unstable. Later, the results based on polytropic models were re-evaluated in the studies of the detailed adiabatic stellar models by Ge et al. (2010). At the same time, detailed codes that traced MT in binaries up to thermal timescale MT, found that the critical mass ratio can be up to 1.1 (e.g. Han et al., 2002).

5.2 Advanced definitions

A common envelope (CE) event is typically defined as two stars sharing the same envelope (for a review, see Ivanova et al., 2013a). The vagueness of this definition reflects the incompleteness and complexity of this area of research. The concept of CE originally appeared as the mechanism to explain the loss of angular momentum and dramatic shrinking of many binary systems Paczynski (1976). There is a continuum of processes ranging from a steady MT through the L_1 point from one component to another and a CE event. The boundary between a CE and a MT is a matter of convention. Based on the aforementioned origin of the term, one could say that during a CE event the system does not behave as a pair of relatively compact objects anymore as is the case in steady MT, instead its dynamical parameters, such as period, evolve substantially on its own crossing timescale and therefore lose physical sense. Mathematically this definition can be written in a number of ways, of which the most straightforward is to consider that the ratio of one of the main dynamical parameters (separation or period) to its temporal derivative is comparable with the crossing timescale (period) of the binary system, e.g.:

$$\frac{P}{\dot{P}} \sim P \tag{5.2}$$

It is a well-known fact that the logarithmic derivatives of the main dynamical parameters in a binary system are all of the same order, so for the purpose of mathematical definition it does not matter which parameter to use.

One can see an important consequence of the definition given by Equation 5.2 if it is rewritten in terms of angular velocity:

$$\frac{\Omega}{\dot{\Omega}} \sim \frac{1}{\Omega}, \tag{5.3}$$

or equivalently

$$\frac{\dot{\Omega}}{\Omega^2} \sim 1. \tag{5.4}$$

The left-hand side of the Equation 5.4 is essentially the ratio of the Euler term of the fictitious force in the co-rotating system of reference, to its centrifugal term (see Section 5.3 for details). In other words, CE happens when the Euler term becomes comparable to the centrifugal term. At the same time the Roche potential approximation, used to describe steady MT from one component to another, breaks down because in this approximation the Euler term of fictitious force is neglected in comparison to the centrifugal term. We see that the following three definitions of CE given so far are equivalent to each other: a) one of the main dynamical parameters substantially changes over one period; b) the Euler term becomes significant compared to the centrifugal term; and c) the Roche potential approximation breaks down. I'd like to show that another definition could be introduced, which is in most cases of giant donors equivalent to these three.

The outer Lagrangian point of the donor, which, depending on the mass ratio can be either called L_2 or L_3, is not usually considered in the models of MT from one component to another. However, in the case of giants, extreme degrees of Roche lobe (in the other words, L_1) overflow can also lead to the overflow of the outer Lagrangian point of the donor, leading to an additional stream of matter flowing through the L_2/L_3 nozzle, which opens in this case.

Our simulations show that in most giants (except the very expanded giants with rarefied envelopes) it occurs approximately at the same time as the criteria for CE discussed in this Section are fulfilled. The demonstration of this can be seen in Section 6.2.

To conclude, the criteria of CE listed in this section all give comparable results. In Section 6.2 I'll show that these criteria are all incompatible with the old simplified criterion, which is based on the comparison of logarithmic exponents, ζ's.

5.3 Euler term

In a non-inertial co-rotating frame fictitious forces appear. It is a common mechanical approach to separate the fictitious force into three components or terms: centrifugal term, Coriolis term and

Euler term. The Roche lobe approximation is based on an approximate potential of gravitational and centrifugal forces in a non-inertial rotating frame, Coriolis and Euler terms are omitted. The Euler term is, as I'll show, small in most cases compared to the centrifugal term. The Coriolis term is significant in mass transferring binaries (Lubow & Shu, 1975b), but its non-potential nature makes it impossible to take it into account in the Roche approximation.

Let's look at the applicability limit of a model that does not include the Euler term. By expressing the Euler term as a fraction of the centrifugal term, we'll see the conditions under which it can be neglected in comparison with the centrifugal term.

$$E = C\frac{d\Omega/dt \times \mathbf{r}}{\Omega \times (\Omega \times \mathbf{r})} \tag{5.5}$$

Here E stands for Euler term, C – centrifugal term, Ω is the angular velocity, t is time and r is radius vector in the co-rotating frame in relation to the center of mass of the system. In flat case, we see that $E/C \sim \frac{d\Omega/dt}{\Omega^2}$, which means that the Euler term becomes important when the angular velocity of the system changes appreciably over one rotation period. We'll see that in many realistic stellar systems involving giant donors it happens approximately at the same time when the donor overfills the potential of its outer Lagrangian point, L_2 or L_3, depending on the mass ratio. This means that at the onset of L_2/L_3 overflow the conventional L_1 MT schemes fail not only because an additional MT nozzle appears at the outer side of the donor, but also because the system as a whole loses its dynamical stability, i.e. begins to evolve substantially on its own dynamical timescale. This signifies a common envelope event.

5.4 Advanced understanding of the stability of the Roche lobe MT

The conventional way to determine stability of a binary system to the MT is to compare the initial responses of the donor radius and the Roche lobe radius to the mass loss. As was mentioned in Section 1, such analysis, if it does not involve actual MT calculations in a binary, is usually done by comparing their mass-radius exponents at the onset of RLOF. In order to do this, the adiabatic radial response of the donor $\zeta_{\rm ad}$ is found from one of the existing approximations (composite polytropes, condensed polytropes, or even simply adopting that for convective donors $\zeta_{\rm ad} = 0$). This adiabatic radial response is used instead of the realistic stellar response.

However, we'd like to stress, that even if the realistic stellar response is obtained, there is no reason to assume that if $\zeta < \zeta_{\rm L}$ at the start of the MT, and a donor's relative RLOF *initially* increases, the instability will necessarily occur. Instead of considering just the moment of RLOF, we can trace

binary evolution through the MT in detail and determine if the instability eventually takes place, or not. The determination of MT instability in a binary system, while the donor is overflowing its RL, requires an alternative (to a simple comparison of the initial ζs) criterion to delineate when the MT proceeds stably, and when it results in a common envelope.

To understand the characteristic behavior of the systems during MT, we performed a large set of simulations with donors of several initial masses ($1, 2, 5, 10, 15, 30, 50 M_{\odot}$). We considered several values of radii for each donor, taken within the range where the donors have non-negligible, greater than approximately $0.3 M_{\rm donor}$ outer convective envelopes, both at the red giant and asymptotic giant branches. We conducted simulations for several initial mass ratios (between 0.9 and 3.5). We assume that a companion is compact, where the compactness only means that we neglect any possible accretor's RLOF.

Further, for these detailed MT sequences we adopted fully conservative MT; any non-conservation in the MT would lead to a relative increase of MT stability. Most of our binary systems were evolved using our modifications: obtaining proper $\epsilon_{\rm g}$, and our method to find MT rates and boundary conditions.

Even for systems with larger initial q than that dictated by the conventional adiabatic stability criterion, the MT rate after RLOF smoothly increases, approaches a peak value and then decreases; the peak MT rate is usually much less than the dynamical MT rate. With the increase of q, the peak MT rate increases. We define as q_{L23} the smallest initial mass ratio for which the binary experiences L_2/L_3-overflow during the MT (see Figure 5.1). We refer to this overflow as L_2/L_3-overflow, as during the MT, the mass ratio can reverse, and L_3-overflow becomes L_2-overflow. This q_{L23} is a function of both the initial mass ratio and the donor's radius. For many initial donor radii, in binary systems with $q = q_{L23}$, the mass of the donor encompassed between the donor's Roche lobe and its L_2/L_3 lobe is very small and the ML rate when L_2/L_3-overflow is approached is far from dynamical. Numerically, we are capable of evolving such systems with $q > q_{L23}$ through the L_2/L_3-overflow, and many of them will not even approach the dynamical MT rate (see Figure 5.1). We, however, do not trust the MT rates obtained in this regime because our stream model only considers the L_1-nozzle.

We adopt therefore that for as long as L_2/L_3-overflow of the donor does not happen, the system is stable. In part, this is confirmed by the three-dimensional hydrodynamical simulations, in which a common envelope is always associated with a severe, albeit very short in duration, L_2/L_3 overflow of the donor (Nandez et al., 2014). Note however, that we consider this to be a *minimum* stability criterion, as the MT in a binary system may remain stable even after the donor's L_2/L_3-overflow takes place, as, e.g., SS 433 shows (e.g., Bowler, 2010; Perez & Blundell, 2010).

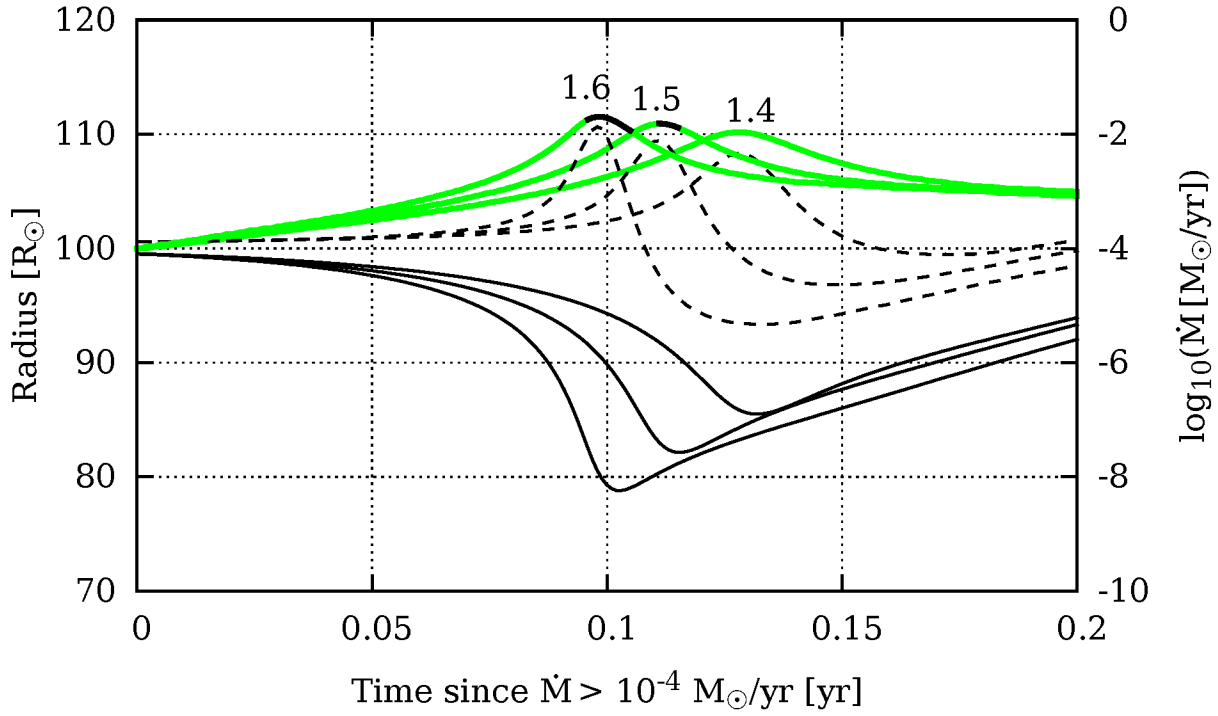

Figure 5.1: The MT rate (green solid lines), and the evolution of the donor's radius (dashed lines) and the donor's Roche lobe radius (solid black lines), shown for the mass ratio with which the binary system does not start L_2/L_3-overflow during the MT (q = 1.4), and when L_2/L_3 takes place (q = 1.5, 1.6). The period of L_2/L_3 overflow is indicated with solid black color on the MT curves. The donor is a $1M_\odot$ and $100R_\odot$ giant at the onset of the MT. The rate of a dynamical MT for this system is $\sim 10M_\odot$ yr^{-1}.

We also compared the surface-averaged effective gravitational acceleration over the L_2/L_3 lobe with the spherically symmetric acceleration that would be expected at its volume radius and found that the difference reaches about 13%.

In addition to the L_2/L_3-overflow condition, we trace whether the binary orbit is changing rapidly. For the latter condition, we adopt that if $|\dot{a}/a|T < 1/50$, the orbit is not changing rapidly, where T is the binary period. Rapid evolution of orbital parameters can invalidate the entire Roche formalism. For example, if angular velocity changes substantially over one period, the Euler term of the fictitious force, which is ignored in the Roche formalism along with the Coriolis term, becomes comparable to the centrifugal term. Note, however, that in Nature, binary systems with a larger $|\dot{a}/a|T$ might not experience dynamical-timescale MT.

The key reason behind the unexpected stability of MT in systems with $q_\zeta < q < q_{L23}$ is that once MT starts, ζ *rises* as the donor's mass decreases (see Figures 6.2, 6.3 and 5.2). At the same time, $\zeta_{\rm L}$ decreases (Figure 5.2). A decrease in $(\zeta_{\rm L} - \zeta)$ means that, as MT proceeds, the stability of the system increases. We define as the *critical mass-point*, $m_{\rm cp}$, the mass of the donor at which $\zeta = \zeta_{\rm L}$. When the donor decreases its mass to the critical mass-point, the ratio of the donor radius to its Roche lobe starts to decrease. Therefore, assuming that the relative RL overflow at the L_2/L_3 equipotential weakly depends on the mass ratio (see below), if there was no L_2/L_3 before the donor mass decreased to $m_{\rm cp}$, the binary system is stable with respect to MT. We have searched for the point when L_2/L_3-overflow starts using our extended set of detailed simulations (see Figure 6.5). It can be seen that the critical mass ratios q_{L23} for which the MT becomes "unstable" are about twice as large as would be predicted by conventional comparison of mass-radius exponents at the onset of the MT.

Let us analyze the results and show how the approximate critical mass ratios can be predicted without doing detailed binary calculations.

To predict whether a system experiences L_2/L_3-overflow during the MT, we need to identify whether at any moment after the start of MT the donor's radius exceeds $R_{\rm L23}$ – the volume radius at which the donor starts L_2/L_3-overflow. In order to do this, we can find the ratio $R_{\rm L23}/R_{\rm L}$ for a range of the donor masses. Note that this critical ratio also depends on the mass ratio. However, we find that this dependence is quite weak, $\ln\left(R_{\rm L23}/R_{\rm L}\right) \approx 0.27 \pm 0.01$ for $0.7 \leq q \leq 4$. Nevertheless, we took this dependence into account in our calculations by examining the ratio $R_{\rm L23}/R_{\rm L}$ not only down to donor mass $m_{\rm cp}$, but also further, almost all the way down to the donor core mass.

The radius of the donor during the MT, when it has shed to mass m, is

$$\ln R(m) = \ln R_0 + \int_{M_0}^{m} \zeta(\dot{M}) dm \ . \tag{5.6}$$

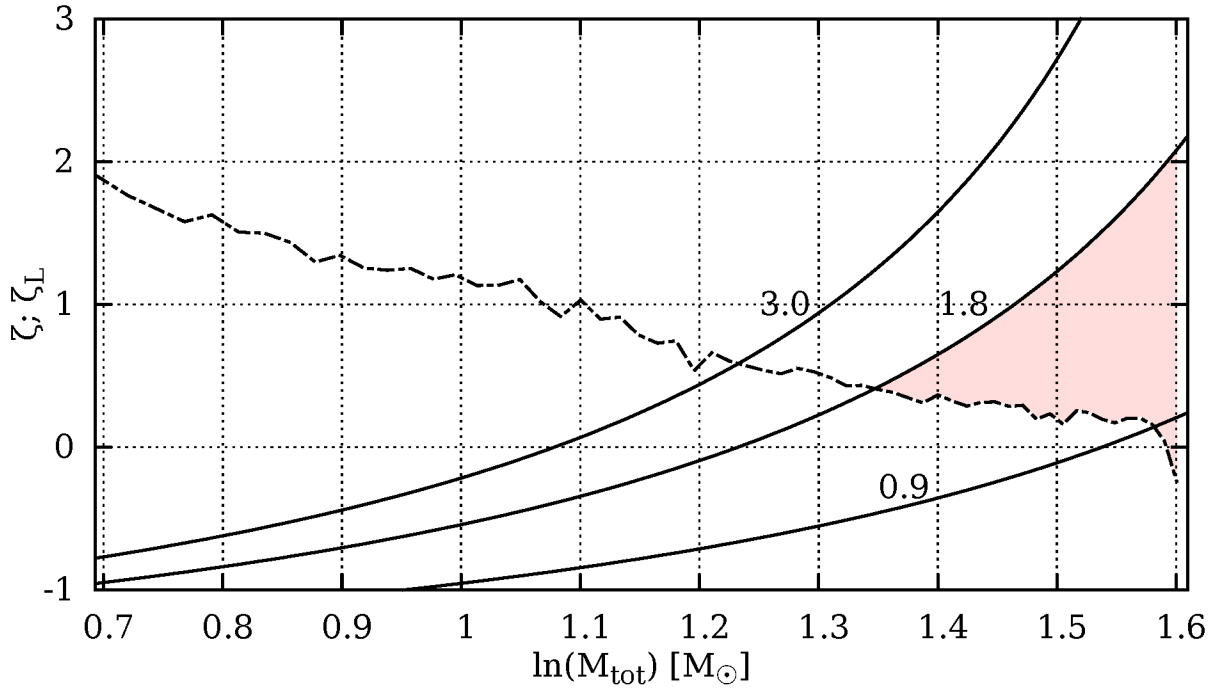

Figure 5.2: ζ for a giant of initial mass 5.0 $M_\odot$ and radius 50 $R_\odot$ subjected to a constant mass loss of 10^{-1} $M_\odot$ yr^{-1} (dot-dashed line). Solid lines show ζ_L for the conservative MT at various initial mass ratios. Intersections $\zeta = \zeta_L$ define the critical mass-points m_{cp}, at which MT starts to decrease. The shaded area is equal to the right part of the Equation 5.7 for $q = 1.8$ and $m = m_{cp}$.

It follows from Section 5.1 that in order to predict the radius of the donor at any moment during fast (saturated) MT, instead of the real ζ one can use $\zeta_{\rm comp}$, which is obtained from the composite polytrope approximation. "Compact" giants, should be expected to expand less than this estimate would predict, and hence be more stable because their $\zeta > \zeta_{\rm comp}$.

Using the definitions of mass-radius exponents (see also Figure 5.2), we can find the approximate radius of the donor at any moment after the start of MT as

$$\ln\left(\frac{R(m)}{R_{\rm L}}\right) = \int_{M_0}^{m} \left(\zeta_{\rm comp} - \zeta_{\rm L}\right) d\ln M \ . \tag{5.7}$$

Now we can find whether the system experiences L_2/L_3-overflow at any moment during the MT and thus produce a semi-analytical estimate of q_{L23} – we will refer to this estimate as "L_2/L_3-overflow condensed polytrope simplification". The application of this new method is shown in Section 6.2.

The theoretical part of the thesis is over. Next chapters will focus on the practical applications of the theoretical part.

Chapter 6

Applications of the improved methods

In this Chapter I will review the practical applications of the theoretical part of the thesis. I will describe the features of mass loss response of the one-dimensional models of single stars, then I will focus on the stability thresholds in detailed binary simulations, i.e., the critical mass ratios at the onset of the Roche lobe overflow that separate stable and unstable MT in a wide range of systems. Finally, we will apply the corrected one-dimensional mass loss and magnetic braking scheme to look for the progenitors of a set of ultra compact X-ray binaries and simulate the evolution of Sco X-1.

6.1 1D response to mass loss

6.1.1 Initial response

First, we can compare the initial reaction of a red giant to constant ML to our prediction made in Section 3.4.1. For example, we take a $5M_\odot$ and $50R_\odot$ giant and subject it to the constant ML rate $\dot{M} = 10^{-3.5} M_\odot$ yr^{-1}. The initial derivative of radius predicted by formula (3.12) is about $-1.7 \cdot 10^5$ cm s^{-1}. With modified boundary conditions and with a timestep of 10^{-4} yr, the code produces $-1.5 \cdot 10^5$ cm s^{-1}. If instead the default hydrostatic boundary condition is used, the code produces $-1.2 \cdot 10^5$ cm s^{-1}.

Second, to compare our results to the ones published earlier, we calculate the behavior of the $0.89\,M_\odot$ and $102R_\odot$ red giant examined by Passy et al. (2012). As in Passy et al. (2012), we subject this giant to the constant ML rate $\dot{M} = 0.1 M_\odot$ yr^{-1}. We evolve one giant using the unmodified `MESA` code with viscosity and timestep setup described in Passy et al. (2012); we call this the "passy-a" model. For the other giant, "passy-b" model, we take into account the circumstances outlined in Section 2.3. In particular, to obtain correct ϵ_g, we evolve this model using a constant time step

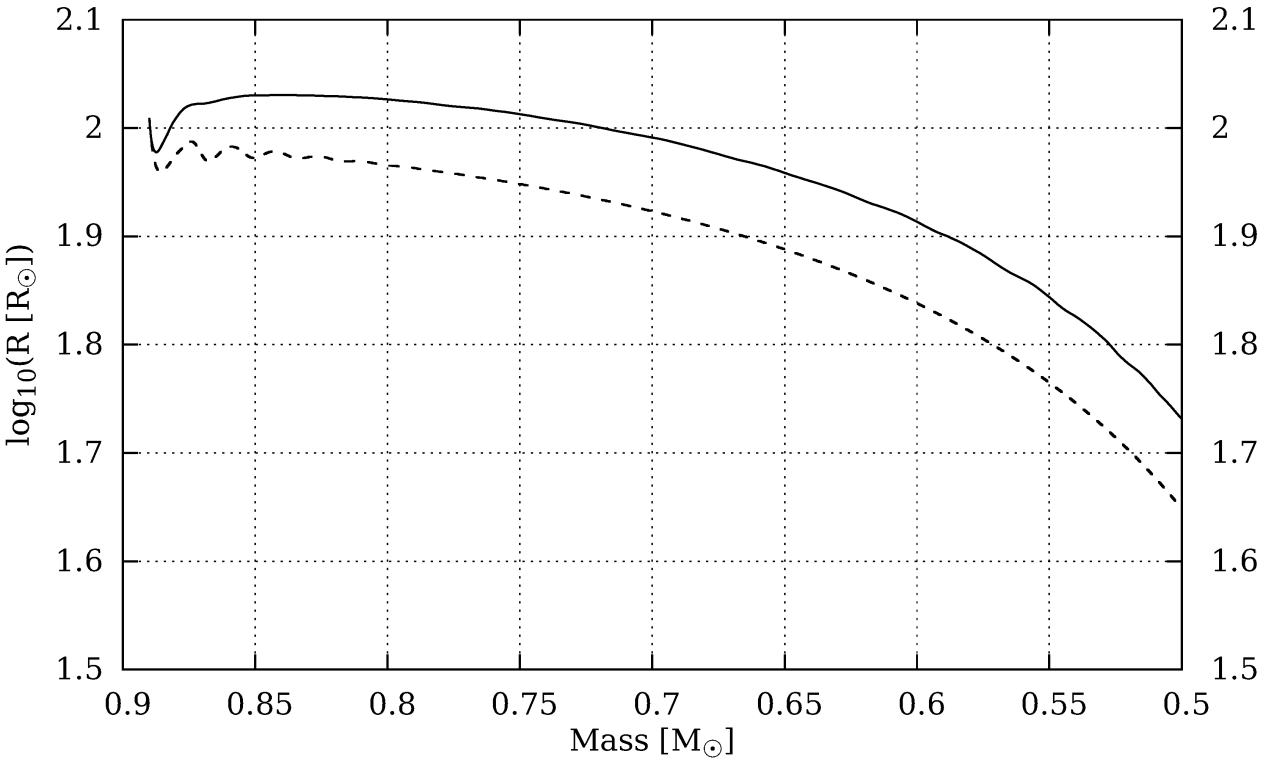

Figure 6.1: Models passy-a and passy-b. A 102 $R_\odot$, 0.89 $M_\odot$ red giant similar to the one considered by Passy et al. (2012) is subjected to constant ML of 0.1 $M_\odot$ yr^{-1}. The solid line represents the result we reproduced following the method described by Passy et al. (2012), which is very similar to the one shown by a red line in their Figure 4. The dashed line represents the result we obtained by compensating for the limitations discussed in Section 2.3, and after removing some pulsation artifacts by disabling composition smoothing at the bottom of the convective envelope.

of 10^{-5} yr. We also remove some pulsation artifacts by disabling composition smoothing at the bottom of the convective envelope.

The initial behavior of the radius in both models has been explained in Section 3.4.1. Note, however, that in our model, the stellar radius is always smaller than that in Passy et al. (2012) (see our Figure 6.1 and their Figure 4). We find that the difference in the value of the radii is mainly due to how accurately the value of ϵ_g is found.

In addition to the initial radius contraction, one can notice ensuing radial oscillations, visible both in the models passy-a and passy-b. We define those non-numerical radial pulsations, excited either by the start of constant ML or, in the case of evolution in a binary, by the rapid growth of the ML rate, as mass loss induced pulsations (MLIPs). These pulsations might be caused by the sonic rarefaction wave, reflected from the bottom of the envelope, which is theoretically predicted to occur in a fluid as it abruptly expands into vacuum, hence we think that they are not of numerical nature. In the model passy-a, these pulsations are largely smoothed out because the timestep in this model grows after the start of simulations and exceeds the dynamical timescale.

A crucial parameter that defines the level of importance of MLIP is the p-mode damping rate η_p, which characterizes the timescale on which a giant roughly attains hydrostatic equilibrium and dynamical oscillations are damped. With contemporary high-precision photometric instruments such as COROT and Kepler, it is possible to obtain high-precision measurements of the profile widths (i.e, damping rates divided by π) of p-modes (see *e.g.* Baudin et al., 2011; Belkacem et al., 2012). Damping rates of intrinsic pulsations of red giants found from those observations are $\eta_p \sim 10^{-1}\pi$ to $10^{1}\pi$. We have also performed numerical experiments to get a handle on how `MESA` treats pulsations, see App. B.

The damping rates, given that the timestep used is much smaller than the pulsation period, depend hugely on the artificial viscosity coefficients: increasing the artificial viscosity increases the damping rates. The damping rates of MLIPs shown in Figure 6.1 are comparable, within an order of magnitude, with those obtained directly from observations. Note that the default artificial viscosity used for the models passy-a and passy-b is very moderate ($l_1 = 0.1$, $l_2 = 0$) and does not substantially affect the damping rates. Due to the lack of wide-range observational calibrations for damping rates across giants of different radii and masses, we do not use an artificial viscosity in our models, except in models passy-a and passy-b, where it is taken into account only for the purpose of comparison with the original paper of Passy et al. (2012).

6.1.2 Realistic radial response

We have performed several simulations where we subjected giants of several initial masses and radii to constant ML, to determine the realistic stellar response defined as:

$$\zeta \equiv \left(\frac{\partial \log R}{\partial \log M} \right) . \tag{6.1}$$

Note that generally ζ is an implicit function of not only the current MT rate, but also of the previous MT, and here we look at ζ for constant MT rates only. We found that:

- At high ML rates, ζ saturates. It becomes mainly a function of the core mass fraction and not of the ML rate (see Figure 6.2 where we show representative examples);
- In "well-expanded" giants, the saturated ζ approaches the behavior of a composite polytrope $\zeta_{\rm comp}$, as in Hjellming & Webbink (1987), with $n = 3/2$ (see Figure 6.3). In more compact giants, ζ is higher than what is expected from the composite polytrope.
- Non-saturated values of ζ are usually lower than the saturated ζ.
- ζ at the very onset of RLOF is often hard to determine due to MLIPs.

6.1.3 The role of recombination

While the radial response seems to be most natural to look at during the MT, we find that other properties of the donor's surface also depend dramatically on how well $\epsilon_{\rm g}$ is obtained. In Section 2.5 we showed that substantial luminosity can be generated if recombination energy is calculated properly. We can compare the surface luminosities of $5M_\odot$ and $50R_\odot$ giant, subjected to a constant ML $\dot{M} = 0.1 M_\odot$ yr^{-1} and evolved with a default time-step adjustment and with a time-step chosen to resolve $\epsilon_{\rm g}$. An estimate provided in Section 2.5 shows that the energy coming from recombination in a giant subjected to ML is approximately

$$W_{\rm rec} \approx 10^5 L_\odot \frac{\dot{M}}{M_\odot {\rm yr}^{-1}} . \tag{6.2}$$

Where does this energy mainly go – is it radiated away as excess luminosity or spent on the star itself, *e.g.*, to increase its thermal or gravitational energy? The unperturbed giant has luminosity only about $L_{\rm donor} \sim 10^3 L_\odot$. The calculations show that a mass-losing giant in which $\epsilon_{\rm g}$ in the superadiabatic layer was calculated properly, has a luminosity about 6 times higher than the mass-losing giant with a default relatively large time-step! The first giant has also become about 50%

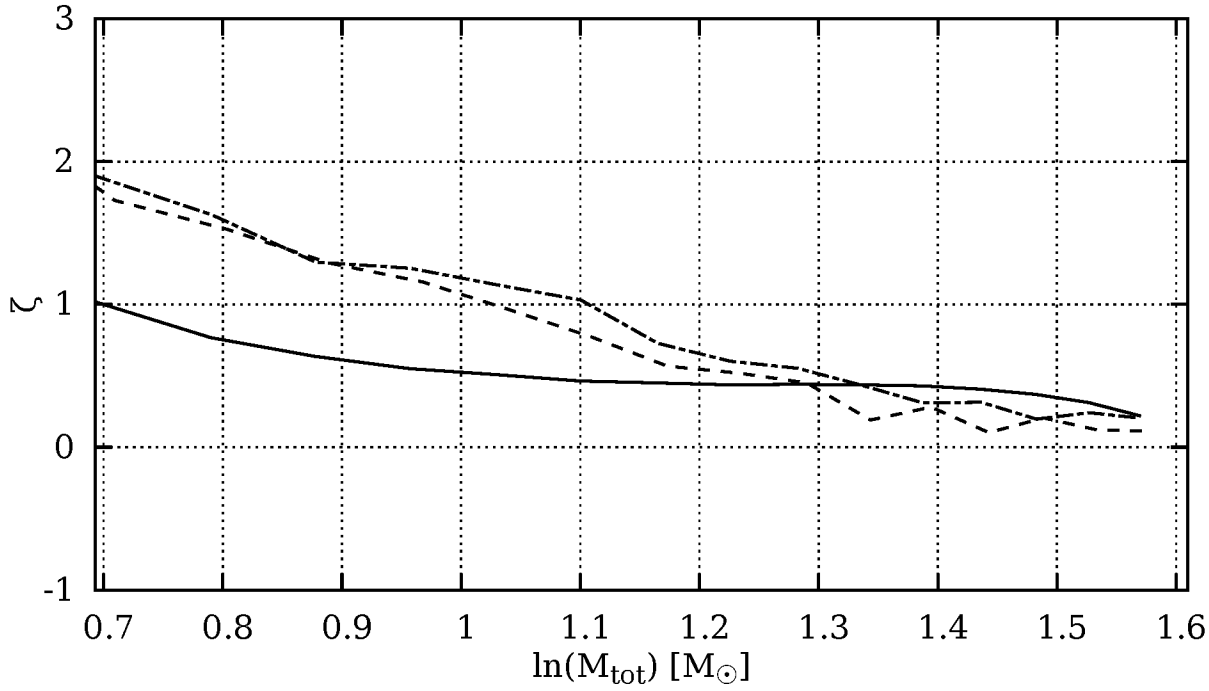

Figure 6.2: ζ for a giant of initial mass 5.0 $M_\odot$ and radius 50 $R_\odot$ subjected to various rates of mass loss (10^{-3}, 10^{-2} and 10^{-1} $M_\odot$ yr^{-1} (solid, dashed and dot-dashed lines respectively).

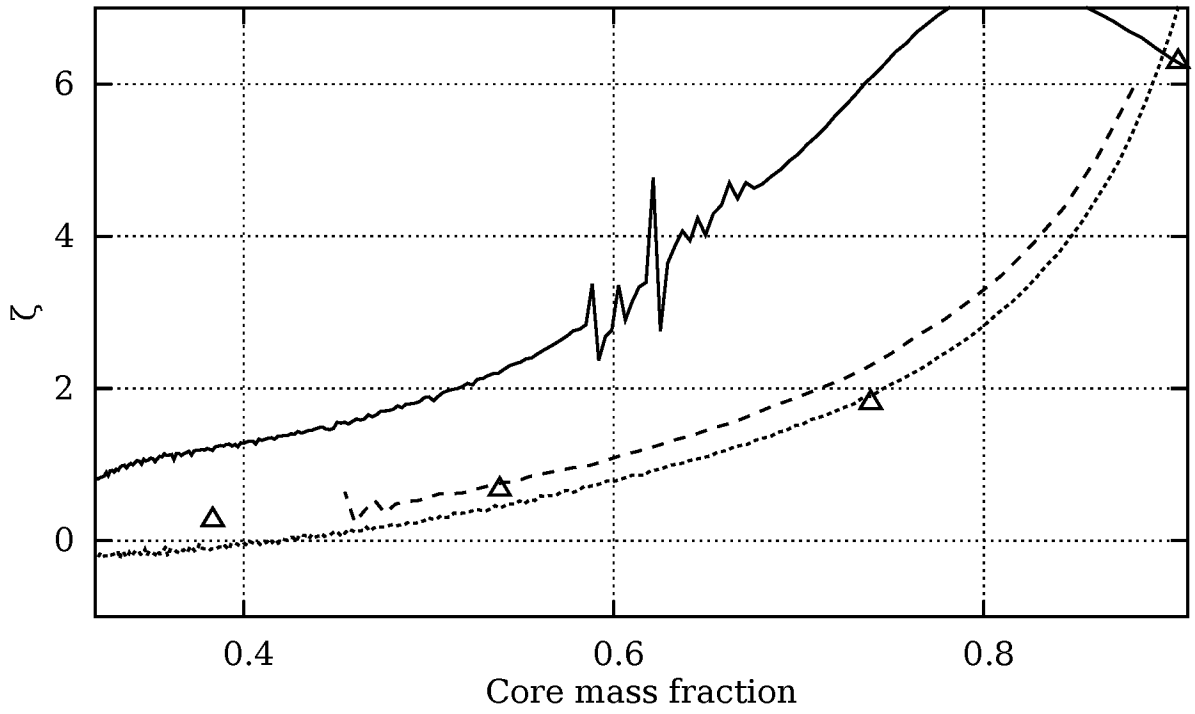

Figure 6.3: ζ for giants at MT rate $10^{-1}\ M_{\odot}\mathrm{yr}^{-1}$. 5.0 $M_{\odot}$ 50 $R_{\odot}$ (solid line), 1.0 $M_{\odot}$ 100 $R_{\odot}$ (dashed line), 5.0 $M_{\odot}$ 200 $R_{\odot}$ (dotted line). ζ_{comp} for a composite polytrope ($n = 3/2$), taken from Hjellming & Webbink (1987), is shown with triangles. Initial portions of the responses with irrelevant dynamical oscillations are removed.

hotter. This increase in luminosity indicates that a large portion of energy from recombination is radiated away, rather than being spent on the star itself. In the case of a $5M_\odot$ and $200R_\odot$ giant, a simple prediction for a luminosity increase and an exact calculation would agree fairly well – in a more expanded giant, less recombination energy was spent on the star itself, and most went directly to surface luminosity. Similarly, the luminosities in the passy-a and passy-b models are different by about 6 times, also as a simple estimate would predict. Interestingly, in the case of $5M_\odot$ giants, the radii obtained by the two methods were not much different, except that in giants evolved with a small time-step we can observe MLIPs.

Of course, very fast MT rates are not commonly observed. However, the path of a star through the fast MT is different, and can define both the stability and/or how the donor appears when the fast MT phase is completed. We also can evaluate that this effect might be important (i.e. provides a difference in the luminosity by more than a few per cent) for as long as

$$\dot{M} \gtrapprox 10^{-7} \frac{M_\odot}{\mathrm{yr}} \times \frac{L_{\mathrm{donor}}}{L_\odot} \tag{6.3}$$

and hence might be important for low-luminosity giant donors and, in general, for all donors transferring mass at the thermal timescale of their envelope.

Indeed, consider the thermal timescale τ_{KH} of the envelope taken as usual

$$\tau_{\mathrm{KH}} \approx 2 \times 10^7 \ \mathrm{yr} \left(\frac{M}{M_\odot} \right)^2 \frac{R_\odot}{R} \frac{L_\odot}{L} \ . \tag{6.4}$$

For most giants $R/R_\odot \gg 2M/M_\odot$, and their envelope thermal timescale MT, M/τ_{KH}, satisfies condition 6.3.

6.2 Stability thresholds and their application

6.2.1 Thresholds

The bird-eye view of the stability thresholds defined according to the criteria listed in Chapter 5 is presented in Figure 6.4. In Figure 6.4 only the case of conservative MT is shown. We have also checked and found that non-conservative MT leads, as expected, to the increase in q_{L23}, increasing it by about 0.3.

More detailed information for the various giants is given in Figure 6.5. In this figure we compare four types of stability thresholds for the initial mass ratio to each other, namely:

- the commonly used condensed polytrope stability thresholds, which are based on the comparison of ζ_{L} and ζ_{ad} at the onset of RLOF;

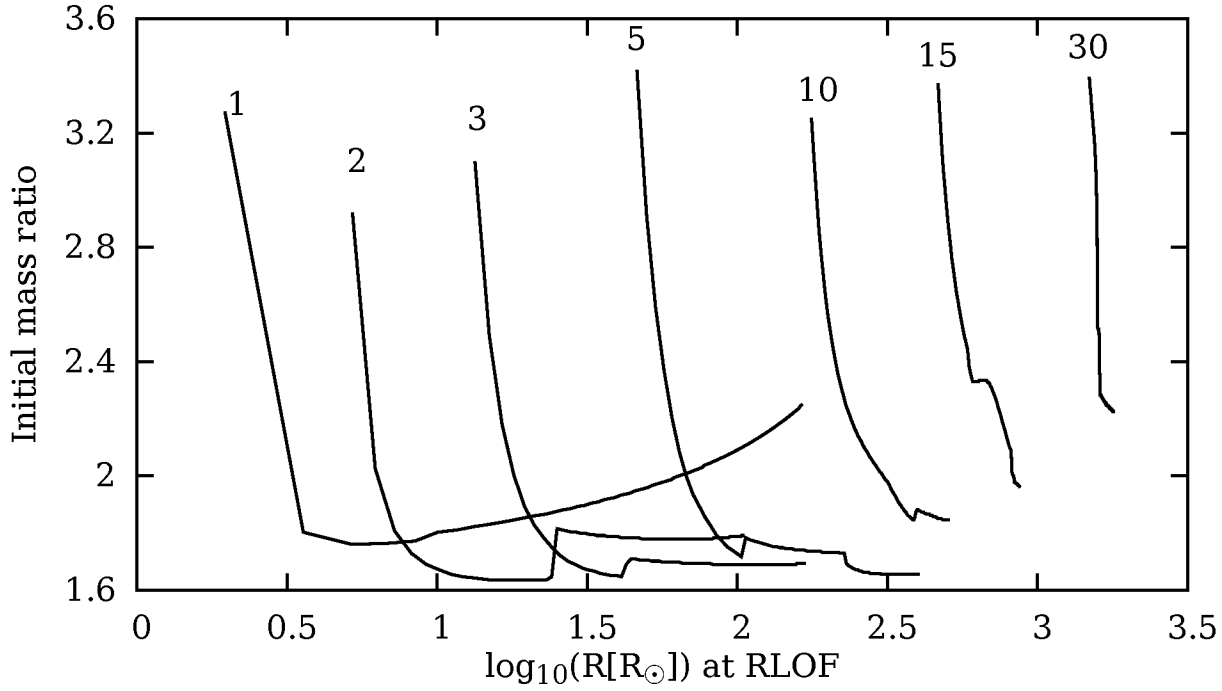

Figure 6.4: Critical mass ratios obtained from the L_2/L_3-overflow simplified composite polytropes for the donors of different initial masses and radii.

- our condensed polytrope stability thresholds which are based on the L_2/L_3-overflow criterion and obtained without detailed simulations;

- thresholds, which are obtained from the combination of detailed simulations and the L_2/L_3-overflow criterion;

- thresholds, which are obtained from the combination of detailed simulations and the dynamical stability criterion $|\dot{a}|P/a > 1/50$.

Figure 6.5 shows that the latter three thresholds are quite comparable to each other and all of them give substantially higher values of the initial critical mass ratio than the first, commonly used criterion that only considers radial responses at the onset of RLOF, but not during the RLOF.

We can see that the condensed polytrope simplification works best for those giants that are neither too compact nor too expanded. In both compact and average-sized giants that approach L_2/L_3-overflow at the critical point, most mass before the critical point is lost at ML rates which are generally much higher than $\sim 10^{-2}\ M_\odot\ \mathrm{yr}^{-1}$, so it's fine to use the saturated value of ζ. At the same time, compact giants have higher saturated values of ζ, which makes them more stable than average-sized giants whose saturated ζ approximately follows the condensed polytrope.

In large giants with very rarefied envelopes, L_2/L_3-overflow occurs at much lower mass loss rates, and the saturated values of ζ become inapplicable. Instead, a lower, non-adiabatic, non-saturated values should be used. This makes these giants less stable. However, such L_2/L_3-overflow will be non-dynamical and does not have to result in a common envelope.

The detailed simulations (Figure 6.5) show that q_{L23} is larger when a donor is more compact and the mass fraction of its convective envelope is smaller. In all detailed simulations we did with donors where the outer convective envelope is non-negligible, q_{L23} is below 3.5, where 3.5 is known as the critical mass ratio leading to a delayed dynamical instability with radiative donors (see, e.g, Ge et al., 2010). It shows therefore that during the development of the outer convective envelope, the convective donors are in the transitional regime. When the convective envelope is well developed, the critical mass ratios are in the range $1.5-2.2$ for most donors.

We conclude that the criterion based on L_2/L_3 overflow is definitely predicting that more binary systems will evolve through their MT in a stable way.

Whether the L_2/L_3 overflow should necessarily lead to a common envelope is not entirely clear. In principle, MT through the L_2/L_3 nozzle can be treated in the same simplified way as that through the L_1 nozzle. It is a subject of our future work.

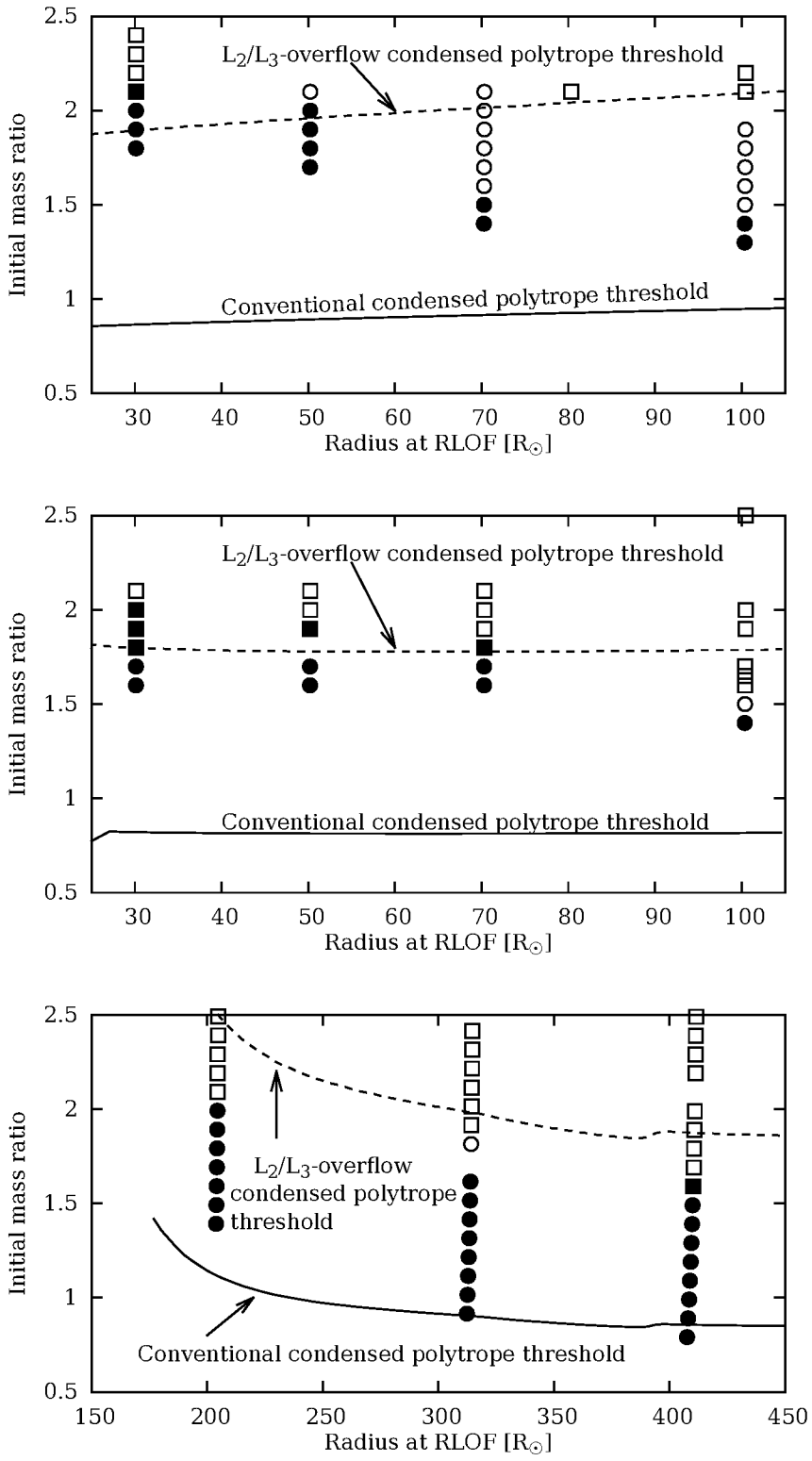

Figure 6.5: The outcomes of the MT sequences for donors of different initial masses. The top panel is for a $1M_\odot$ donor, the middle panel is for a $2M_\odot$ donor and the bottom panel is for a $10M_\odot$ donor. A square symbol indicates that $|\dot{a}|T/a > 1/50$, otherwise, the symbol is a circle. If a symbol is filled, then no L_2/L_3 overflow is experienced, if a symbol is empty, then the system experiences L_2/L_3-overflow. Our L_2/L_3-overflow condensed polytrope simplification is shown with a dashed line, and q_ζ – the conventional condensed polytrope threshold – is shown with a solid line.

6.2.2 Application to double compact objects

The material in this section is adapted from Pavlovskii, Belczynski and Ivanova in preparation.

The formation of close black hole - black hole binaries and, consequently, the rate of Galactic double compact object (DCO) mergers depends strongly on the stability of MT (MT) from massive giants to their compact companion, a black hole (BH) or a neutron star (NS) (Dominik et al., 2012).

The episode of the MT that affects DCO rates the most, takes place when the initially most massive companion has already become a compact object, and the second companion, now most massive, starts to evolve from the MS, and overfills its Roche lobe. The mass ratio in this system with a first-formed compact object is large, and, by conventional MT stability criterion for either convective or radiative donors, the MT is deemed to be dynamically unstable and must result in a common envelope event (CEE). Depending on the energy balance, the outcome of the CEE is either the merger of the two companions, or the ejection of the common envelope. In the latter case the formed close binary may evolve into a DCO and merge later within the Hubble time, thus becoming a source of detectable gravitational waves.

It was shown that for BH-BH binaries the decisive episode of the MT predominantly takes place when their donor is at a Hertzsprung gap (Dominik et al., 2012). A donor in this case does not necessarily have a well developed density contrast between the core and the envelope. While the outcome of a CEE in a case of a well-developed giant donor is not yet well understood and is commonly parametrized with the energy budget formalism (for a review, see Ivanova et al., 2013b), the applicability of the energy formalism for a donor with a not well-developed density contrast is not justified. This uncertainty, on whether the MT results in a merger or that a CEE may create a close binary, was investigated by Dominik et al. (2012). They found that the Galactic DCO merger rate changes by more than an order of magnitude depending on whether binary formation via CEE is plausible via the energy formalism, or if a merger takes place (see, e.g., their Fig. 19). It hints that the stability of the mass transfer from such a donor (i.e., whether or not the CE even takes place) should also significantly affect the Galactic DCO merger rate.

In this thesis we propose a third outcome: we find that the MT is stable for a large range of donor's radii and mass ratios. We discuss here why the MT is stable and present the detailed MT calculations covering a large parameter space. This allows us to derive the parametrized criterion for stability, suitable for future studies using population synthesis codes.

Understanding the stability of the MT from Hertzsprung gap donors

Population synthesis codes, to treat MT, require parametrized stability thresholds, which can be based on whether the donor is convective or radiative, on the mass ratio of the binary companions

at the onset of the RLOF, on the mode of MT (the assumption on how conservative is the MT) and sometimes on the additional features of the nature of the donor and/or of the accretor (e.g., `StarTrack`, Belczynski et al., 2012).

A common mechanism underlies all types of runaway MT instabilities – insufficient shrinkage of the donor upon the mass loss compared to the change of the radius of the Roche lobe. This response on the MT, of both the donor and the Roche lobe, is known as the mass-radius exponent, abbreviated as ζ, and is defined as the logarithmic derivative of the giant's radius with respect to its mass:

$$\zeta = \frac{\partial \log R}{\partial \log M}. \tag{6.5}$$

It is was suggested in the past that the donor's response $\zeta_{\rm don}$ is low for stars with convective envelopes – the simplified polytropic stars were found to expand upon the mass loss (Hjellming & Webbink, 1987). That led to a classical understanding that if the donor has a convective envelope at the moment of Roche lobe overflow, the mass ratio is above the critical, ~ 0.8, and the MT is fully non-conservative, then the ensuing mass transfer will be dynamically unstable (Hjellming & Webbink, 1987; Soberman et al., 1997). Later, when the reaction of realistic stellar models was studied, it has been shown that the convective envelopes do not necessarily expand upon the mass loss, and the critical mass ratio for a stable MT can even be larger than 1 (Woods & Ivanova, 2011).

In more recent studies, two new effects important for MT were explored (Pavlovskii & Ivanova, 2015b).

First, a MT framework was developed that can follow the MT beyond the L_1 overflow, by calculating the current RL overflow MT rate until L_2/L_3 overflow occurs, if the latter does happen. A model that has overfilled its outer Lagrangian point can still be simulated, but the MT through this point is not taken into account. Usually by the time it happens the MT itself is already dynamically unstable and the Euler term is comparable to the centrifugal term, i.e. the Roche lobe approximation itself breaks down. As an immediate application, it was found that for donors with deep convective envelopes, the critical mass ratio is about twice as previously thought, above 1.6, allowing very massive donors without entering a CEE. In this paper, we will be using that MT framework.

Second, it was shown that the critical mass ratio for giants with shallow convective envelopes approached the critical mass ratio characteristic for radiative donors, about 3.5. This effect is important for Hertzsprung gap donors that play a role in BH-BH binary formation, and needs more attention than was given previously.

A massive donor's structure can be in general quite complex and include both formally radiative layers with only slightly increasing specific entropy in mass or formally convective layers in which

the entropy decreases quite fast. The response of the donor is not solely defined by whether a convective or radiative layer is being removed during MT, but is a complex function of the donor's structure as a whole, which can be only determined with detailed simulations.

A donor with a shallow or not developed at all convective envelope, may still contain an area with a relatively flat entropy profile. When, during the MT the donor's outer layers are steadily eaten to expose the area with a sufficiently flat entropy profile, ζ decreases dramatically and, it might lead in some cases to the delayed dynamical instability (DDI), if the evolved mass ratio was not decreased enough. This way even underdeveloped massive subgiant donors with compact accretors can in principle be the progenitors of DCO, which is an important thing to consider in the current population synthesis codes.

The two described above effects lead to the qualitatively new stability picture for the massive giant donors. Models of massive giants are frequently not robust and exhibit numerical artifacts that affect their radial response to mass loss. Thus, their binary evolution is harder to predict than that of relatively low-mass giants, for which the detailed simulations were supplied in Pavlovskii & Ivanova (2015b). In this paper we will perform detailed simulations for such massive donors, with the aim to find the range of donor's radii at the moment of RLOF, such that the MT, for a given mass ratio, will be not affected by either of the following instabilities:

- The first instability is the HG expansion instability that appears in donors which at the moment of RLOF are experiencing a period of fast thermal-timescale HG expansion. This expansion is so rapid and the outer layer of these donors are so dense that it almost immediately (within a few thousand years) leads to extremely fast MT and dynamical instability. We define the radius that a donor should reach before RLOF to avoid this instability as $R_{\rm S}$.

- The second instability is a dynamical instability that appears in donors with a sufficiently developed convective envelope. We define the minimum critical radius, which a donor should reach before RLOF to experience this instability as $R_{\rm U}$.

We note also that there is a third instability – DDI-type instability. It might take place in some donors that overfill the Roche lobe when their radius is between the first two – $R_{\rm S}$ and $R_{\rm U}$. This instability does not appear immediately after RLOF. Instead, the first RLOF leads to stable MT, after which a part of the hydrogen-rich envelope is lost and the donor detaches. That lost envelope was radiative initially. Later, the donor overfills the Roche lobe again and the remaining envelope is consumed to expose its middle convective layer (which is still hydrogen-rich). At this point the donor expands dramatically and experiences a very fast dynamically unstable MT and a CEE.

Detailed MT Simulations

To calculate the detailed evolution of the giants and their behavior during the RLOF, we use the MT framework as described in Pavlovskii & Ivanova (2015b). This MT code is an extension to the `MESA/binary` binary module that uses for the evolution of single stars the `MESA/star` stellar code (Paxton et al., 2011a, 2013).

For donors, we consider stars of several ZAMS masses – 20, 30, 40, 80 $M_\odot$ with solar metallicity and 0.1 $Z_\odot$ and evolve them employing the Vink wind prescription (Vink et al., 2001). We then place each star in a binary containing a 7 $M_\odot$ black hole. The initial binary separation at the start of MT is varied from a few tenths to a few thousands of $R_\odot$. Different initial binary separations correspond to different radii of the star when it evolves and overfills the Roche lobe. After the start of the MT, we examine whether or not the MT is dynamically unstable, using a modified criterion outlined in Pavlovskii & Ivanova (2015b), namely, $\dot{M}P/M > 2\%$, where P is orbital period. Note that in this way we can detect either immediate or delayed dynamical instability, whichever takes place in a given system.

For example, the donor with ZAMS mass 30 $M_\odot$ and $Z = 0.1Z_\odot$ has two critical points (see Table 6.1). The first critical point happens when the speed of the thermal-timescale expansion of the star during the HG becomes insufficient to cause the extremely fast unstable MT after the RLOF. This critical point is located between the radii of 87 and 103 $R_\odot$ at the moment of RLOF, 87 $R_\odot$ corresponds to immediately unstable and 103 $R_\odot$ to immediately stable MT. Stars that reach the RLOF between the end of the MS and this critical point experience unstable MT almost immediately, in a few thousand years after the RLOF.

For donors with ZAMS masses 30-40 $M_\odot$, unstable donors would have their thermal-timescale expansion approximately $(\partial R/\partial t)_{\rm ev} \geq 0.0023$ $R_\odot$/yr (as measured in unperturbed stars). The donors with ZAMS mass of $20M_\odot$ are always stable after the end of the main sequence. The maximum $(\partial R/\partial t)_{\rm ev}$ in these stars during their HG is 0.0021 $R_\odot$/yr. For most massive donors, with the initial mass of $80M_\odot$, MT with a $7M_\odot$ BH is always unstable. With a twice more massive BH, and mass ratio close to that of a binary with the donor that has initial ZAMS mass of $40M_\odot$ and a $7M_\odot$ BH, the value of $(\partial R/\partial t)_{\rm ev}$ that separates stable and unstable regime is slightly larger, about 0.09 $R_\odot$/yr.

A second critical point corresponds to the moment when the donor grows large enough on the giant branch to develop a convective envelope (a donor may have had convective layers in its envelope previously, but instability is developed when the convective zone reaches the surface, see Figure 6.6 and Table 6.1). For example, for a 30 $M_\odot$ red giant the second critical point corresponds to the radius between 991 and 1111 $R_\odot$ at RLOF, where the latter radius leads to instability and the

donor has outer convective zone, and in the former case the MT is stable at the beginning.

Stars that experience RLOF between the first and the second critical point proceed with dynamically stable MT. We note that the donors between two critical points can experience L_2/L_3 overflow, which is detected, but not treated in our framework. This overflow is not likely to lead to dynamically unstable MT because the outer layers of these stars are quite rarefied and the corresponding mass loss rates are too low to cause any dynamical instability.

Let's consider for example a $30M_\odot$ donor with the initial radius of 750 $R_\odot$ at the moment of RLOF. At the start of RLOF the outer envelope of the star is radiative, the star has a convective core with a mass $\approx 5\ M_\odot$ and an inner convective layer stretching from ≈ 8 to 14 $M_\odot$. The rest of the star is radiative. A dynamical timescale MT in this donor can be estimated as a 1 $\mathrm{M_\odot\ yr^{-1}}$, while the maximum attained MT rate does not exceed $\sim 0.01\ M_\odot\ \mathrm{yr}^{-1}$. The relative RLOF (by how much the donor exceeds its Roche lobe radius, in units of the Roche lobe radius) reaches 37%, but the mass of the star outside of the Roche lobe is less than 0.5% of the donor mass. The binary experiences a brief period of L_2/L_3 overflow during which the MT rate reaches $0.005\ M_\odot\ \mathrm{yr}^{-1}$. In total, 4.1 $\mathrm{M_\odot}$ were removed during L_2/L_3 RLOF that has lasted 1000 years. Note, that the stream via L_2/L_3 nozzles should be negligible compared to the stream flowing via L_1.

After the giant's ζ_R becomes larger than ζ_RL and the degree the of donor's RLOF becomes small, MT rate falls to $\approx 10^{-5}\ M_\odot\ \mathrm{yr}^{-1}$ and finally the donor detaches. By the time the donor had detached,$\approx 11.6M_\odot$ is removed, leaving a $10\ M_\odot$ envelope above the core, which is predominantly radiative with a convective layer from 10.5 to 12.3 $M_\odot$. The mass ratio of the donor to the BH, by the time the MT stopped, is ~ 2.5. The binary has shrunk, and the donor radius at the end is only about 107 $\mathrm{R_\odot}$ (see Table 6.1).

A donor that has a radius below R_S doesn't experience L_2/L_3 overflow. The L_1 MT rate reaches about 10 $\mathrm{M_\odot\ yr^{-1}}$, at which point the stellar code fails to converge. This is a direct consequence of the fast intrinsic evolutionary expansion rate of these donors.

A donor that has a radius larger than R_U, experiences unstable MT. The L_1 MT rate reaches about $0.27\ M_\odot\ \mathrm{yr}^{-1}$. The mass of the envelope at this moment is reduced to 26.4 $\mathrm{M_\odot}$. At this fast MT the condition $\dot{M}P/M < 2\%$ is not satisfied anymore, which constitutes dynamical-timescale MT. The dynamical MT that leads in this case to a common envelope, will start therefore with a less-massive envelope, starting in a binary with different orbital parameters than would be formed when a whole envelope is present.

The complete results for under-solar metallicity are presented in Table 6.1. This mapping between donor's radius, mass at the moment of Roche lobe overflow and stability of the ensuing MT can be directly used by the population synthesis codes.

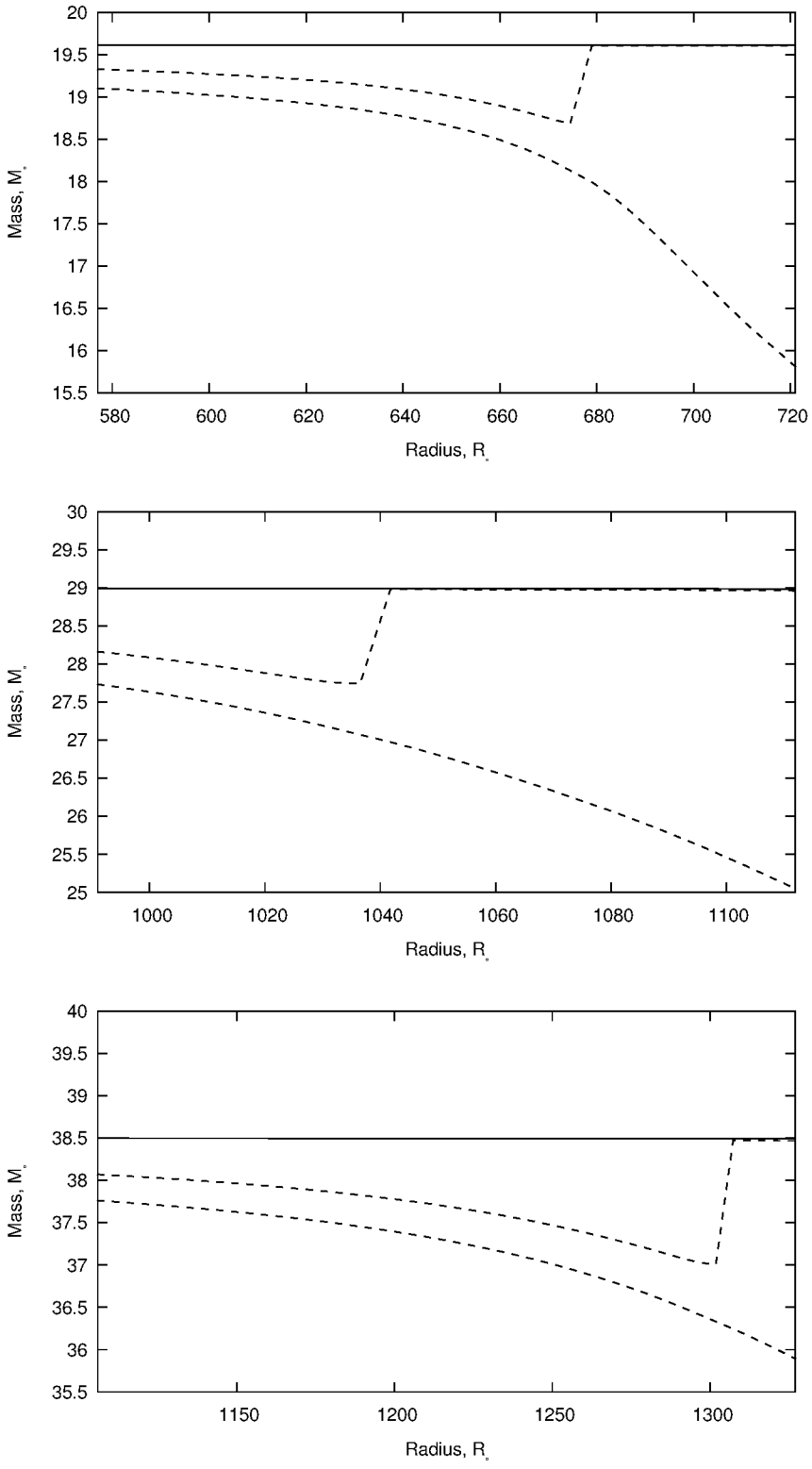

Figure 6.6: Development of the convective envelope (between the dashed lines), which leads to instability at $R_{\rm U}$ in 20 $M_{\odot}$ (top panel), 30 $M_{\odot}$ (middle panel) and in 40 $M_{\odot}$ (bottom panel) giants, Z=0.1Z$_{\odot}$.

Table 6.1: Stability of MT in giants obtained with initial $Z = 0.1Z_{\odot}$

$M_{d,ZAMS}/M_{\odot}$	$M_d/M_{\odot}$	$M_{BH}/M_{\odot}$	$R_S/R_{\odot}$	$(\partial R/\partial t)_{ev}$	$R_U/R_{\odot}$
20	20	7	12-27 (if any)	<0.0021	577-721
30	29	7	87-103	0.0033-0.0002	991-1112
40	38-39	7	310-354	0.0024-0.0022	1106-1327
80	72-75	7	unstable	–	unstable
80	72-75	14	134-156	0.07-0.10	1721-2007

$M_{d,ZAMS}$ – donor mass at ZAMS, M_d – donor mass at RLOF, M_{BH} – mass of the black hole, R_S – first critical radius (boundary of the instability caused by the intrinsic evolutionary expansion at HG), $(\partial R/\partial t)_{ev}$ – intrinsic evolutionary expansion rate at the onset of RLOF, R_U – second critical radius (boundary of the instability caused by developing convective envelope). "If any" means that it is not known with certainty whether the former type of instability takes place in a giant since for all models after the end of MS that we have checked, the MT is stable.

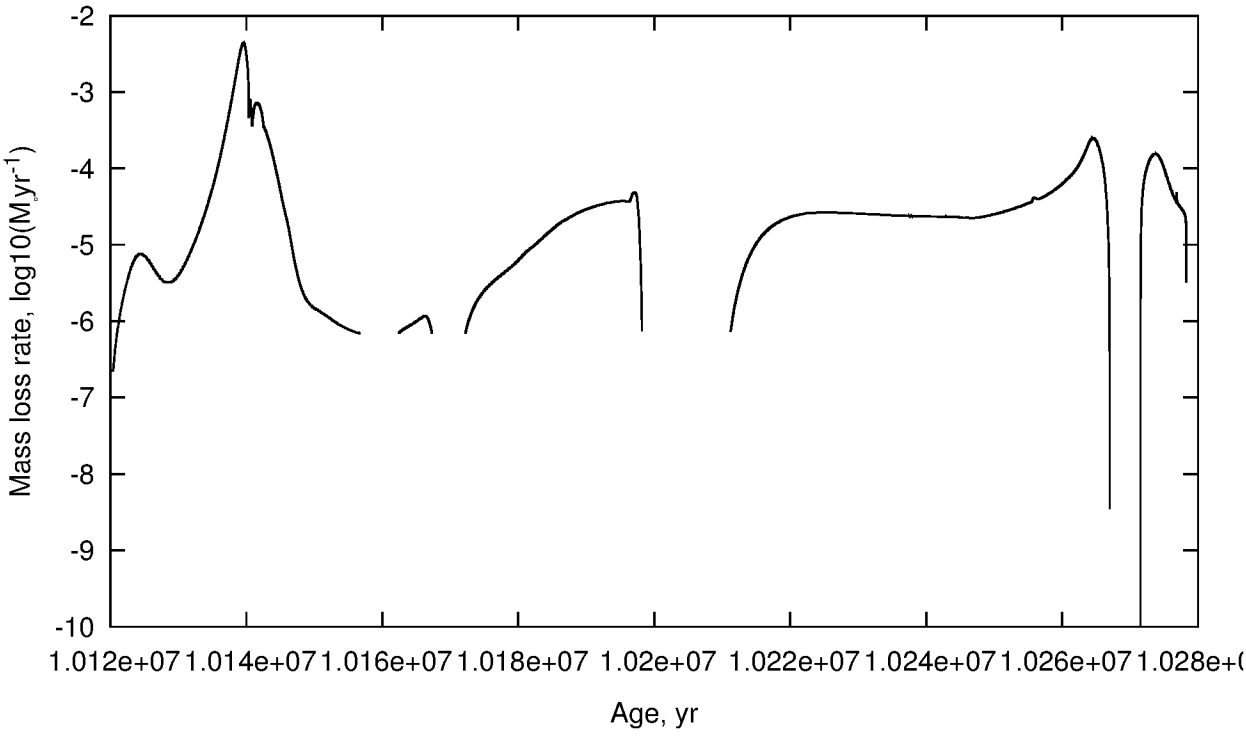

Figure 6.7: History of MT from a 20 $M_{\odot}$ giant with radius at RLOF 144 $R_{\odot}$ with Z=0.1Z$_{\odot}$.

Table 6.2: Properties of stable MT sequences with initial $Z = 0.1Z_{\odot}$

$M_i/M_{\odot}$	$M_f/M_{\odot}$	$R_i/R_{\odot}$	$R_f/R_{\odot}$	$m_{core}/M_{\odot}$ at RLOF	$m_{core}/M_{\odot}$ final	Burning
19.6	7.2	144	50	6.1	7.2	H shell, He core
19.6	7.3	577	200	6.1	7.3	H shell, He core
29.3	9.7	103	3	8.4	8.5	H shell, He core
29.1	17.5	751	107	8.8	10.0	H shell, He core
38.6	26.0	1106	103	11.5	12.1	H shell, He core

M_i – donor mass at RLOF, M_f – donor mass after the end of MT, R_i – donor radius at RLOF, m_{core} – He-CO core mass, Burning – modes of nuclear burning in the donor at the onset of RLOF.

Such systems as shown in Figure 6.7 proceed with stable MT after the RLOF. It means that they are unlikely to experience the common envelope phase (unless the donor reattaches again to the Roche lobe in future and loses enough mass to reach the DDI). This rules out the possibility of them appearing as DCO mergers. Because the MT rate in these systems reaches very high values, these systems are likely to appear as ultra luminous X-ray sources (ULXs). ULXs are sources that are more luminous than $\gtrsim 10^{39}$ erg/s, exceeding the Eddington limit for a stellar-mass BH. One of the famous examples of such an object is ULX M82 X-2, discovered by NuSTAR(Bachetti et al., 2014). To exceed this cut-off luminosity by a factor of 30, as it is observed in the ULX M82 X-2, one requires MT rates of at least $7.5 \times 10^{-6}\ M_{\odot}\mathrm{yr}^{-1}$, assuming the 0.07 Schwarzschild black hole conversion factor. The MT rates in the system shown in Figure 6.7 are more than enough for that.

Formation of ULX systems with very massive donors and a stellar mass BH accretor was ruled out in the past since it was though that dynamically unstable mass transfer should occur. For example, Bachetti et al. (2014) showed that ULX M82 X-2 consists of a massive giant donor and a NS accretor and has an extreme mass ratio of more than 3.5. Fragos et al. (2015) have shown that it is possible to obtain such systems assuming non-conservative MT to a neutron star accretor, donors masses below $8M_{\odot}$ and an orbital period between 1 and 3 days. With the revised stability for substantially more massive donors and wider initial orbital periods, we should be able to produce a large population of ULXs systems with BH donors.

Conclusions

We showed that systems with high mass ratios, which were earlier thought to experience a CE event and with certain probability form a DCO can, nevertheless, avoid a CE and have stable MT, which prevents them from appearing as DCO mergers. We expect such systems to appear as ULXs. A finer table of stability criteria for systems of various mass ratios and donor radii at the onset

of RLOF is required to conduct binary population synthesis simulations with the StarTrack code. In addition, even the models, in which the first considered episode of RLOF was stable, have to be followed through to the point when their inner convective layers are exposed by mass loss to make sure that they don't experience the DDI. For these reasons we continue to conduct additional detailed simulations for under-solar and solar metallicities.

6.3 Simulation of Sco X-1

This material in this section is adapted from Pavlovskii & Ivanova (2015a).

Sco X-1 is the first extrasolar X-ray source discovered and is the brightest persistent X-ray source beside the Sun (Giacconi et al., 1962). The source has been extensively observed since its discovery in both radio and X-ray, and is classified as a low-mass X-ray binary (LMXB) for which a number of parameters have been obtained (see Section 6.3.1).

The evolution of a close binary after the compact object formation, and, specifically, the MT (MT) rate during an LMXB phase, are governed by angular momentum loss. In a persistently accreting short-period binary with a giant or subgiant donor, the dominant angular momentum loss mechanism is magnetic braking (Rappaport et al., 1982). It is crucial that the first detailed numerical study of the population of short-period LMXBs has shown an unexpectedly strong mismatch between the MT rates in the theoretical population of LMXBs and the observationally-inferred mass accretion rates of known LMXBs (Podsiadlowski et al., 2002). Most of the observed LMXBs, including Sco X-1, were found to have mass accretion rates at least an order of magnitude higher than the theoretically expected MT rates for the same orbital periods (although it was unclear whether observational selection effects could cause this effect).

This alarming mismatch between theory and observations, albeit mainly noticed only by theorists doing detailed studies of MT in LMXBs, has prompted several new ideas to explain how the magnetic braking operates in LMXBs. For example, Justham et al. (2006) suggested that Ap and Bp stars with radiative envelopes, due to their high magnetic fields and stellar winds could nevertheless experience stronger than usual magnetic braking. Another idea, also related to the nature of the donor, was that a stronger magnetic braking could be achieved in short-period LMXBs if they have pre-MS donors (Ivanova, 2006). How the transferred material can affect the orbital evolution also was explored. For example, Yungelson & Lasota (2008) resolved the magnetic braking problem by proposing that accretion discs in LMXBs are truncated, and Chen & Li (2006) explored the role of the circumbinary disc. At the moment, none of these ideas have become the mainstream method for producing LMXBs in population studies, despite the inability of the standard magnetic

braking theory to explain the LMXBs that are well studied. It is important to add that all the mentioned ideas were explored on the set of very short-period LMXBs, with orbital periods less than about 10 hours, and are not applicable to LMXBs with larger orbital periods, like Sco X-1.

These facts led us to revisit the way magnetic braking is treated in LMXBs with subgiant and giant donors. We take the well-observed prototype low-mass X-ray binary – Sco X-1 – as an example for our simulations. We provide its observationally-derived properties in Section 2. In Section 3, we outline our revised prescription for magnetic braking. We provide detailed MT simulations for the case of Sco X-1 in Section 4.

6.3.1 Observed parameters of the system

From spectroscopic data, Steeghs & Casares (2002) infer the upper limit of its mass ratio to be 0.46 (see the brief overview of the important observed parameters in Table 6.3). Assuming that the lowest-velocity emission lines originate at the inner Lagrangian point, using the radio inclination data from Fomalont et al. (2001) and setting the accretor mass to 1.4 $M_{\odot}$ gives a probable value of mass ratio 0.30 and donor mass $0.42 M_{\odot}$, in agreement with Mata Sánchez et al. (2015), who find the donor mass to be between 0.28 and 0.70 $M_{\odot}$. The orbital period of the system is the best determined quantity, and is $P = 0.787313 \pm 0.000015$d (Hynes & Britt, 2012).

The donor has been identified to have spectral class K4 or later, and luminosity class IV, subgiant (Mata Sánchez et al., 2015). The intrinsic effective temperature of the donor then should not be hotter than 4800 K. This upper limit includes uncertainties in the spectral class determination as discussed in Cox (2000), for a subgiant the intrinsic effective temperature is likely lower than this upper limit.

The X-ray luminosity of this system, as measured in 2-20 keV range, is 2.3×10^{38} ergs^{-1} (Bradshaw et al., 1999). An estimate of its bolometric luminosity, from the bolometric flux and distance gives $L_b = 3.6 \pm 0.8 \times 10^{38}$ ergs^{-1} (Watts et al., 2008). If the accreting star is 1.4 $M_{\odot}$, the accreted material is 70% hydrogen and opacities are provided by Thomson scattering, then the critical Eddington luminosity for this system is $L_{\rm Edd,TS} = 2.1 \times 10^{38}$ ergs^{-1}. This system is slightly above the Thomson scattering Eddington limit. The minimum MT rate that can support this bolometric luminosity for a non-rotating neutron star is $\dot{M}_{\rm min} = 3.5 \pm 0.8 \times 10^{-8}$ M$_{\odot}$yr^{-1} (for a 1.4 $M_{\odot}$ neutron star with a radius of 11.5 km), and if one takes into account only X-ray output, then $\dot{M}^{X}_{\rm min} \approx 2.2 \times 10^{-8}$ M$_{\odot}$yr^{-1}.

There is evidence for the presence of a jet originating at the accretor, for details see Mirabel & Rodríguez (1999). We have not found any data on the possible circumbinary disk, which means that the non-conservative mode of MT, in which the specific angular momentum of the lost material

Table 6.3: Observational properties of Sco X-1

Quantity	Value	Reference
Mass ratio	$\approx$0.30 but $\lesssim$0.46	S02
Donor spectral class	later than K4	M15
Donor luminosity class	IV	M15
Period, d	0.787313$\pm$0.000015	H12
Distance, kpc	2.8$\pm$0.3	B99
X-ray flux [2-20keV], erg s^{-1} cm^{-2}	$2.4 \cdot 10^{-7}$	B99
Bolometric flux, erg s^{-1} cm^{-2}	$3.88 \cdot 10^{-7}$	W08

Sources: S02 – Steeghs & Casares (2002), H12 – Hynes & Britt (2012), B99 – Bradshaw et al. (1999), W08 – Watts et al. (2008), M15 – Mata Sánchez et al. (2015).

is equal to that of the accretor is plausible. The possible transient nature of Sco X-1 has, to our knowledge, never been discussed, which implies that it is in a steady state, in which the relationship between accretion rate and X-ray luminosity stays roughly the same with time.

6.3.2 Magnetic braking

It is widely accepted that magnetic braking – the removal of angular momentum from a rotating star by the action of a magnetically coupled stellar wind – is crucial for studies of the formation and evolution of a number of classes of close binaries. It has been most deeply addressed for the case of cataclysmic variables (for details, see Knigge et al., 2011), but it also plays an important role for LMXBs.

It was Schatzman (1962) who recognized first that the slowing down of single stars can take place when the material lost from the stellar surface is kept in co-rotation with the star by the magnetic field. As a result, the specific angular momentum carried by the gas is significantly greater than in a spherically symmetric stellar wind. The corotation can be achieved if a star possesses a substantial magnetic field. The strength of the magnetic field has been linked to the generation of a magnetic field by dynamo action in a deep convective envelope.

Skumanich (1972) had found observationally that, in MS stars of spectral class G, the equatorial rotation velocities decrease with time, t, as $t^{-0.5}$. This timescale of angular momentum removal can take place if the rate of angular momentum loss, $\dot{J_{\rm MB}}$, is proportional to Ω^3, where Ω is the stellar rotational velocity. After being calibrated to the observed angular momentum losses in main sequence stars in open clusters, this law is usually referred to as the Skumanich magnetic braking law, and can be written in a generic form as considered by Rappaport et al. (1983):

$$\dot{J_{\rm mb,Sk}} = -3.8 \cdot 10^{-30} M R_\odot^4 \left(\frac{R}{R_\odot}\right)^\gamma \Omega^3 \text{ dyne cm} . \tag{6.6}$$

Here M and R are the mass and radius of the star that is losing its angular momentum via magnetic braking, and γ is a dimensionless parameter from 0 to 4. Magnetic braking is observationally absent in low-mass MS stars; this was linked to the possible halt of the dynamo mechanism in almost fully convective MS stars. For fast rotators, it has been discussed that the dipole magnetic field can create a dead zone that traps the gas, or alternatively that once B has reached some maximum value, it saturates and can not increase any further (e.g. Mestel & Spruit, 1987; Ivanova & Taam, 2003; Andronov et al., 2003). In either case, $\dot{J_{\rm MB}}$ has a shallower dependence on Ω, approaching Ω^2, and its value is smaller than the Skumanich law would predict.

Let us estimate what MT rate the Skumanich magnetic braking provides. For a binary system with a mass ratio $q = 0.3$ and assuming a conservative MT, one can find that the accretion rate is

$$\frac{\dot{M}}{M} \approx -2\frac{\dot{J_{\rm MB}}}{J_{\rm orb}} \tag{6.7}$$

and

$$\begin{aligned} \dot{M} &= 6.1 \cdot 10^{-9} M_\odot \text{yr}^{-1} \times \\ &\left(\frac{R}{R_\odot}\right)^\gamma \left(\frac{a}{R_\odot}\right)^{-2} \left(\frac{1\text{day}}{P_{\rm orb}}\right)^2 \frac{M+M_2}{M_2} \frac{M}{M_\odot} . \end{aligned} \tag{6.8}$$

Here M_2 is the mass of the binary companion. For a system of a 0.4 $M_\odot$ subgiant and a 1.4 $M_\odot$ neutron star at the observed period, the Skumanich prescription with γ from 0 to 4, $\dot{M} = 2.6$ to 6×10^{-10} $\text{M}_\odot\text{yr}^{-1}$. Clearly, as was found in the previous studies, the Skumanich law provides the MT rate that is two orders of magnitude lower than the observed mass accretion rate, and is independent of how we evolve the star.

We note however that Sco X-1 is an evolved star. In this case, it is important to realize that the Skumanich magnetic braking law was *scaled* to match the observations of MS stars. This implicitly included two assumptions: (i) the wind mass loss is at the MS rate, and (ii) the magnetic field strength is only changing with the angular velocity.

Let us consider how these two quantities can affect the rate of angular momentum loss via magnetic braking. From continuity, and assuming an isotropic wind;

$$\dot{M}_{\rm w} = 4\pi R_{\rm A}^2 \rho_{\rm A} v_{\rm A} = 4\pi R^2 \rho_{\rm S} v_{\rm S} \ . \tag{6.9}$$

Here $R_{\rm A}$ is the radius of the Alfven surface, $\rho_{\rm A}$ and $v_{\rm A}$ are the density and the speed of the material that crosses it; R is the radius of the star, $\rho_{\rm S}$ and $v_{\rm S}$ are density and velocity of the wind at the star's surface. The angular momentum loss through the Alfven surface is then

$$\begin{aligned} \dot{J}_{\rm MB} &= -4\pi\Omega \int_0^{\pi/2} \rho_{\rm A} v_{\rm A} R_{\rm A}^2 (R_{\rm A}\sin\theta)^2 \sin\theta d\theta \\ &\simeq -\frac{2}{3}\dot{M}_{\rm w}\Omega R_{\rm A}^2 \end{aligned} \tag{6.10}$$

Here we assumed for simplicity that $R_{\rm A}$ does not depend on θ, which is not necessarily true. The Alfven surface is defined as the surface where the wind speed $v_{\rm w}$ becomes the Alfvenic speed, v_A, or in other words, the magnetic pressure and ram pressure are balanced (e.g., Mestel, 1968; Mestel & Spruit, 1987)

$$\frac{1}{2}\rho_{\rm A} v_{\rm A}^2 \simeq \frac{B(r)^2}{8\pi} \ . \tag{6.11}$$

In the case of a radial magnetic field $B(r) = B_{\rm S}R^2/r^2$, and in a case of a dipole field, $B(r) = B_{\rm S}R^3/r^3$, where B_S is the surface magnetic field. For a radial field,

$$\frac{1}{2}\rho_{\rm A} v_{\rm A}^2 \simeq \frac{B_{\rm S}^2}{8\pi}\frac{R^4}{R_{\rm A}^4} \ . \tag{6.12}$$

To close the system, one more important assumption is needed, about the wind velocity along the magnetic streamlines, and this is where most of the uncertainty is hidden. The most often considered option is to assume that the system is isothermal. Then one can consider the generalized Bernoulli equation for a rotating system inside the co-rotating zone (e.g., Equation A8 in Mestel & Spruit, 1987) . In this case, it can be shown that the velocity at the Alfven surface is reduced to the wind sonic velocity c_w(Mestel & Spruit, 1987); then

$$R_{\rm A} \simeq B_{\rm S}\frac{R^2}{\sqrt{\dot{M}c_{\rm w}}} \ . \tag{6.13}$$

With the further standard assumption of $B_{\rm S} = B_0\Omega$ (later in this Section we will show where this assumption comes from) we recover the same functional dependence as in the empirical Skumanich law (see Equation 6.6):

$$\dot{J}_{\rm MB} \propto B_{\rm S}^2 \Omega R^4 \propto B_0^2 \Omega^3 R^4 \ . \tag{6.14}$$

For a dipole field and a similar thermally-driven wind, one can similarly obtain

$$R_{\rm A} \simeq B_{\rm S}^{1/2} \frac{R^{3/2}}{(v_{\rm A}\dot{M}_w)^{1/4}} \tag{6.15}$$

An additional assumption that the isothermal wind velocity is of order the surface escape velocity when it reaches the Alfven surface (Justham et al., 2006) leads to

$$R_{\rm A} \simeq B_{\rm S}^{1/2} \frac{R^{13/8}}{(\sqrt{2GM}\dot{M}_w)^{1/4}} \tag{6.16}$$

and produces a functional dependence of the form (Justham et al., 2006)

$$\dot{J}_{\rm MB} \propto \dot{M}_w^{1/2} B_{\rm S} R^{13/4} \Omega \propto \dot{M}_w^{1/2} R^{13/4} \Omega^2 \ . \tag{6.17}$$

If one assumes that the Bernoulli equation is legitimate, then the other two limiting cases are that the velocity at the Alfven surface can be reduced either to the local escape velocity, or is of order $\sim \Omega R_{\rm A}$. These assumptions will lead to different powers of Ω and stellar wind mass loss rate in the magnetic braking torque, thus there is no unique way to obtain $\dot{J}_{\rm MB}$. This uncertainty is also reflected in the existence of several prescriptions for the magnetic braking law, and the use of a free value for the parameter γ in the prescription of Equation 6.6.

Compared to main sequence stars, subgiants are generally colder, and hence the assumption of isothermal wind velocity inside the Alfven sphere may not hold – not even considering that the wind can be accelerated by the magnetic fields. Indeed, even for the Sun, we know that the temperature of the wind is substantially higher than the surface temperature, and also that the wind is both heated and accelerated via several mechanisms (e.g., Cranmer et al., 2007). Therefore, the generalized, albeit convenient, Bernoulli equation as in Mestel & Spruit (1987) is not valid.

Similarly to the Sun, it was found in MHD simulations of red giant winds that they are also accelerated (Suzuki, 2007). Unlike the Sun, red giant winds are also structured, and can form bubbles, and hence a method that assumes the existence of the Alfven sphere might not be applicable. We can nonetheless examine what self-consistent winds (Suzuki, 2007) in a radial field may imply, by considering their red giant models that are closest to the case of Sco X-1 donor, models II and III. Importantly, in their models, density drops with distance as $\propto R^{-3}$. As a result, from continuity, velocity grows linearly with distance. At the Alfven surface, the velocity of the wind may reach a value that is about the surface escape velocity (we recognize that this not necessarily the case for larger giants where the winds are slower than surface escape velocity, see also discussion in

Cranmer & Saar, 2011). Then $R_{\rm A}$ can be expressed only using the surface values of the star, with the direct dependence on $\dot{M}_{\rm w}$ disappearing,

$$R_{\rm A} = \frac{B_{\rm S}^2}{8\pi} \frac{R^2}{GM\rho_{\rm S}} \ , \tag{6.18}$$

where $\rho_{\rm S}$ is linked to the density at the wind base and is determined by hydrostatic equilibrium in the stellar photosphere (Suzuki, 2007). As a result, we arrive at the functional form for the rate of loss of the angular momentum in a red giant as

$$\dot{J}_{\rm MB} \propto \dot{M}_{\rm wind} \Omega B_{\rm S}^4 R^4 \ . \tag{6.19}$$

Note that here the dependence on the wind ML rate does not disappear, unlike the standard case that is the isothermal solution in a radial field. A similar consideration of a dipole field would produce an angular momentum loss rate that is proportional to $\dot{M}_{\rm wind} \Omega B_{\rm S}^{4/3} R^{8/3}$. As one can see, varying the geometry of the magnetic field changes the power law with which the magnetic field enters in the functional form. But it is the assumptions on reaching the Alfven surface for the stars' surface escape velocity and on the density profile that keep the functional form proportional to the wind mass loss rate.

Now we address the surface value of the magnetic field. It has been discussed in the past that the dynamo activity scales with the dynamo number N_D (e.g., Parker, 1971; Hinata, 1989; Meunier et al., 1997). The dynamo number is related to the Rossby number as $N_{\rm D} \sim Ro^{-2}$, where Rossby number is defined as $Ro = 1/(\Omega\tau_{\rm conv})$, where $\tau_{\rm conv}$ is the convective turnover time (Noyes et al., 1984). Ivanova (2006) has discussed that in LMXBs with donors that are not on the MS, this has to be taken into account as

$$B_{\rm S} = B_{\rm S}^0 \frac{\tau_{\rm conv}}{\tau_{\rm conv}^0} \frac{\Omega}{\Omega^0} \ . \tag{6.20}$$

Here the indices "0" are for values of some star with respect to which the magnetic braking law should be calibrated.

Considering the two factors discussed above, we propose to examine the angular momentum loss rate that is equivalent to consideration of the Skumanich law in Equation (6.6) but with two additional scaling ("boost") factors, wind-boost and τ-boost:

$$\dot{J}_{\rm MB} = \frac{\dot{M}_{\rm w}}{\dot{M}_\odot} \left(\frac{\tau_{\rm conv}}{\tau_{\rm conv}^\odot} \right)^\eta \dot{J}_{\rm MB,Sk} \ . \tag{6.21}$$

The power η with which the τ-boost enters in the equation can vary, it is two for the empirical Skumanich law and can be as high as four in the case of a giant wind as discussed above (see

Table 6.4: Magnetic braking in an unperturbed 1 $M_\odot$ star

$\log_{10}(R/R_\odot)$	$\dot{M}_{\rm Reim}/\dot{M}_\odot$	$\tau_{\rm conv}/\tau^\odot_{\rm conv}$
0.27	4	3.7
0.95	260	9.2
1.23	1413	9.9
1.43	4500	11.0
1.57	10325	11.8

$\tau_{\rm conv}$ – convective turnover timescale. Wind is calculated as in Reimers (1975).

Equation 6.19).

To account for the wind-boost, for the solar wind loss rate we take $\dot{M}_\odot = 2.5 \cdot 10^{-14}\ M_\odot$ per year (Carroll & Ostlie, 1995). For subgiant and giant wind mass loss rates, we adopt the standard Reimers wind prescription (Reimers, 1975):

$$\dot{M}_{\rm Reim} = 4 \cdot 10^{-13} \frac{R}{R_\odot} \frac{L}{L_\odot} \frac{M_\odot}{M}\ {\rm M_\odot yr^{-1}}\ , \tag{6.22}$$

where L is donor's luminosity. The values of the expected boost in an unperturbed 1 $M_\odot$ giant are provided in Table 6.4. We ran the same accretion rate estimate for the magnetic braking prescription as in Equation 6.21, where in order to obtain L we took into account the donor's effective temperature. If the boost by the convective turnover time (which we can only find when a proper giant model with lost mass will be obtained) is neglected, we obtain 0.74 to 1.7×10^{-8} $\rm M_\odot yr^{-1}$, which is close to the observed range.

6.3.3 Detailed evolution and MT

For the simulation of binary MT through the inner Lagrangian point (L_1), we use our framework (Pavlovskii & Ivanova, 2015b) based on the `MESA` code[1]. `MESA` is a modern set of stellar libraries described in Paxton et al. (2011a, 2013). We obtain the binary evolutionary tracks for systems with varying initial parameters. The donor mass at ZAMS was varied from 0.9 to 1.8 $M_\odot$ and the initial neutron star mass was varied from 1.24 to 1.6 $M_\odot$. For a fixed combination of masses from these ranges we adjust the initial period to find the tracks that pass as close as possible to the point of $q = 0.30$, $P = 0.787$, which corresponds to the observed parameters of Sco X-1. We use solar metallicity for the donor.

[1]Modules for Experiments in Stellar Astrophysics, http://mesa.sourceforge.net

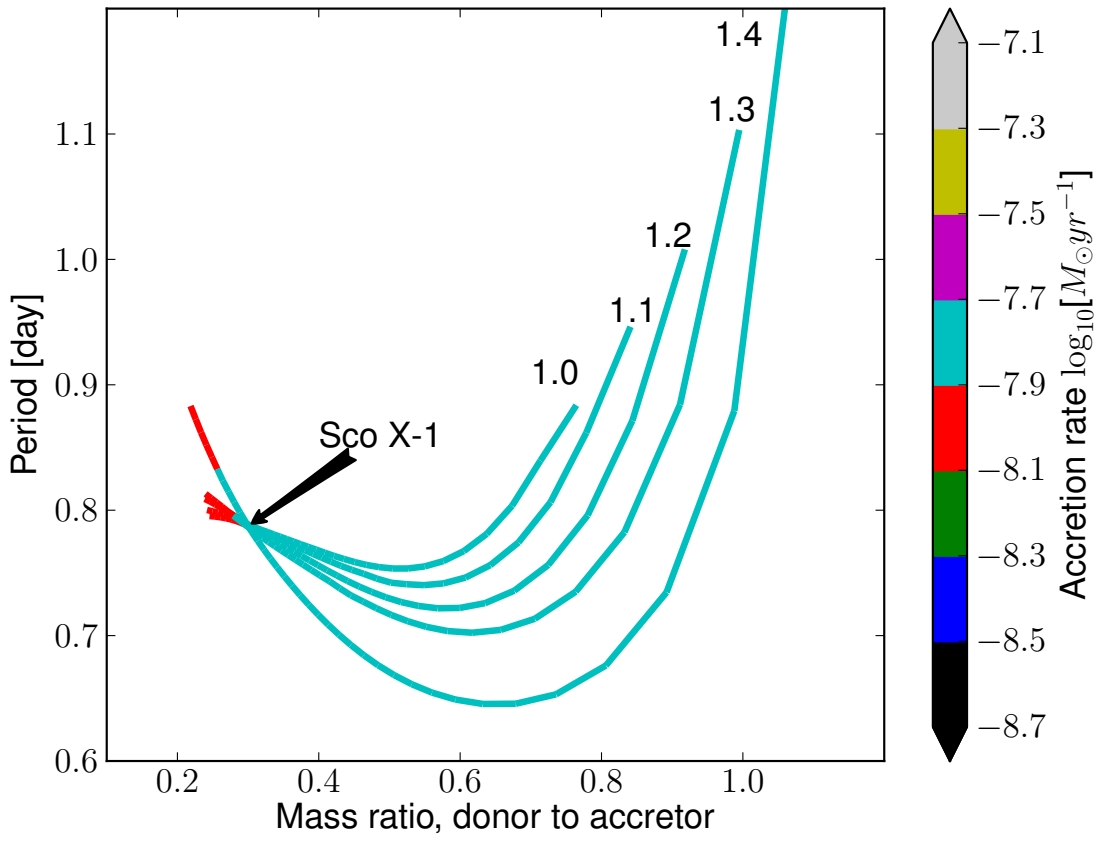

Figure 6.8: Models employing the "wind-boosted" magnetic braking law, given by Equation 6.21. Each track corresponds to the evolution of a binary system that crosses the point corresponding to the observed parameters of Sco X-1, i.e. $q = 0.30$, $P = 0.787$. Tracks start when more than 0.01 $M_\odot$ has been accreted. The numbers denote the initial donor masses in solar masses. The initial NS (accretor) mass for all tracks is 1.3 $M_\odot$. Color denotes current mass accretion rate. Note that these simulated mass accretion rates agree with observations.

We assume that the compact companion was already a neutron star when the initially less massive star overfilled its Roche lobe for the first time at the subgiant stage. We assume that the accretion rate is limited by Thomson scattering to $\dot{M}_{\rm Edd,TS} = 4\pi cR/(0.2(1+X))$, where R is the neutron star radius, taken to be 11.5 km, and X is the hydrogen abundance in the outer layers of the donor. The excess material above $\dot{M}_{\rm Edd,TS}$ is assumed to be taken away from the system carrying the specific angular momentum of the accretor.

We also assume that the components are circularized at all times, and that magnetic braking torque applied to the donor brakes the whole system via the tidal interaction. We utilize both the standard and wind-boosted prescriptions for the magnetic braking.

The results of these simulations for both wind-boosted and regular magnetic braking are shown in Figures 6.8, 6.9 and 6.10. As can be seen in Figure 6.8, in the wind-boosted model the accretion rate at the Sco X-1 point becomes closer to the observational estimate obtained in Equation (6.3.1) as the donor's initial mass increases: the rates are respectively 1.4, 1.5, 1.5, 1.5, 1.8, 2.0 $\times 10^{-8}$ $M_\odot yr^{-1}$, whereas the observed rate is 2.2 $\times 10^{-8}$ $M_\odot yr^{-1}$. Note also that the obtained value of accretion rate is close to the estimate obtained in Section 6.3.2. For the models utilizing the regular magnetic braking prescription (Fig. 6.9), accretion rates vary from 0.1 to 0.2 $\times 10^{-8}$ $M_\odot yr^{-1}$, which is more than an order of magnitude less than that observed.

Varying the initial mass of the NS and taking more massive donors does change the shape of the tracks that pass through the Sco X-1 point, but the key feature remains unchanged: the wind-boosted tracks have mass accretion rates at the Sco X-1 point comparable to the observations – for all tracks the mass accretion rate at the Sco X-1 point is 2.0 $\times 10^{-8}$ $M_\odot yr^{-1}$, while the unboosted tracks lack this agreement, reaching a maximum accretion rate of 0.4 $\times 10^{-8}$ $M_\odot yr^{-1}$ (see Figures 6.10 and 6.11).

We find that systems with a more massive initial NS mass and donor mass experience non-conservative MT at the Sco X-1 point. For these systems, in the order of increasing donor ZAMS mass from 1.5 $M_\odot$ to 1.9 $M_\odot$, the MT rates are 2.3, 2.7, 3.3, 3.3, 2.5 $\times 10^{-8}$ $M_\odot yr^{-1}$ (see Figure 6.11). Among the tracks shown in Figure 6.8, only the one obtained with a 1.5 $M_\odot$ donor ZAMS mass is non-conservative with MT rate 2.2 $\times 10^{-8}$ $M_\odot yr^{-1}$. All tracks obtained with the classical MB prescription have conservative MT at the Sco X-1 point.

The effective temperature of the donor is 4661 K for a 1.0 $M_\odot$ donor and a 1.3 $M_\odot$ NS, and increases further with both initial donor mass and NS mass. For example, a 1.1 $M_\odot$ donor with a 1.3 $M_\odot$ NS would already have $T_{\rm eff} = 4692$ K and a 1.0 $M_\odot$ donor with a 1.42 $M_\odot$ NS has $T_{\rm eff} = 4710$ K. Because the maximum effective temperature of the donor is 4800 K, systems with donor ZAMS mass $\gtrsim 1.6$ $M_\odot$ are unlikely to be the progenitors because in this case even for a

$1.3M_\odot$ neutron star the resulting effective temperature of the donor exceeds the 4800 K limit. If we fix the mass of the neutron star at 1.42 $M_\odot$, then based on the observed accretion rate, the most likely ZAMS mass of the donor is between 1.4 and 1.5 $M_\odot$.

Finally one can estimate to what degree the difference in convective turnover timescale could affect these results. For this estimate one needs to know how the convective turnover time of the donor at the Sco X-1 point relates to the solar convective turnover time. In our models the ratio $\tau_{\rm conv}/\tau^{\odot}_{\rm conv}$ at the Sco X-1 point reaches 4. The magnetic braking torque could be additionally boosted by this factor, however this will not affect the mass accretion rates in those models, which already accrete at the Eddington rate, e.g. those shown in Figure 6.11. We note that without any wind boost, and only considering the boost of the magnetic field due to convective turnover, the observed accretion rates can also be achieved, but we do not have detailed tracks for this case. We note that in the case when wind-boosting is not taken into account, η should be taken as 2 in Equation 6.21.

Using the wind-boosted MB law, for every considered combination of the initial masses of the donor and compact object we were able to find the initial period that led the binary system to the observed period and mass ratio of Sco X-1 and to an accretion rate comparable to that of Sco X-1. None of the above combinations required us to set the initial orbital period of the binary to less than 1.15 days.

We find two-mode behavior that depends on whether the initial MT is conservative MT (with a donor less massive than $\sim 1.5\ M_\odot$) or non-conservative MT (donor more massive than $\sim 1.5\ M_\odot$). If the donor is less massive than about 1.5 $M_\odot$, the more massive a donor is, the weaker the dependence of the final period (at $q = 0.3$) is on the initial period. For donors more massive than $1.5M_\odot$ the tendency reverses: the higher is the donor mass, the stronger is the dependence of final period on the initial period.

6.3.4 Conclusion

We have conducted detailed simulations of the binary evolution of Sco X-1. Our simulations show that the commonly used prescription for magnetic braking, which is based on the observations of MS stars, does not work in the case of Sco X-1, where the donor is an evolved star (subgiant). Namely it provides a substantially lower mass accretion rate than observed, by at least an order of magnitude.

We suggest a different model of magnetic braking, which is suitable for stars with strong winds, such as the subgiant donor in Sco X-1. It turns out that this new model makes possible the formation of a binary system with parameters that closely match Sco X-1 from a wide range of progenitor

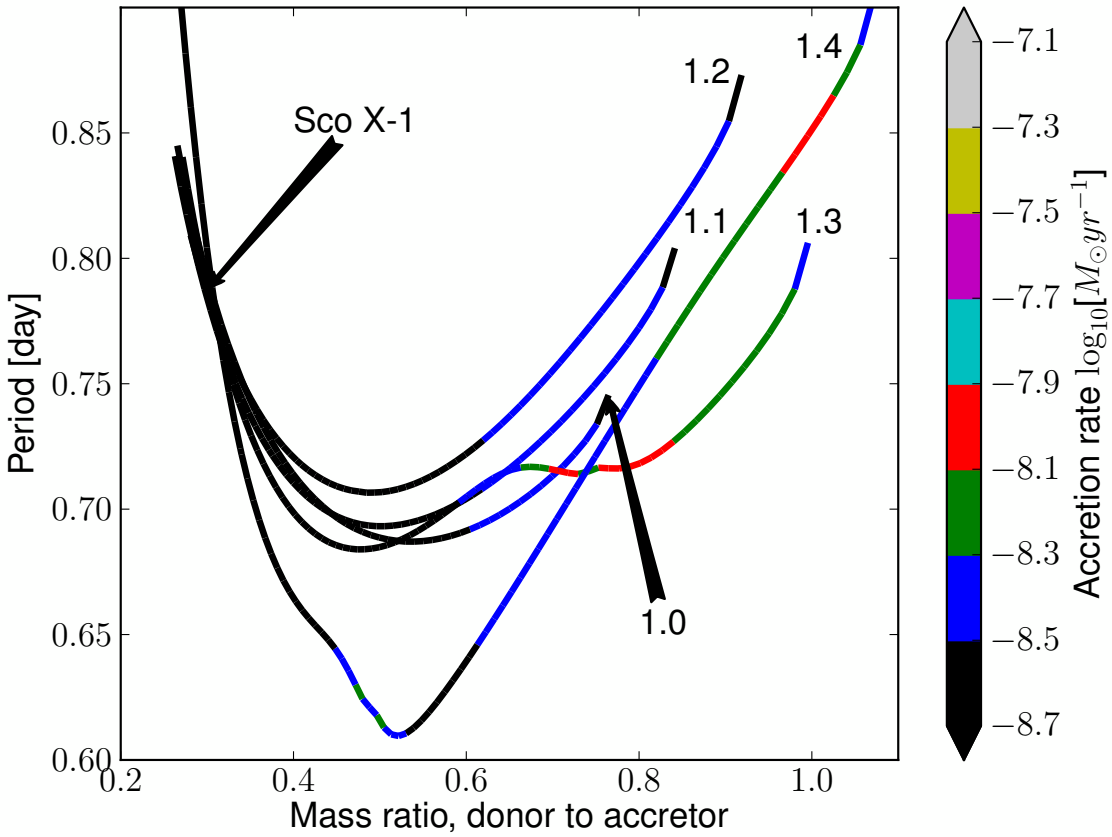

Figure 6.9: Same as in Figure 6.8, but employing the conventional magnetic braking law, given by Equation 6.6 with $\gamma = 3$. Note that the simulated mass accretion rates disagree with observations.

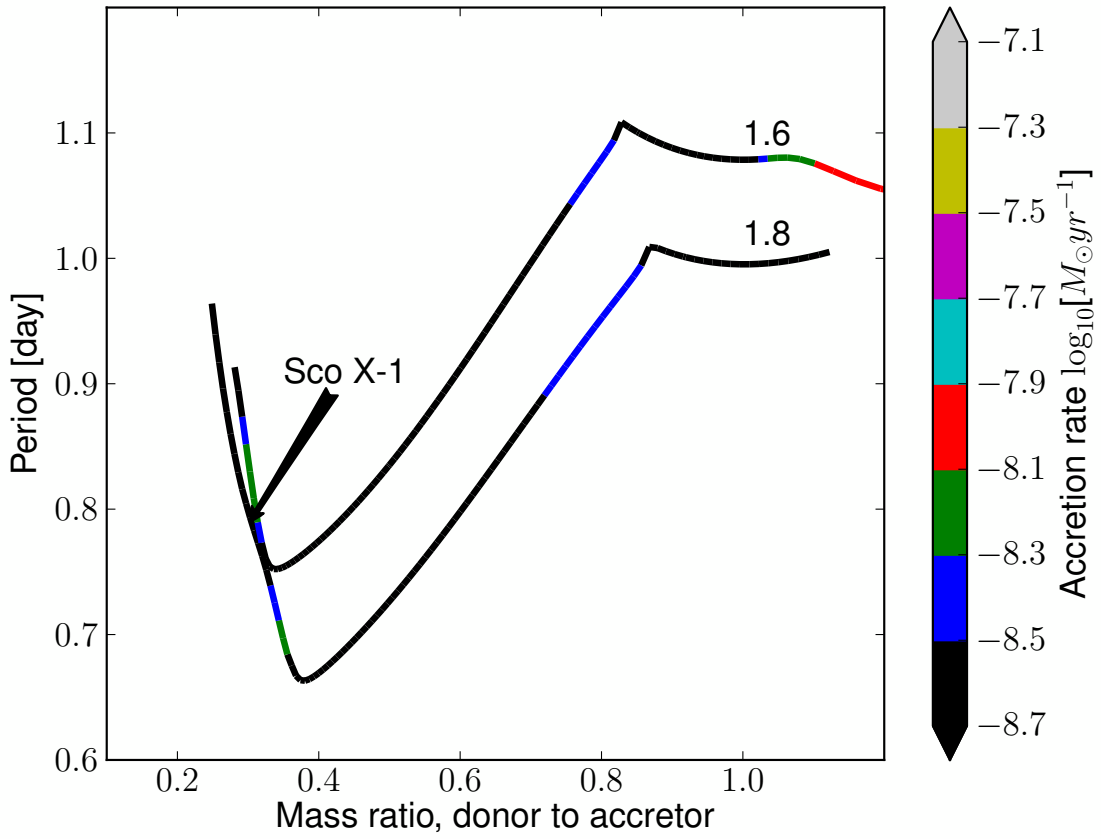

Figure 6.10: Same as in Figure 6.9, but for initially more massive donors and initial NS mass 1.42 $M_\odot$. The simulated mass accretion rates are still too low.

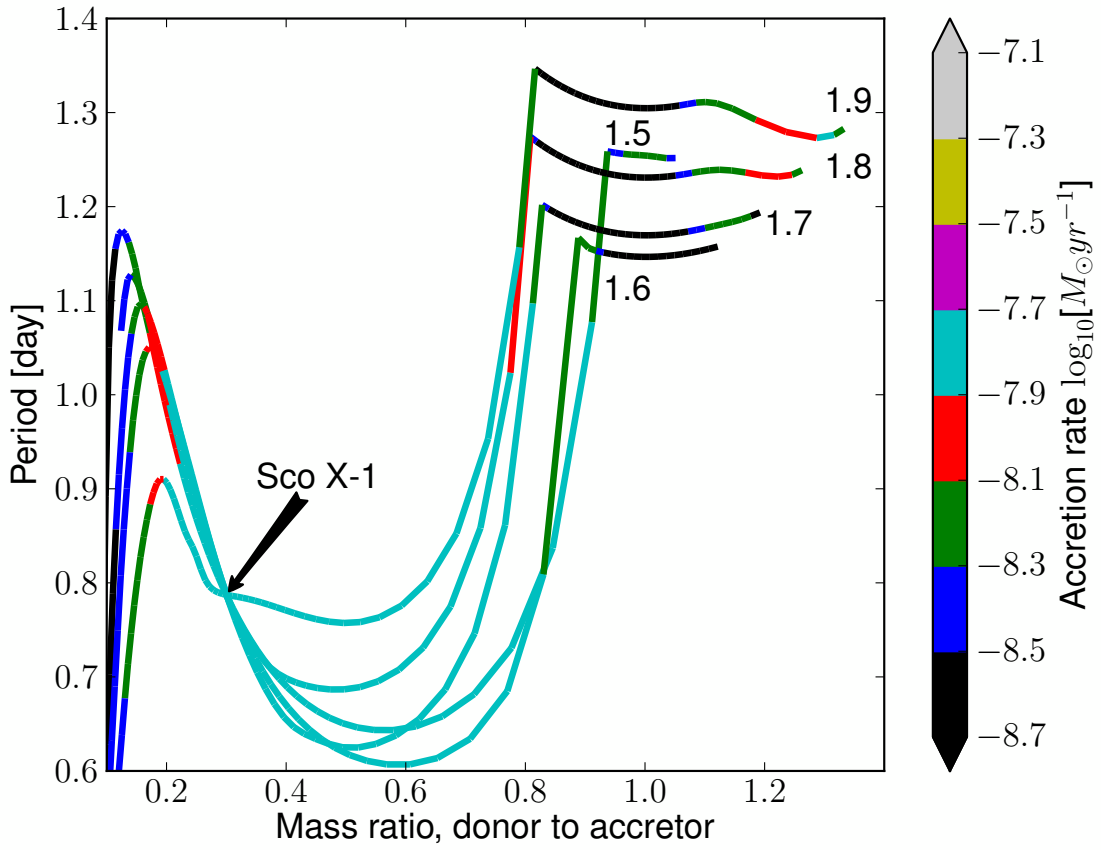

Figure 6.11: Same as in Figure 6.8, but for initially more massive donors and initial NS mass 1.42 $M_\odot$. The simulated mass accretion rates agree with observations.

systems. In select models (see Fig. 6.11) with the observed period and mass ratio of Sco X-1 we obtain as little as $\approx 10\%$ discrepancy between the simulated and observed accretion rate and in all cases the accretion rate is comparable to the observations. The commonly used prescription gives an accretion rate approximately an order of magnitude lower than observed.

Based solely on the known period, mass ratio and accretion rate, we couldn't constrain the parameters of the possible progenitor system. By varying the initial period we were able to obtain a binary with the observed period, mass ratio and comparable mass accretion rate from initial NS masses in the range of 1.24 to 1.6 $M_\odot$ and donor ZAMS masses from 1.0 to 1.6 $M_\odot$. However, based on the maximum observed effective temperature of the donor, which is 4800 K, the systems with donor ZAMS mass $\gtrsim 1.6\ M_\odot$ are unlikely to be the progenitors because in this case even for a $1.3 M_\odot$ neutron star the resulting effective temperature of the donor exceeds the 4800 K limit. We find that the effective temperature of the Sco X-1 donor rises with both the donor ZAMS mass and the initial NS mass. Under the standard assumption that the NS mass is 1.42 $M_\odot$, the most likely ZAMS mass of the donor is from 1.4 to 1.5 $M_\odot$, based on the observed accretion rate.

Keeping in mind the existing problems with binary simulations of the known LMXBs, we anticipate that this new magnetic braking model can (and should) be used in the simulations of other LMXBs with giant or subgiant donors and compact accretors. For example, for the majority of LMXBs mentioned in Podsiadlowski et al. (2002), the observed mass accretion rate is approximately an order of magnitude higher than expected. There is also a major mismatch between the observed period decay in A0620-00 and the period decay expected for this system from the standard magnetic braking prescription. The observed decay is ~ 0.6 ms yr^{-1} (González Hernández et al., 2014). An estimate that assumes conservative MT and the standard MB law with $\gamma = 3$ (Equation 6.6) provides the period decay to be ~ 0.05 ms yr^{-1} (see also for discussion González Hernández et al., 2014). Applying the wind-boosted modified magnetic braking law we obtain the decay of 0.35 ms yr^{-1}, which is closer to the observed value; a τ-boost that increases the surface magnetic field can explain the remaining discrepancy. We note that this system is a candidate circumbinary disk system (Wang & Wang, 2014), and hence may have an additional mode for the angular momentum loss.

The LMXBs in elliptical galaxies, where they are thought to be the main source of X-ray radiation, can be observed with quite low detection limits of $\sim 10^{36}$erg s^{-1}. These data can be used in conjunction with population synthesis models to examine the formation scenarios of LMXBs. When an X-ray luminosity function (XLF) of an elliptical galaxy is simulated with population synthesis models, it turns out to be very sensitive to the MB prescription used (Fragos et al., 2008). Depending on the other free parameters of the population synthesis model, the discrepancy between

XLFs obtained from different MB prescriptions reaches an order of magnitude. The probability that a simulated XLF is consistent with the observed one also differs drastically for different MB prescriptions, from practically zero to comparable to unity, and the majority of population synthesis models still give results that are very unlikely to be consistent with the observations (Fragos et al., 2008). With the boosted model for magnetic braking, we also can foresee that not only mass accretion rates can be different, but also a class of LMXB systems, deemed to be transient with the standard magnetic braking, will become persistent. We anticipate that the new generation of population synthesis models made to simulate the XLF functions of elliptical galaxies, if switched to our modified model of magnetic braking, might give substantially different results.

6.4 MT in ultra compact X-ray binaries

This material in this section is adapted from Pavlovskii & Ivanova (2013) and Heinke et al. (2013).

6.4.1 Too high MT rates in UCXBs

Recent observations show that, at long orbital periods ≥ 40 minutes, there are two groups of UCXBs widely separated in their MT rates (Heinke et al., 2013). The first group is well known and consists of transient sources with very low average MT rates, $\sim 10^{-11} M_{\odot}$ per yr. However, unexpectedly, the other group consists of permanent sources with average MT rates of at least two order of magnitude higher for the same orbital periods (Fig. 6.12). While in the first group an UCXB can belong to either the Galactic field, or be located in the direction of the bulge or in a globular cluster, in the second group all three UCXBs – 4U 1626-67, 4U 0614+09, 4U 1916-053 – belong only to the Galactic field.

The first group of long-period transient UCXBs is rather well understood in terms of MT sequence of cooling WDs (WDs). The consideration that WDs are not completely degenerate at the start of the MT, and hence have some final entropy in the center, provides a range in possible MT rates for the same period. This effect is minimal for large periods, as MT was going on for already very long time and WDs are close to completion of their cooling (Deloye & Bildsten (2003), see also Fig. 6.12).

As for the second group of long-period persistent UCXBs, gravitational wave radiation can not provide such high MT rate even if a WD donor has finite entropy. One alternative is to invoke an angular momentum loss mechanism that is stronger than gravitational wave radiation. Donor wind mass loss (van Haaften et al. 2012; see discussion above) is one possibility. Alternatively, if an accretor does not accept all the donor's material, a circumbinary disk (CBD) could form. A CBD,

[!p]

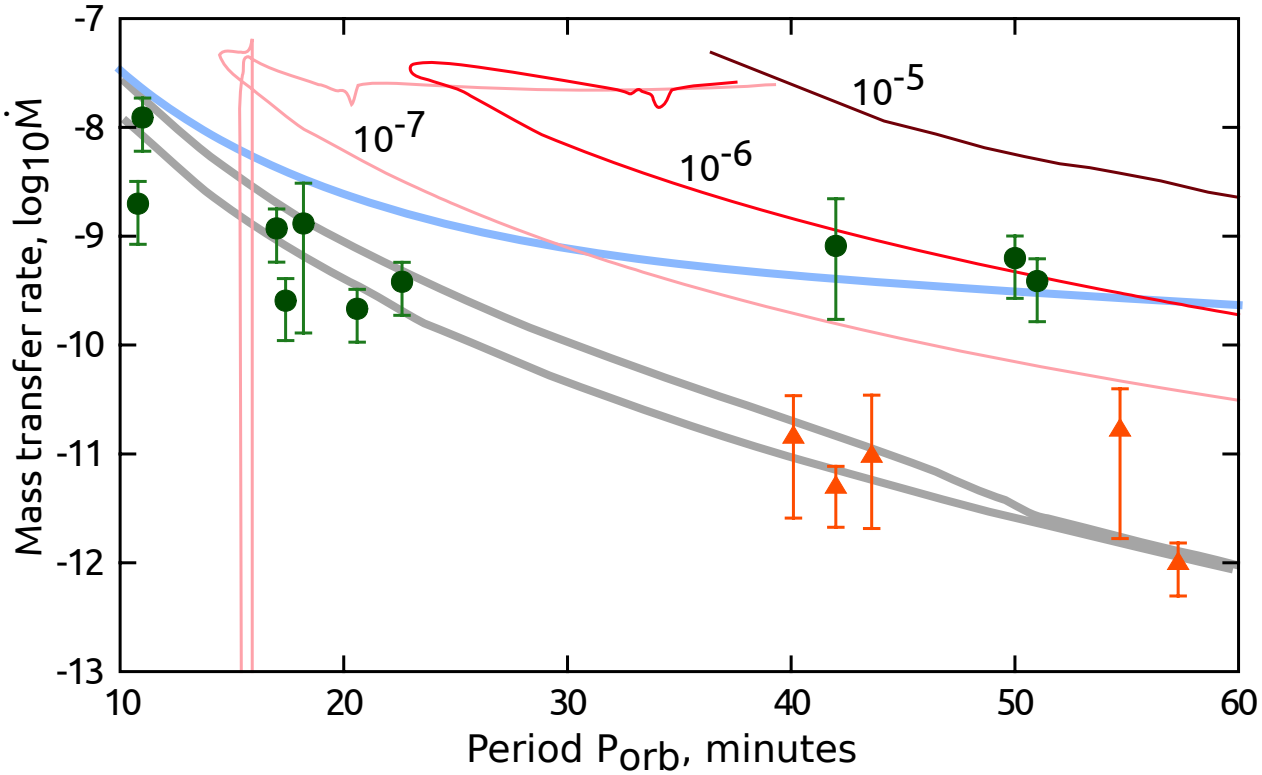

Figure 6.12: Periods and MT rates for observed UCXBs compared to theoretical MT tracks of: a) partially degenerate WD donors (thick solid lines); b) WD donors evolved with a tidal torque of CBD where the mass ending up in CBD is adopted to be 10 times higher than in a calibrated model (thick dashed line); c) He remnants evolved under gravitational wave radiation after their formation with fast initial post-CE mass loss rate (thin lines, mass loss rates are indicated on the diagram in units of $M_{\odot}/yr$). Observational data for persistent sources are shown with circles and ellipses (ellipses denote sources with anomalously high MT rates) and for transient sources with triangles (Heinke et al. (2013)). He remnants were obtained using the stellar evolution code `MESA` (Paxton et al. (2011a)).

as it rotates slower than the binary orbits, provides a tidal torque on the binary, removing its orbital angular momentum (see Spruit & Taam, 2001, for more details on a simple CBD model). The strength of that tidal torque depends on the physics of the CBD, mainly its viscosity and the scale height, as well as on what fraction of the donor's mass loss ends up in the CBD, denoted as δ. The physics of the CBD can be further simplified, as for a standard $\alpha-$viscosity disk the loss of angular momentum takes a simple form (Shao & Li, 2012):

$$\dot{J}_{\rm CBD} = A(GM)^{2/3}\delta\dot{M}_{\rm donor}t^{1/3} \tag{6.23}$$

Here $A = (3\alpha\beta^2/4)^{1/3}$, where α is the viscosity parameter and β is the ratio of the scale height of the disk to its radius; with values for a standard disk $\alpha = 0.01$ and $\beta = 0.03$, $A \approx 0.02$. t is time after the start of the MT. Studies performed for cataclysmic variables suggested that $\delta \ll 1$, and its value is of order 10^{-4} to 10^{-3} (Taam et al., 2003). Further analysis showed that for a standard CBD in a binary system with an orbital period of about 1 hour, $\delta \sim 6\times10^{-4}t_9^{-1/3}$ (where $t_9 = t/10^9$ years; Shao & Li 2012).

Using this formalism, a WD donor can drive a MT rate of $2\times10^{-10}M_\odot$ per yr at a period > 40 minutes (note this is the minimum MT rate in the second group), if the CBD model has $\delta \gtrsim 0.0025$. This is several times larger than it should be for this evolutionary stage, typically $\delta \sim 3\times10^{-4}$. See Fig. 6.12 where we show an example WD track with a very strong CBD included.

A second option begins with an initially slightly evolved MS donor with a helium-rich core, where the orbit shrinks due to magnetic braking, and can reach ultra compact periods (Nelson et al., 1986; Podsiadlowski et al., 2002). Such an evolutionary sequence can produce MT rates of 10^{-9} $M_\odot$/year, and thus explain the second group of systems. This evolution requires rather finely tuned initial parameters to reach ultra compact orbits, producing very few systems with periods below 1 hour, and almost none below 30 minutes (van der Sluys et al., 2005). This evolutionary sequence may leave some hydrogen in the core, a clear observable difference with the other sequences (Nelemans et al., 2010).

6.4.2 Alternative donors

For a third alternative, a He star can be produced by a common envelope event and inspiral via gravitational waves until it makes contact at short periods while still fusing He at its center (see Yungelson 2008; Nelemans et al. 2010; van Haaften et al. 2012). This avoids the fine-tuning difficulties with the evolved main-sequence star evolution. Naked He star donors generally have radii much larger than WDs of the same mass, where this radius is also a function of its final entropy (we demonstrate this dependence in Figs. 6.13 and 6.14, where we show radius and central temper-

ature T_c evolution for a naked He core of a giant with initial mass of 5 $M_\odot$, evolved with different mass loss rates using the stellar code MESA. Once a naked He star is formed – through a common envelope event – it also may start He burning in the core (note that whether it burns or not depends on the naked He star mass). This burning may be fully completed (in the sense that the core is fully converted to a carbon-oxygen core) during the mass loss sequence, depending on the initial post-common envelope binary separation, on how close to the giant tip the donor was before the common envelope event, and how fast the He star is losing mass (see Fig. 6.15). As a result of this burning, a very low-mass carbon-oxygen donor can be formed, although in some cases He fusion is simply stopped by the rapid expansion of the donor and drop of its central temperature. For example, we note that very rapid mass loss leads to donor expansion and cooling, hence burning is rapidly depleted and a C/O core might not form. Continued He burning is more likely to provide an inflated donor, vs. a donor that had a composite He/C/O core before the MT (see Figs. 6.13 and 6.14). At some point, the He donor starts to expand with continued mass loss - note that this can happen due to various reasons, e.g., due to the core's conversion into a C/O core, or to adiabatic expansion due to rapid mass loss. The point where the nuclear burning turns off can also be roughly identified as where the He star tracks begin to expand outwards to longer periods again (see Fig. 6.16).

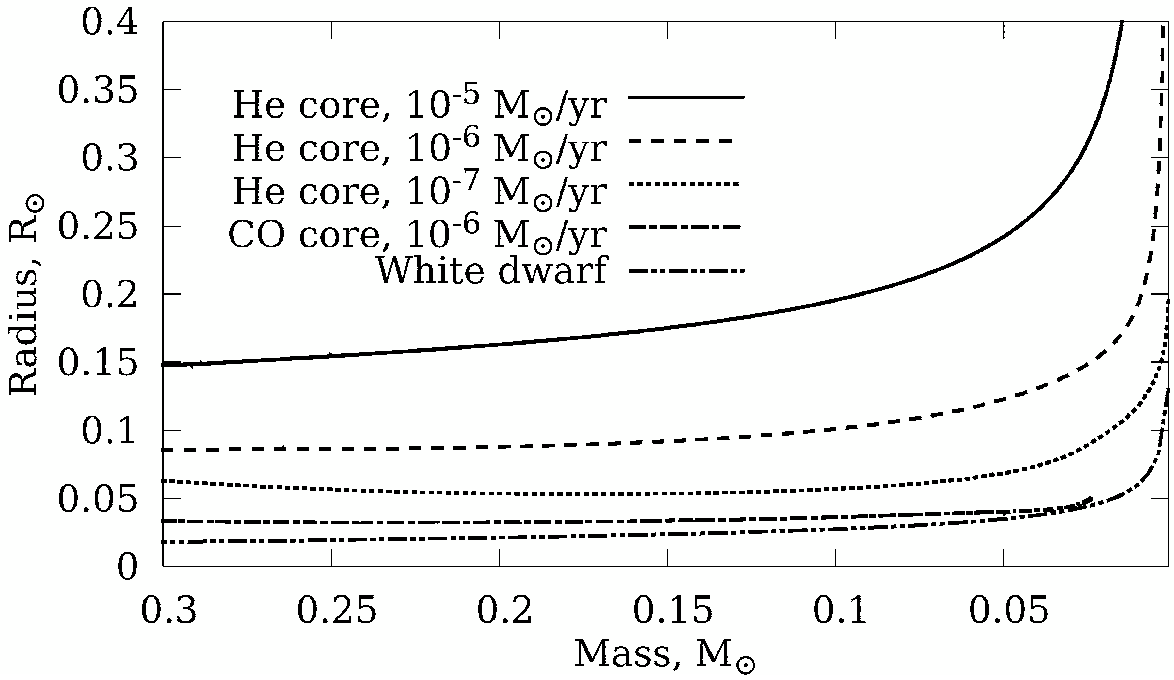

Figure 6.13: Evolution of mass and radius for He stars at different initial mass loss rates from our MESA calculations, including a He star stripped down to its CO core, vs. the evolution of a WD (Tout et al. 1997, their eq. 17, a rough approximation for either He or CO WDs). Note that the radii for He stars are substantially larger than WDs of the same mass.

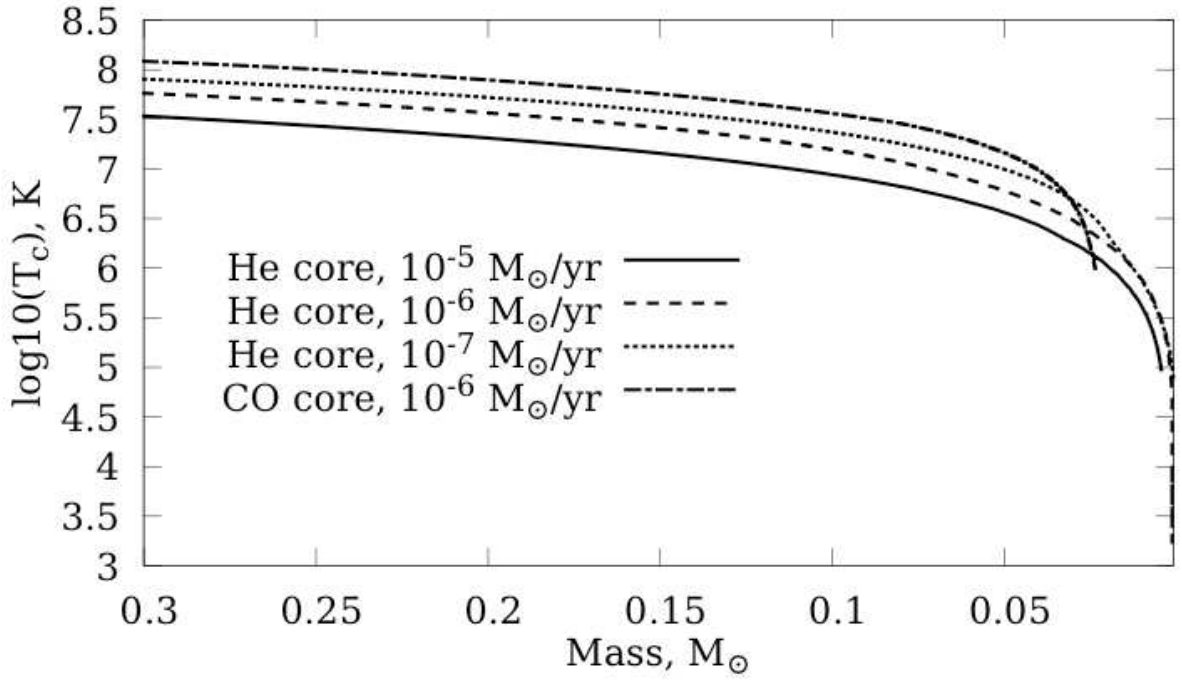

Figure 6.14: Temperature evolution with time of He stars at different initial mass loss rates, including a He star stripped down to its CO core, from our MESA calculations. Note that He stars can retain high central temperatures down to very low masses.

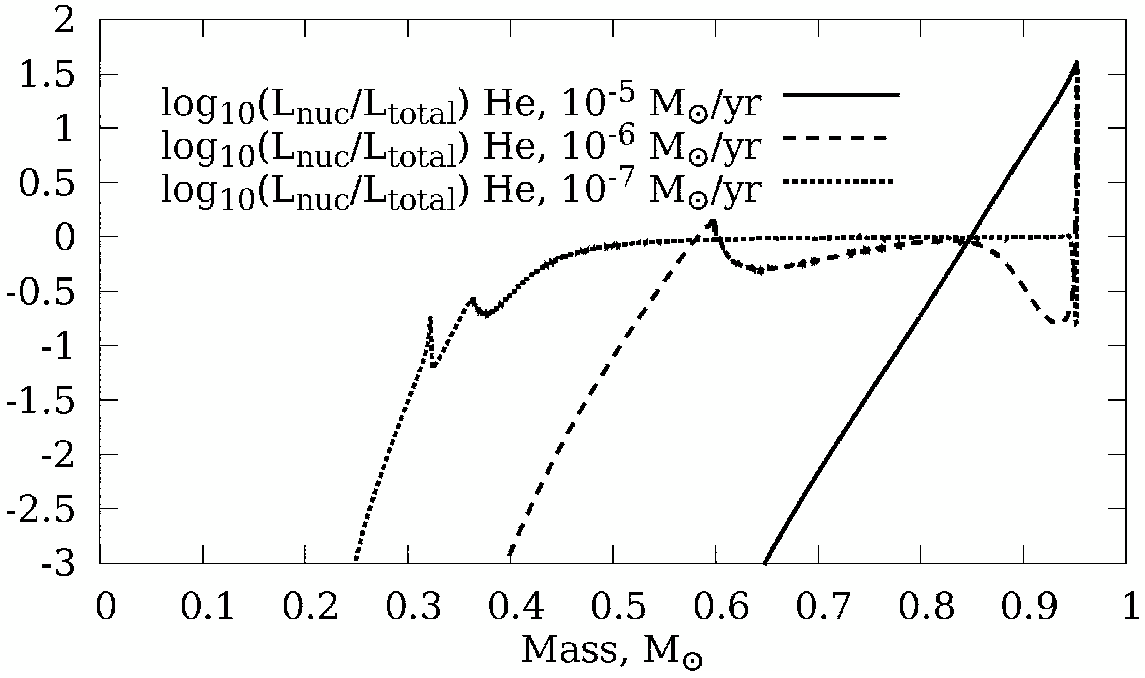

Figure 6.15: Evolution of the nuclear burning luminosity as a fraction of the total luminosity for He stars at different initial mass loss rates from our MESA calculations. Note that the nuclear burning turns off more quickly for higher mass-loss rates due to rapid donor expansion. The large initial nuclear luminosity (which may be larger than the total emitted luminosity) is due to the just-completed common envelope stage.

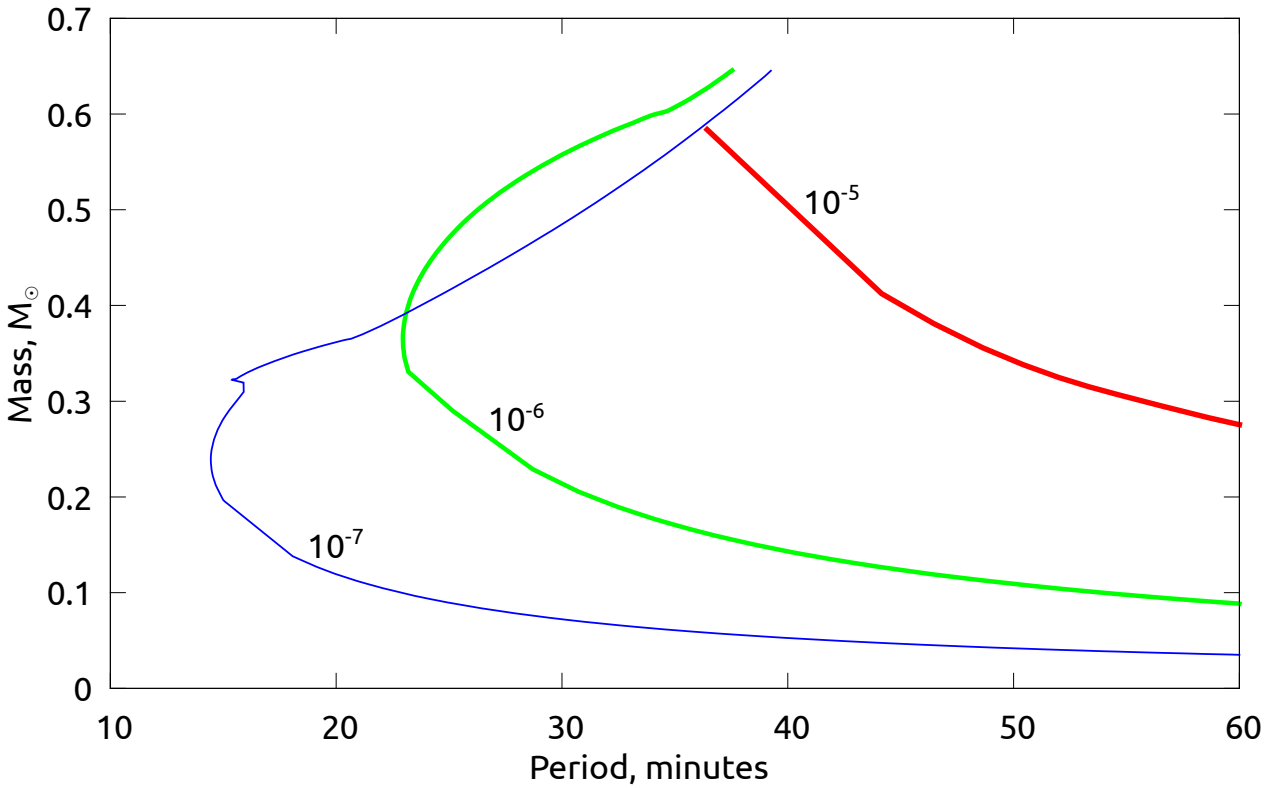

Figure 6.16: Mass evolution vs. orbital period of He stars at different initial mass loss rates; tracks as in Fig. 6.12 These tracks are consistent in masses, orbital periods, and MT rates (see Fig. 6.12) with the known information on 4U 1626-67 and 4U 1916-053.

If a He star *retained* its entropy in the center due to either faster (in the past) MT, or due to nuclear burning, tidal heating, or ongoing irradiation, it can provide the observed MT rates requiring only gravitational wave radiation without invoking a CBD. We tested this situation by applying a fast mass loss rate to a He star model in MESA, and then checking what MT rate this star (which is out of thermal equilibrium) will have if it is in a binary evolving only under gravitational radiation (see Fig. 6.12). Non-degenerate He star cores (appropriate for the intermediate-mass progenitors required) expand upon mass loss from the outer envelope (Deloye & Taam, 2010; Ivanova, 2011; Ivanova et al., 2013a). Thus, they can continue to drive MT as the orbit expands, giving MT rates up to 10^{-3} $M_{\odot}$/year for some fraction of the core. A fully self-consistent calculation of the evolution of He stars in binary systems has not yet been performed, and the stage where the core will stop expanding is not well established. MESA does not include tidal heating or donor irradiation, which could increase the inferred mass loss rates.

If the donor is an (inflated) He star evolving under gravitational wave radiation only, then MT rates do not significantly exceed the Eddington rate during most of the mass loss evolution, while still transferring ~ 0.5 $M_{\odot}$ (Fig. 6.16). If an accretor accepts most of the transferred mass below the Eddington limit, then the NS in such a binary could grow significantly more massive than a NS with a WD donor, potentially forming a NS with $M \gtrsim 2M_{\odot}$. This is in contrast with WD UCXB evolution; cold WDs more massive than 0.08 $M_{\odot}$, upon starting MT, will exceed the Eddington limit (Bildsten & Deloye, 2004), so cannot efficiently transfer more than $\sim$0.1 $M_{\odot}$ to the NS.

He stars may show a wide range of surface abundances, depending on the initial post-common-envelope orbital period, which sets how long the star burns He before MT stops fusion. Nelemans et al. (2010) present extensive calculations of the evolution and abundances of He stars. In the initial, rapid epoch of orbital shrinkage, the outer, unburnt helium layers are consumed (note that this epoch is very brief, $< 10^7$ years, and thus difficult to observe). After period minimum, the C/O fusion products are revealed, though some He is still available. Nelemans et al. (2010) show that wider initial orbital periods (e.g. 200 minutes) give primarily C and O chemical compositions at $P_{orb} > 30$ minutes, with reduced He. This matches the inferred compositions of 4U 1626-67 (substantial C, O, and Ne, Schulz et al. 2001; Werner et al. 2006) and 4U 0614+09 (C and O dominate Nelemans et al. 2004; while X-ray bursts indicate the presence of He without H, Kuulkers et al. 2010). Schulz et al. (2001) claimed an overabundance of Ne in local absorbing material around 4U 1626-67, which would be hard to explain with a He star (or any star hot enough to provide this MT rate), since the Ne can only sink to the core in a cold WD. However, the evidence for overabundant Ne in absorption seems to have disappeared, leaving only the strong Ne X-ray emission lines as more ambiguous evidence for Ne's abundance Krauss et al. (2007).

We note that the He star mechanism to create longer-period, high-mass-transfer systems cannot work in globular clusters, due to the relatively high masses of the initial donors ($>$2.3 $M_{\odot}$) and short lifetimes of the systems (Yungelson, 2008). This is consistent with the lack of UCXB systems with unusually high MT rates for their orbital period, like 4U 1626-67 or 4U 1916-053, in globular clusters. The lack of the He star mechanism in globular clusters also can explain part of the difference in the distribution of orbital periods between globular cluster and field UCXBs (that field UCXBs have longer periods) which was noted by Zurek et al. (2009).

Chapter 7

Conclusion

In this thesis we studied MT in binaries. We introduced several methodological improvements to how MT in binaries is simulated in the following areas:

- Treatment of the outer layers of giant stars in stellar evolutionary codes.
- Response of single stars to mass loss.
- Treatment of MT in binaries on timescales longer than dynamical.
- Criteria for the onset of the common envelope.
- Magnetic braking in systems with giant or subgiant donors.

and applied these methodological improvements to the following problems:

- Stability criteria used in the population synthesis codes;
- Detailed evolution and possible progenitor of Sco X-1 and other low-mass X-ray binaries;
- MT in ultra compact X-ray binaries;

We find that the response of giant stars to mass loss depends on whether recombination in the outer layer of the star is treated correctly. This relates to both radial response (properly treated giants expand less) and the effective temperature of the giant (difference in effective temperature for a properly treated giant could be a high as several times). We also find that the response depends on whether the hydrodynamical term is included in the applied boundary conditions. The use of the appropriate hydrodynamical boundary condition enables us to explain the initial response of the hydrodynamical models subjected to mass loss. This response was found earlier by other authors but wasn't explained correctly.

We suggest an improved scheme of binary MT that among other improvements enables one to track whether or not the equipotential corresponding to the outer Lagrangian point of the donor is overfilled during the MT. At this moment the commonly used L_1 MT schemes become inapplicable. We propose two new criteria for the onset of the common envelope: i) based on how fast the orbital parameters of the binary system evolve, and ii) whether the equipotential of the outer Lagrangian point of the donor is overfilled. We find that they are comparable to each other and both of the criteria predict much more stability for giant donors than the classic criteria. We find that the critical mass ratios for which the MT is unstable are almost twice as large as previously believed, e.g. from 1.6 to 2.2 for conservative MT and even higher for non-conservative MT. We also find that the critical mass ratio gradually decreases to this value as the convective envelope becomes deeper, so underdeveloped giants with shallow convective envelope are capable of even more stable MT. Our modifications to the `MESA` code are implemented in a way that allows anyone to use our MT framework by simply adding a few additional options to their setup.

We also suggest an improved model for the treatment of magnetic braking in the binary systems with giant or subgiant donors, which in our opinion should replace the commonly used prescription based on the Skumanich law, which was calibrated on MS stars. This model takes into account the increased rate of isotropic mass loss from giants and subgiants. Using our improved MT framework based on the `MESA` code (which among other things contains the improved treatment of magnetic braking) we look into the possible detailed evolution and progenitors of the low-mass X-ray binary, Sco X-1. We find that the use of our framework with the new prescription for magnetic braking resolves the long-standing problem of a higher-than-expected mass accretion rate in this system. Based on our simulations we limit the maximum mass of a progenitor to less than 1.6 $M_{\odot}$. We expect that the higher-than-expected mass accretion rates in several other low-mass X-ray binaries can be explained in a similar way.

We find that the new stability criteria for giant and subgiant donors should be taken into account in the modern population synthesis code, StarTrack. The rate of Galactic mergers of the double compact objects that are detectable sources of gravitational radiation will, as we foresee, be substantially affected by these new criteria.

We use our framework to study MT in the ultra compact X-ray binaries. We consider a non-degenerate He-rich remnant after a CE event, which is colder and more inflated than if it was completely degenerate. We place this remnant into the binary and find that it produces a substantially higher MT rate than a degenerate helium WD, at least for a while. This explains the observed high MT rates in some ultra compact X-ray binaries.

Our way of treating MT has, of course, certain limitations.

Heyney-type hydrodynamical treatment of one-dimensional single stars, used in modern stellar codes, is not suitable to study shocks that might appear in the stellar envelope during fast MT. We have also shown that the mixing length theory of convection fails at fast mass loss rates (see Chapter 3). It hints that a new non-local (both temporally and spatially) convective treatment might be necessary in these cases.

We don't treat the process of accretion and the structural changes in the accretor. We use a simple parametrization for the fraction of mass lost from the system and assume that it has accretor's specific angular momentum. Both the fraction of lost mass and its specific angular momentum might vary in time, which may substantially affect the stability thresholds.

The radial response of the donor to mass loss depends very strongly on the relative mass of its radiative He-rich core. This relative core mass, in its turn, depends on the overshooting prescription used for the stellar evolution. There is, therefore, an uncertainty in the stability thresholds caused by the uncertainty in the prescription for overshooting.

We use the Roche model, which involves the ad-hoc assumption of *volume correspondence* to connect the one-dimensional model of the donor star and the three-dimensional MT model. Also, the Roche model doesn't take into account the Euler and Coriolis components of the fictitious force. The former component might only matter if the angular velocity of the system changes appreciably over one period, which happens only in dynamically unstable systems. The latter is known to affect the shape of the gas flows (Lubow & Shu, 1975b). We use simplified assumptions for the shape of the flow and the position of sonic surface.

The complete synchronization of the donor with the orbital angular velocity of the binary, caused by tidal interaction, is assumed in all explicit MT schemes, including ours. This assumption may not always hold for radiative donors or donors with shallow convective envelopes. Note that the same assumption is also used in our model of magnetic braking.

We don't treat optically thin MT in our scheme. For some types of donors, e.g., for low-mass giant donors this type of MT might be important (see Section 4.1.2).

Our explicit MT scheme might not be suitable for those systems that lose a large fraction of mass through the $L2/3$ nozzle, which is sometimes the case for giants with very rarefied envelopes. To treat the MT in these systems one could implement a similar simplified model of gas flows through the $L2/3$ nozzle, which is one of our future goals.

We expect our framework to be mainly applied to simulate MT in various binary systems with compact accretor and a donor that overflows its Roche lobe. It does not necessarily have to be a giant star because our MT scheme is general and can be used with certain modifications (like changing the resolution in potential) for any type of donor. Our stability framework can be used

to explore the formation channels of compact binaries and the mergers of double compact objects, including detecting the delayed dynamical instability in these systems. In general, our framework for MT in X-ray binaries can be used to study the possible progenitors of SN1a supernovae and the spin rates of the black holes. Also, detailed studies of MT in X-ray binaries with neutron stars are important because accretion can spin them up and produce recycled (e.g., millisecond) pulsars, which affects the distribution of their periods.

References

Andronov, N., Pinsonneault, M., & Sills, A. 2003, ApJ, 582, 358

Bachetti, M., Harrison, F. A., Walton, D. J., Grefenstette, B. W., Chakrabarty, D., Fürst, F., Barret, D., Beloborodov, A., Boggs, S. E., Christensen, F. E., Craig, W. W., Fabian, A. C., Hailey, C. J., Hornschemeier, A., Kaspi, V., Kulkarni, S. R., Maccarone, T., Miller, J. M., Rana, V., Stern, D., Tendulkar, S. P., Tomsick, J., Webb, N. A., & Zhang, W. W. 2014, Nature, 514, 202

Baudin, F., Barban, C., Belkacem, K., Hekker, S., Morel, T., Samadi, R., Benomar, O., Goupil, M.-J., Carrier, F., Ballot, J., Deheuvels, S., De Ridder, J., Hatzes, A. P., Kallinger, T., & Weiss, W. W. 2011, A&A, 529, A84

Bedding, T. R. 2011, eprint arXiv:1107.1723

Belczynski, K., Wiktorowicz, G., Fryer, C. L., Holz, D. E., & Kalogera, V. 2012, ApJ, 757, 91

Belkacem, K., Dupret, M. A., Baudin, F., Appourchaux, T., Marques, J. P., & Samadi, R. 2012, A&A, 540, L7

Bildsten, L. & Deloye, C. J. 2004, ApJ, 607, L119

Bildsten, L., Paxton, B., Moore, K., & Macias, P. J. 2012, ApJ, 744, L6

Bowler, M. G. 2010, A&A, 521, A81

Bradshaw, C. F., Fomalont, E. B., & Geldzahler, B. J. 1999, ApJ, 512, L121

Buzasi, D., Catanzarite, J., Laher, R., Conrow, T., Shupe, D., Gautier, III, T. N., Kreidl, T., & Everett, D. 2000, ApJ, 532, L133

Carroll, B. W. & Ostlie, D. A. 1995, An Introduction to Modern Astrophysics (Benjamin Cummings)

Chen, W.-C. & Li, X.-D. 2006, MNRAS, 373, 305

Christensen-Dalsgaard, J. 2011, eprint arXiv:1110.5012

Cox, A. N. 2000, Allen's astrophysical quantities

Cox, J. & Giuli, T. 1968, Principles of stellar structure (GORDON AND BREACH, Science Publishers, Inc.)

Cranmer, S. R. & Saar, S. H. 2011, ApJ, 741, 54

Cranmer, S. R., van Ballegooijen, A. A., & Edgar, R. J. 2007, ApJS, 171, 520

De Donder, E. & Vanbeveren, D. 2004, NewAR, 48, 861

Deloye, C. J. & Bildsten, L. 2003, ApJ, 598, 1217

Deloye, C. J. & Taam, R. E. 2010, ApJ, 719, L28

Dominik, M., Belczynski, K., Fryer, C., Holz, D. E., Berti, E., Bulik, T., Mandel, I., & O'Shaughnessy, R. 2012, ApJ, 759, 52

Dziembowski, W. A., Gough, D. O., Houdek, G., & Sienkiewicz, R. 2001, MNRAS, 328, 601

Eggleton, P. 2006, Evolutionary Processes in Binary and Multiple Stars

Eggleton, P. P. 1967, MNRAS, 135, 243

—. 1973, MNRAS, 163, 279

—. 1983, ApJ, 268, 368

Fomalont, E. B., Geldzahler, B. J., & Bradshaw, C. F. 2001, ApJ, 558, 283

Fragos, T., Kalogera, V., Belczynski, K., Fabbiano, G., Kim, D.-W., Brassington, N. J., Angelini, L., Davies, R. L., Gallagher, J. S., King, A. R., Pellegrini, S., Trinchieri, G., Zepf, S. E., Kundu, A., & Zezas, A. 2008, ApJ, 683, 346

Fragos, T., Linden, T., Kalogera, V., & Sklias, P. 2015, ApJ, 802, L5

Ge, H., Hjellming, M. S., Webbink, R. F., Chen, X., & Han, Z. 2010, ApJ, 717, 724

Giacconi, R., Gursky, H., Paolini, F. R., & Rossi, B. B. 1962, Physical Review Letters, 9, 439

Goldreich, P. & Keeley, D. A. 1977, ApJ, 212, 243

González Hernández, J. I., Rebolo, R., & Casares, J. 2014, MNRAS, 438, L21

Guenther, D. B., Demarque, P., Buzasi, D., Catanzarite, J., Laher, R., Conrow, T., & Kreidl, T. 2000, ApJ, 530, L45

Han, Z., Podsiadlowski, P., Maxted, P. F. L., Marsh, T. R., & Ivanova, N. 2002, MNRAS, 336, 449

Heinke, C. O., Ivanova, N., Engel, M. C., Pavlovskii, K., Sivakoff, G. R., Cartwright, T. F., & Gladstone, J. C. 2013, ApJ, 768, 184

Herwig, F. 2000, A&A, 360, 952

Hinata, S. 1989, Ap&SS, 153, 1

Hjellming, M. S. & Webbink, R. F. 1987, ApJ, 318, 794

Houdek, G., Balmforth, N. J., Christensen-Dalsgaard, J., & Gough, D. O. 1999, A&A, 351, 582

Hynes, R. I. & Britt, C. T. 2012, ApJ, 755, 66

Ivanova, N. 2006, ApJ, 653, L137

—. 2011, ApJ, 730, 76

Ivanova, N., Justham, S., Chen, X., De Marco, O., Fryer, C. L., Gaburov, E., Ge, H., Glebbeek, E., Han, Z., Li, X.-D., Lu, G., Marsh, T., Podsiadlowski, P., Potter, A., Soker, N., Taam, R., Tauris, T. M., van den Heuvel, E. P. J., & Webbink, R. F. 2013a, A&ARv, 21, 59

—. 2013b, A&A Rev., 21, 59

Ivanova, N. & Taam, R. E. 2003, ApJ, 599, 516

—. 2004, ApJ, 601, 1058

Justham, S., Rappaport, S., & Podsiadlowski, P. 2006, MNRAS, 366, 1415

Kevorkian, J. & Cole, J. D. 1985 (Springer)

Kippenhahn, R. & Weigert, A. 1994, Stellar Structure and Evolution (Springer-Verlag Berlin Heidelberg New York)

Knigge, C., Baraffe, I., & Patterson, J. 2011, ApJS, 194, 28

Kolb, U. & Ritter, H. 1990, A&A, 236, 385

Krauss, M. I., Schulz, N. S., Chakrabarty, D., Juett, A. M., & Cottam, J. 2007, ApJ, 660, 605

Kuhfuss, R. 1986, A&A, 160, 116

Kuulkers, E., in't Zand, J. J. M., Atteia, J.-L., Levine, A. M., Brandt, S., Smith, D. A., Linares, M., Falanga, M., Sánchez-Fernández, C., Markwardt, C. B., Strohmayer, T. E., Cumming, A., & Suzuki, M. 2010, A&A, 514, A65

Lubow, S. H. & Shu, F. H. 1975a, ApJ, 198, 383

—. 1975b, ApJ, 198, 383

—. 1976, ApJ, 207, L53

Mata Sánchez, D., Muñoz-Darias, T., Casares, J., Steeghs, D., Ramos Almeida, C., & Acosta Pulido, J. A. 2015, ArXiv e-prints

Mestel, L. 1968, MNRAS, 138, 359

Mestel, L. & Spruit, H. C. 1987, MNRAS, 226, 57

Meunier, N., Proctor, M. R. E., Sokoloff, D. D., Soward, A. M., & Tobias, S. M. 1997, Geophysical and Astrophysical Fluid Dynamics, 86, 249

Mirabel, I. F. & Rodríguez, L. F. 1999, ARA&A, 37, 409

Nandez, J. L. A., Ivanova, N., & Lombardi, Jr., J. C. 2014, ApJ, 786, 39

Nelemans, G., Jonker, P. G., Marsh, T. R., & van der Klis, M. 2004, MNRAS, 348, L7

Nelemans, G., Yungelson, L. R., van der Sluys, M. V., & Tout, C. A. 2010, MNRAS, 401, 1347

Nelson, L. A., Rappaport, S. A., & Joss, P. C. 1986, ApJ, 304, 231

Noyes, R. W., Hartmann, L. W., Baliunas, S. L., Duncan, D. K., & Vaughan, A. H. 1984, ApJ, 279, 763

Paczynski, B. 1965, AcA, 15, 89

Paczyński, B. 1971, ARA&A, 9, 183

Paczynski, B. 1976, in IAU Symposium, Vol. 73, Structure and Evolution of Close Binary Systems, ed. P. Eggleton, S. Mitton, & J. Whelan, 75

Paczyński, B. & Sienkiewicz, R. 1972, Acta Astronomica, 22, 73

Parker, E. N. 1971, ApJ, 164, 491

Passy, J.-C., Herwig, F., & Paxton, B. 2012, ApJ, 760, 90

Pavlovskii, K., Belczynski, K., & Ivanova, N. 2015, in preparation

Pavlovskii, K. & Ivanova, N. 2013, in IAU Symposium, Vol. 291, IAU Symposium, ed. J. van Leeuwen, 468–470

Pavlovskii, K. & Ivanova, N. 2015a, MNRAS, submitted

—. 2015b, MNRAS, 449, 4415

Paxton, B., Bildsten, L., Dotter, A., Herwig, F., Lesaffre, P., & Timmes, F. 2011a, ApJs, 192, 3

—. 2011b, ApJs, 192, 3

Paxton, B., Cantiello, M., Arras, P., Bildsten, L., Brown, E. F., Dotter, A., Mankovich, C., Montgomery, M. H., Stello, D., Timmes, F. X., & Townsend, R. 2013, ApJs, 208, 4

Paxton, B., Marchant, P., Schwab, J., Bauer, E. B., Bildsten, L., Cantiello, M., Dessart, L., Farmer, R., Hu, H., Langer, N., Townsend, R. H. D., Townsley, D. M., & Timmes, F. X. 2015, ArXiv e-prints

Perez, M. S. & Blundell, K. M. 2010, MNRAS, 408, 2

Petrova, A. V. & Orlov, V. V. 1999, AJ, 117, 587

Podsiadlowski, P. 1991, Nature, 350, 136

Podsiadlowski, P., Rappaport, S., & Pfahl, E. D. 2002, ApJ, 565, 1107

Portegies Zwart, S. F. & Verbunt, F. 1996, A&A, 309, 179

Rappaport, S., Joss, P. C., & Webbink, R. F. 1982, ApJ, 254, 616

Rappaport, S., Verbunt, F., & Joss, P. C. 1983, ApJ, 275, 713

Rasio, F. A. & Livio, M. 1996, ApJ, 471, 366

Reimers, D. 1975, Memoires of the Societe Royale des Sciences de Liege, 8, 369

Ritter, H. 1988, A&A, 202, 93

Samadi, R. 2011, in Lecture Notes in Physics, Berlin Springer Verlag, Vol. 832, Lecture Notes in Physics, Berlin Springer Verlag, ed. J.-P. Rozelot & C. Neiner, 305

Savonije, G. J. 1978, A&A, 62, 317

Schatzman, E. 1962, Annales d'Astrophysique, 25, 18

Schulz, N. S., Chakrabarty, D., Marshall, H. L., Canizares, C. R., Lee, J. C., & Houck, J. 2001, ApJ, 563, 941

Sepinsky, J. F., Willems, B., Kalogera, V., & Rasio, F. A. 2007, ApJ, 667, 1170

—. 2009, ApJ, 702, 1387

Shao, Y. & Li, X.-D. 2012, ApJ, 745, 165

Skumanich, A. 1972, ApJ, 171, 565

Soberman, G. E., Phinney, E. S., & van den Heuvel, E. P. J. 1997, A&A, 327, 620

Spruit, H. C. & Taam, R. E. 2001, ApJ, 548, 900

Steeghs, D. & Casares, J. 2002, ApJ, 568, 273

Suzuki, T. K. 2007, ApJ, 659, 1592

Taam, R. E., Sandquist, E. L., & Dubus, G. 2003, ApJ, 592, 1124

Toonen, S., Claeys, J. S. W., Mennekens, N., & Ruiter, A. J. 2014, A&A, 562, A14

Toonen, S. & Nelemans, G. 2013, A&A, 557, A87

Tout, C. A., Aarseth, S. J., Pols, O. R., & Eggleton, P. P. 1997, MNRAS, 291, 732

van der Sluys, M. V., Verbunt, F., & Pols, O. R. 2005, A&A, 431, 647

van Haaften, L. M., Voss, R., & Nelemans, G. 2012, A&A, 543, A121

Vink, J. S., de Koter, A., & Lamers, H. J. G. L. M. 2001, A&A, 369, 574

Wang, X. & Wang, Z. 2014, ApJ, 788, 184

Watts, A. L., Krishnan, B., Bildsten, L., & Schutz, B. F. 2008, MNRAS, 389, 839

Webbink, R. F. 1985, Stellar evolution and binaries, ed. J. E. Pringle & R. A. Wade, 39

Werner, K., Nagel, T., Rauch, T., Hammer, N. J., & Dreizler, S. 2006, A&A, 450, 725

Woods, T. E. & Ivanova, N. 2011, ApJ, 739, L48

Woods, T. E., Ivanova, N., van der Sluys, M. V., & Chaichenets, S. 2012, ApJ, 744, 12

Yungelson, L. R. 2008, Astronomy Letters, 34, 620

Yungelson, L. R. & Lasota, J.-P. 2008, Astronomy and Astrophysics, 488, 257

Zurek, D. R., Knigge, C., Maccarone, T. J., Dieball, A., & Long, K. S. 2009, ApJ, 699, 1113

Appendix A

Changes in MESA

This section lists the technical details of the changes introduced to the MESA code to obtain the results of this thesis. Changes are listed with respect to the MESA release 5596. The actual difference files are available by an e-mail request to the author[1].

A.1 Changes to the MESA/atm module

The boundary condition equation is modified to contain the effective force field instead of just the gravitational field (see Eq. 3.7). The radiative pressure at zero optical depth is modified due to an error in the MESA code, which comes from the error in the classical textbook Cox & Giuli (1968) used by the MESA developers. Instead of the original defective formula

$$1.6 \times 10^{-4} \kappa \frac{L}{L_\odot} \frac{M}{M_\odot}, \tag{A.1}$$

where κ is Rosseland mean opacity at the surface, L and M are luminosity and mass of the star we use

$$\frac{1}{6} a T_{\rm eff}^4, \tag{A.2}$$

where a is radiative constant, $T_{\rm eff}$ is the effective temperature of the star.

A.2 Changes to the MESA/mlt module

The expression for the force field in the standard MLT scheme (Cox & Giuli, 1968) is modified to include the fictitious force, that depends on the local acceleration. Originally in MESA the external

[1] pavlovsk@ualberta.ca

force field was assumed to be equal to the external gravitational field for the purpose of convection, which is only valid in the absence of local accelerations, i.e. in hydrostatic equilibrium.

This change ultimately affects the convective conductivity , which is proportional to the external force field. E.g., when the external force field is zero, there is no convection, hence the convective conductivity is zero.

A.3 Changes to the `MESA/star` module

The outermost cell used to be treated hydrostatically disregarding whether or not the code is run in hydrodynamical mode. We've changed this: now in hydrodynamical mode the outermost cell is treated also hydrodynamically. This change was possible because of the hydrodynamical boundary condition that we also introduced (see Section A.1) for details). The new boundary condition now allows to consistently treat the outer cell hydrodynamically.

Acceleration terms were introduced to the temperature equation and to the expression for radiative gradient as explained in Section 3.3.2. These terms are necessary to make the temperature equation consistent simultaneously with the modified MLT module, which is discussed in Section A.2, and with the radiative gradient in radiative zones. In radiative zones the acceleration terms in the expression for radiative gradient and temperature equation mutually vanish. This is not surprising because the external force field is not taken into account in the radiative diffusion approximation, used to treat heat transfer in radiative regions.

A.4 Changes to the `MESA/binary` module

A new explicit MT scheme is added, which is implemented along the lines of Section 4.1. The user may choose the scheme "Pavlovskii" in the same way as the other schemes, which will result in MT being calculated in a new way. Because this new scheme uses realistic 3D integrations (see Section 4.1.1 for details), it is not compatible with the old code that calculates the Roche lobe radius in the binary using the Eggleton prescription. Hence, the code is modified to use a binary data file with a geometrical table to determine the Roche lobe radius from mass ratio and binary separation. There is a setting that allows the user to switch back to the Eggleton approximation, but it is not recommended to use this setting when the "Pavlovskii" explicit MT scheme is used.

A.5 Additional modules written in C++ and data files

Additional modules written in C++ are:

- The module that conducts realistic Roche geometry integrations to determine the volume of the Roche lobe and the area of the nozzle for a given dimensionless Roche potential.
- The module that conducts adiabatic integrations with the realistic equation of state implemented in `MESA/eos` to obtain the thermodynamical parameters of gas at the sonic surface.
- A wrapper that provides a C++ interface for a subset of the `MESA/eos` module.

The Roche geometry integrations are conducted in the following way: first a Newton-Raphson solver finds intersections between various lines passing through the center of the donor and the shell composed of the Roche lobe and the sonic surface. Then, the positions of these intersections are used to calculate the volume of the shell using a three-dimensional integration with the Simpson method. Areas of the nozzles for different equipotentials are calculated in the same way, but the L_1 point is used instead of the center of the donor, only those lines that lie within the sonic surface are considered and the resulting integral is two-dimensional.

These calculations are conducted for multiple equipotentials and multiple values of mass ratio. The resulting tables that contain mass ratios, dimensionless potentials and the corresponding Roche lobe volumes and nozzle areas are written to a binary file. This file is loaded into memory as needed. Because of this no Roche geometry integrations are conducted at runtime.

Adiabatic integrations along the streamlines to the sonic point are conducted with the Runge-Kutta-Fehlberg integrator that comes with the GNU Scientific Library[2].

[2] https://www.gnu.org/software/gsl/

Appendix B

Pulsations in MESA models

Red giants are known to have intrinsic oscillations (for reviews, see Bedding 2011, Christensen-Dalsgaard 2011, and references therein). The MESA code was developed taking into account the hydrodynamical term in the pressure equation (Paxton et al., 2011b), hence it is capable (with certain limitations, see Chapter 3) of modeling stellar oscillations. This capability is important for the studies of ML from red giants because a rapidly increasing ML rate does induce dynamical pulsations in a red giant (see Section 6.1 and model passy-b). Here, we explore the ability of MESA to model radial oscillations, and compare our results with observations and numerical studies performed by other methods.

As an example, the oscillations of interest were observed by Buzasi et al. (2000) in a 4 $M_{\odot}$ and $\sim 28R_{\odot}$ K0 giant (α UMa) with the WIRE satellite. They observed about 10 low-frequency radial modes with the fundamental mode at 1.82 μHz, which corresponds to a period of ≈ 0.017 yr. Guenther et al. (2000) and later works Dziembowski et al. (2001) attempted to model the oscillation properties observed by Buzasi et al. (2000), and found that although the overall agreement of their simulation with observations is satisfactory, modes 3, 5 and 7 predicted by their codes were not observed by Buzasi et al. (2000) (see Table B.1).

We modeled a similar red giant – with a mass of $4M_{\odot}$ and radius of $\sim 28R_{\odot}$ – using MESA (release 4028), in hydrodynamical mode. For this evolution we adopted the MESA overshooting parameter $f = 0.02$ (Herwig, 2000), default artificial viscosity coefficients $l_1 = 0.1$; $l_2 = 2$ and constant timestep 10^{-5} yr.

A very rough spectral density estimate of oscillations (Figure B.2) in a $4M_{\odot}$ red giant that we modeled with MESA shows 7 distinct oscillatory modes (Table B.1) that are in good agreement with the ones obtained in earlier estimates by Guenther et al. (2000) and Dziembowski et al. (2001). In particular, all frequencies given by MESA (except for the main mode frequency) exceed the corresponding frequencies given by the simulations of Guenther et al. (2000), and are less than the

Table B.1: Radial p-mode frequencies of αUMa: observations and simulations

n	B2000	G2000	D2001	MESA
0	1.82 ± 1.484	2.67	2.83	2.88
1	4.84 ± 0.98	5.01	5.30	5.16
2	7.86 ± 0.77	7.00	7.42	7.12
3	not excited	8.94	9.46	9.05
4	11.41 ± 0.59	10.65	11.29	10.90
5	not excited	12.38	13.09	12.56
6	15.00 ± 0.71	14.24	15.03	14.56
7	not excited	16.00	16.86	
8	18.25 ± 0.71	17.85	18.80	
9	20.90 ± 0.67	19.73	20.78	

Frequencies are given in μHz. B2000 – observational results from Buzasi et al. (2000); G2000 – numerical results by Guenther et al. (2000), values are given for 4.0 $M_{\odot}$ model; D2001 – numerical results by Dziembowski et al. (2001), values for the model with parameters $a^2 = 900$ and $b^2 = 2000.$; MESA – this work. In our work, the frequencies are taken as maxima of the periodogram (Figure B.2), over the period of 27.1 yr. No spectral fitting has been carried out because of a complicated pattern of damping and excitation of modes.

corresponding frequencies obtained by Dziembowski et al. (2001).

It has to be anticipated, however, that the oscillations produced by MESA and the oscillations observed in αUMa by Buzasi et al. (2000) have different origins. Hence, their amplitudes are completely unrelated. In real giants, intrinsic oscillations are thought to appear due to turbulent convection (for review, see Samadi (2011)), the same mechanism responsible for excitation of p-modes in MS stars. It was first shown by Goldreich & Keeley (1977) that turbulent convective eddies can exchange significant amounts of energy with p-modes.

In stellar models produced by MESA, radial oscillatory modes can be excited by those changes in stellar structure that produce local accelerations. Examples of such changes include numerical artifacts, abrupt nuclear processes (Bildsten et al., 2012) and ML (Section 6.1). Artificial viscosity damps oscillations, and therefore their amplitude depends on the viscosity coefficients.

In our models, the numerical artifact responsible for the majority of oscillations is the smoothing of convective boundaries. When the bottom of the convective zone moves up (or the top of convective zone moves down) in mass, MESA performs a linear smoothing of the abundance gradient in the newly non-convective region. This leads to sharp changes in the abundances of several neighboring cells and, consequently, to the local sharp change in pressure that produces local accelerations and creates velocity waves in the interior. These waves are responsible for the majority of the excitation of "intrinsic" radius oscillations. If this effect is removed, the amplitude of radial p-modes is suppressed to $\sim 10^{-3}$ times the default setup (this ratio varies for different giants).

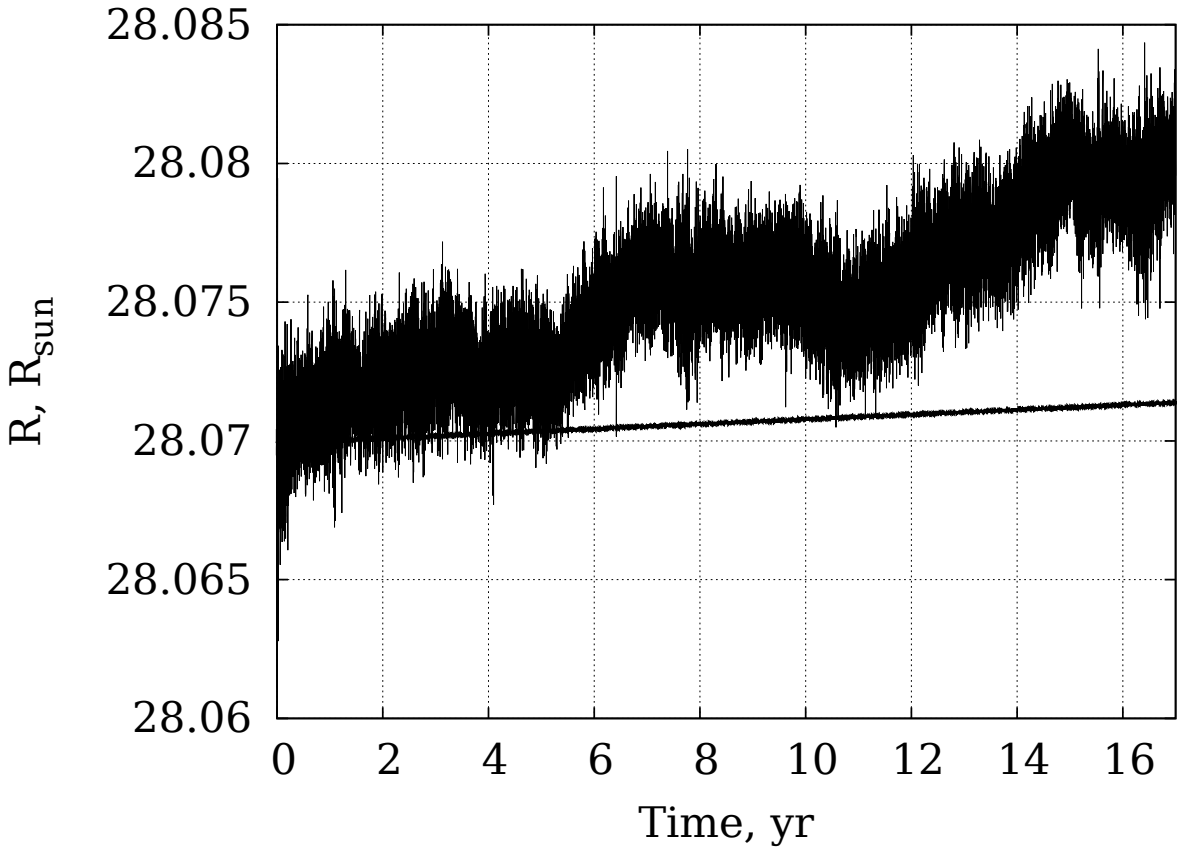

Figure B.1: Intrinsic oscillations of a 4 $M_{\odot}$ red giant of 28$R_{\odot}$ (upper line). The lower line shows the evolution of the radius when the major sources of p-mode excitation are excluded (see text for details).

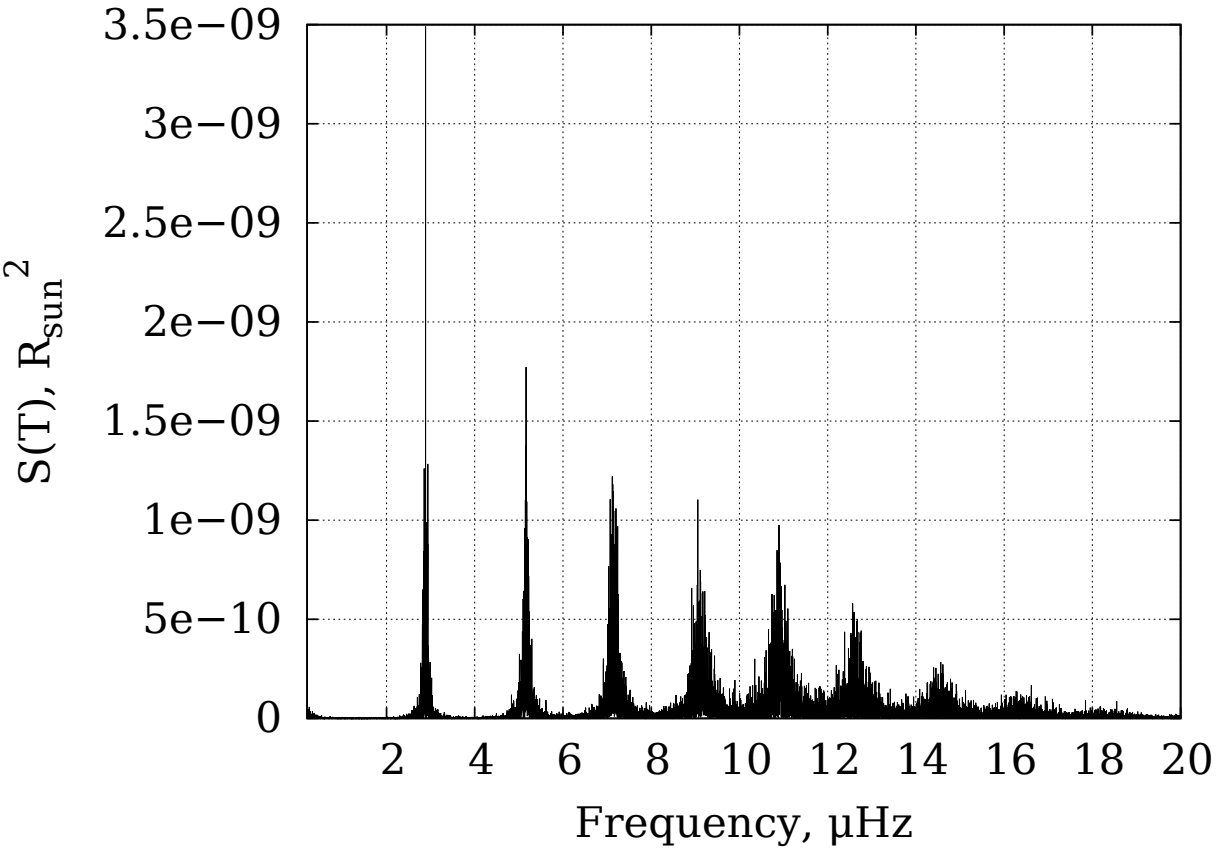

Figure B.2: Raw Schuster periodogram of detrended evolution of radius in a 4 $M_{\odot}$ red giant.